Current and Temperature Distributions in Proton Exchange Membrane Fuel Cell

by

Ibrahim Alaefour

A thesis
presented to the University of Waterloo
in fulfillment of the
thesis requirement for the degree of
Doctor of Philosophy
in
Mechanical Engineering

Waterloo, Ontario, Canada, 2012

AUTHOR'S DECLARATION

I hereby declare that I am the sole author of this thesis. This is a true copy of the thesis, including any required final revisions, as accepted by my examiners.

I understand that my thesis may be made electronically available to the public.

Ibrahim Alaefour

Abstract

Proton exchange membrane fuel cell (PEMFC) is a potential alternative energy conversion device for stationary and automotive applications. Wide commercialization of PEMFC depends on progress that can be achieved to enhance its reliability and durability along with cost reduction. It is desirable to operate the PEMFC at uniform local current density and temperature distributions over the surface of the membrane electrode assembly (MEA). Non-uniform distributions of both current and temperature over the MEA could result in poor reactant and catalyst utilization as well as overall cell performance degradation. Local current distribution in the PEMFC electrodes are closely related to operating conditions, but it is also affected by the organization of the reactant flow arrangements in PEMFCs. Reactant depletion and water formation along the flow channel leads to current variation from the channel inlet to the exit, which leads to non-uniformity of local electrochemical reaction activity, and degradation of the cell performance. Flow arrangements between the anode and cathode streams, such as co-, counter- and cross- flow can exacerbate the effect of the non-uniformity considerably, producing complex current distribution patterns over the electrode surfaces. Thus, understanding of the local current density and its spatial characteristics, as well as the temperature distributions under different physical and operating conditions, is crucially important in order to develop optimum design and operational strategies. Despite the importance of the influence of the flow arrangement on the local current and temperature distributions under various operating conditions, few systematic studies have been conducted experimentally to investigate this effect.

In this research, an experimental setup with special PEMFC test cells are designed and fabricated in-house, in order to conduct in-situ mapping of the local current and temperature distributions over the electrode surfaces. A segmented flow field plate and the printed circuit board (PCB) technique is used to measure the current distribution in a single PEMFC. In situ, nondestructive temperature measurements are conducted using thermocouples to determine the actual temperature distribution. Experimental studies have been conducted to investigate the effect of different flow arrangements between the anode and cathode (co-, counter-, and

cross- flow) on the local current density distribution over the MEA surface. Furthermore, local current distribution has been characterized for PEMFCs under various operating conditions such as reactant stoichiometry ratios, reactant backpressure, cell temperature, cell potentials, and relative humidity for each one of the reactant flow arrangements. The dynamic characteristics of the local current in PEMFC under different operating conditions also have been studied. Temperature distributions along the parallel and serpentine flow channels in PEMFs under various operating conditions are also investigated. All independent tests are conducted to identify and optimize the key design and operational parameters for both local current and temperature distributions.

It has been found that the local current density distribution is strongly affected by the flow arrangement between the anode and cathode streams and the key operating conditions. It has also been observed that the counter-flow arrangement generates the most uniform distribution for the current density, whereas the co-flow arrangement results in a considerable variation in the current density from the reactant gas stream inlet to the exit. Low stoichiometry ratio of hydrogen at the anode side has a predominant effect on the current distribution and cell performance. Further, it has been found that the dynamic characteristics and the degree of fluctuation of local current density inside PEMFC are strongly influenced by the crucial operating conditions. In-situ, nondestructive temperature measurements indicate that the temperature distribution inside the PEMFC is strongly sensitive to the cell's current density. The temperature distribution inside the PEMFC seems to be virtually uniform at low current density, while the temperature variation increases up to 2 ^{o}C at the high current density. Finally, the present work contribution related to the local current and temperature distributions is required to understand the effect of each individual or even several operating parameters combined together on the local current and temperature distributions. This will help to develop an optimum design, which leads to enhancing the reliability and durability in operational PEMFCs.

Acknowledgements

First and Foremost, I would like to thank my supervisor, Dr. Xianguo Li, for his guidance throughout my Ph.D. program. His encouragement and support are very much appreciated. I would also like to thank my committee members, Dr. David Johnson, Dr. John Z. Wen, and Dr. Zhongwei Chen, and Dr. Andy (Xueliang) Sun form University of Western Ontario for taking the time to review my thesis. Their comments are very valuable and highly appreciated.

I would like to thank the staff of the Mechanical Engineering Department at the University of Waterloo for their support and friendship. Also, I want to thank all my group members at the 20/20 Laboratory for their support and encouragement throughout my Ph.D. program.

I appreciate the financial support from the Libyan Government through the Libyan Ministry of Higher Education and the Canadian Bureau for International Education (CBIE).

Last but not the least; I would like to express my eternal gratitude to my family who has given me endless love and support throughout my entire life. I would like especially to thank my wife and sons for their understanding and patience throughout my endeavors.

Table of Contents

List of Figures

List of Tables

Nomenclature

A_C	Cross section area of flow channel (m^2)
b	Bias errors (limits)
CV	Coefficient of variation
D_h	Hydraulic diameter of the flow channel (m)
f	Friction factor
h	Height of the flow channel (m)
I	Current density (A/cm^2)
L	Length of the flow channel (m)
L_e	Length of hydrodyanmic entrance
$\dot{m}$	Mass flow rate (kg/sec)
N	Number of tests
$\dot{N}$	Molar flow rate (mol/sec)
P	Pressure (kPa)
p	Precision error
Δp	Pressure drop along the flow channel (kPa)
R	Resistance (Ω)
Rh	Relative humidity
Re	Reynolds number
T	Temperature (^oC)
U	Flow stream velocity (m/sec)
w	Channel width (m)
u	Measurement uncertainty
V	Cell potential (V)
x	Current density value (A/cm^2)
$\bar{X}$	Average of current density value (A/cm^2)

Greek letters

σ	Standard deviation
ρ	Fluid density (kg/m^3)
μ	Dynamic viscosity (kg/m.s)

Superscripts/subscripts

a	Anode
act	Activation loss
b_{yk}	Individual bias limits
conc	Concentration loss
gas	Gas mixture
H_2	Hydrogen gas
in,a	Anode inlet
in,c	Cathode inlet
cell	Cell characteristic
vap	Water vapour
Omh	Omhic loss
Total	Total pressure
O_2	Oxygen gas
R	Resistance
rev	Reversible

Abbreviations

AFC	Alkaline fuel cell
ANSI	American National Standards Institute
CL	Catalyst layer
DAQ	Data acquisition system
DI	De-ionized water
DMFC	Direct methanol fuel cell
FCATS	Fuel Cell Automated Test Stations
GDL	Gas diffusion layer
HOR	Hydrogen oxidization reaction
MEA	Membrane electrode assembly surface
MCFC	Molten carbonate fuel cell
ORR	Oxygen reduction reaction

PAFC	Phosphoric acid fuel cell
PTFE	Polytetrafluoroethylene
PFSA	Perfluorosulfonic acid
PCB	Printed circuit board
SOFC	Solid oxide fuel cell
SEM	Scanning electron microscope
SLE	Special limits of error

Chapter 1
Introduction

1.1 Background

Fuel cells are electrochemical devices that convert the chemical energy of reactants directly into electrical energy as long as the fuel and oxidant are supplied [1]. Fuel cells can be classified into different categories based on the operating temperature or the type of electrolyte. The most common classification of fuel cells is according to their electrolyte material. Common types of fuel cells include polymer electrolyte membrane or proton electrolyte membrane fuel cell (PEMFC), direct methanol fuel cell (DMFC), alkaline fuel cell (AFC), solid oxide fuel cell (SOFC), phosphoric acid fuel cell (PAFC), and molten carbonate fuel cell (MCFC). The first three types are also known as low-temperature fuel cells which operate at about 80 ^{o}C, whereas the last two types are commonly known as high-temperature fuel cells, which operate at high temperatures of up to 1000 °C. Each type of cell is used for one or more power generation applications. DMFCs are widely used as a power source for portable applications [2]. SOFCs and MCFCs are commonly used as stationary and cogeneration power plants. PEMFCs are one of the promising power sources for transportation and on-site co-generation stationary applications due to their attractive features, including fast startup time, zero emissions, high power density, and simple design configuration. These advantages clearly demonstrate the practical feasibility of the PEMFC. However, it has not become commercially very feasible because of operating and technical barriers, such as high cost, reliability, and durability [3, 4]. During the operation of PEMFC, very complex and tightly related transport phenomena occur inside each individual cell component. These transport phenomena include mass and heat transfer, protons and electronics transport, and heat and water transport simultaneously with electrochemical kinetic process.

It is desirable to operate the PEMFC at uniform distributions of both the local current density and temperature over the membrane electrode assembly surface (MEA) because non-

uniform current distribution in a PEMFC could result in poor reactant and catalyst utilization, low energy efficiency, and possible corrosion processes inside the fuel cell [1]. Local current distribution and its dynamic characteristics in the fuel cell can be strongly affected by various operating conditions as well as the organization of the reactant flow arrangement between the anode and cathode streams especially in practical PEMFCs of large cell sizes [2, 4]. For instance, reactant depletion along the flow channel leads to current variation from the channel inlet to the exit, and degrades the cell performance; flow arrangements between the anode and cathode streams, such as co-, counter-, and cross-flow can exacerbate this effect considerably, resulting in complex current distribution patterns over MEA surfaces.

An operating PEMFC converts about 50% of the chemical energy available in the reactants to useful electricity, and the rest turns into heat [4]. By-products of heat and water should be continuously removed in order to ensure safe operation and optimum performance of the fuel cell. Heat generation leads to non-uniform temperature distribution in the cell and performance degradation. It is desirable for PEMFCs to operate at isothermal conditions because temperature variation changes local relative humidity and causes water phase changes (condensation/evaporation). Isothermal operating conditions also yield the best cell performance. In addition, the temperature distribution and water content inside PEMFC affect the electrochemical reaction in the catalyst layer, the hydration/dehydration of the polymer membrane, the ionic transport, and the supply of reactant. Thus, understanding the distributions of both local temperature and current density inside the fuel cell is essential for developing proper water and heat management, which lead to improved cell reliability and durability.

1.2 Operating Principles of a PEMFC

A PEMFC converts the chemical energy of a fuel and an oxidant directly into electric energy. It is composed of a polymer electrolyte sandwiched between two platinum catalyzed electrodes made of a porous material with high electrical conductivity, typically carbon fiber

paper or carbon cloth treated with polytetrafluoroethylene (PTFE) because of its hydrophobic property [1].

All types of fuel cells operate on the same basic principle. At the anode, a fuel is oxidized into electrons and protons, and at the cathode, oxygen is reduced to oxide species. The basic operational principle of a PEMFC is illustrated in Figure 1.1. Humidified hydrogen is supplied to the flow channel field of the anode side, and then diffuses through the gas diffusion layer (GDL) toward the platinum catalyst layer (CL). An electrochemical reaction takes place when the hydrogen reaches the CL, splitting the hydrogen atom into positive protons and negative electrons as given below:

$$\textit{Anode reaction (Reaction I)}: \qquad \mathrm{H_2} \rightarrow 2\mathrm{H^+} + 2\mathrm{e^-} \tag{1.1}$$

This reaction is known as the hydrogen oxidization reaction (HOR).

The electrolyte membrane facilitates the proton transport from the anode to the cathode, while forcing the electron to travel through the external circuit, thus producing the useful electrical power output. At the cathode, humidified air is supplied to the flow channel field, and transported via the GDL toward the platinum catalyst layer, where it reacts with the protons from the anode and the electrons from the external circuit to produce water and heat. The electrochemical equation that describes the process that occurs at the cathode side is known as the oxygen reduction reaction (ORR):

$$\textit{Cathode reaction (Reaction II)}: \quad 2\mathrm{H_2} + \frac{1}{2}\mathrm{O_2} + 2e^- \rightarrow \mathrm{H_2O} \tag{1.2}$$

By combining the equations 1.1 and 1.2, the overall electrochemical reaction occurs in PEMFC as:

$$H_2 + \frac{1}{2}O_2 \rightarrow H_2O + Heat + Work \tag{1.3}$$

The only liquid in the fuel cell is water; thus, corrosion problems are minimal. Water management in the membrane is critical for efficient performance: the fuel cell must operate

under conditions in which the byproduct water evaporation rate is slower than its production rate to keep the membrane hydrated. The effect of water generation and formation along the flow channels issue will be discussed further in the following chapters.

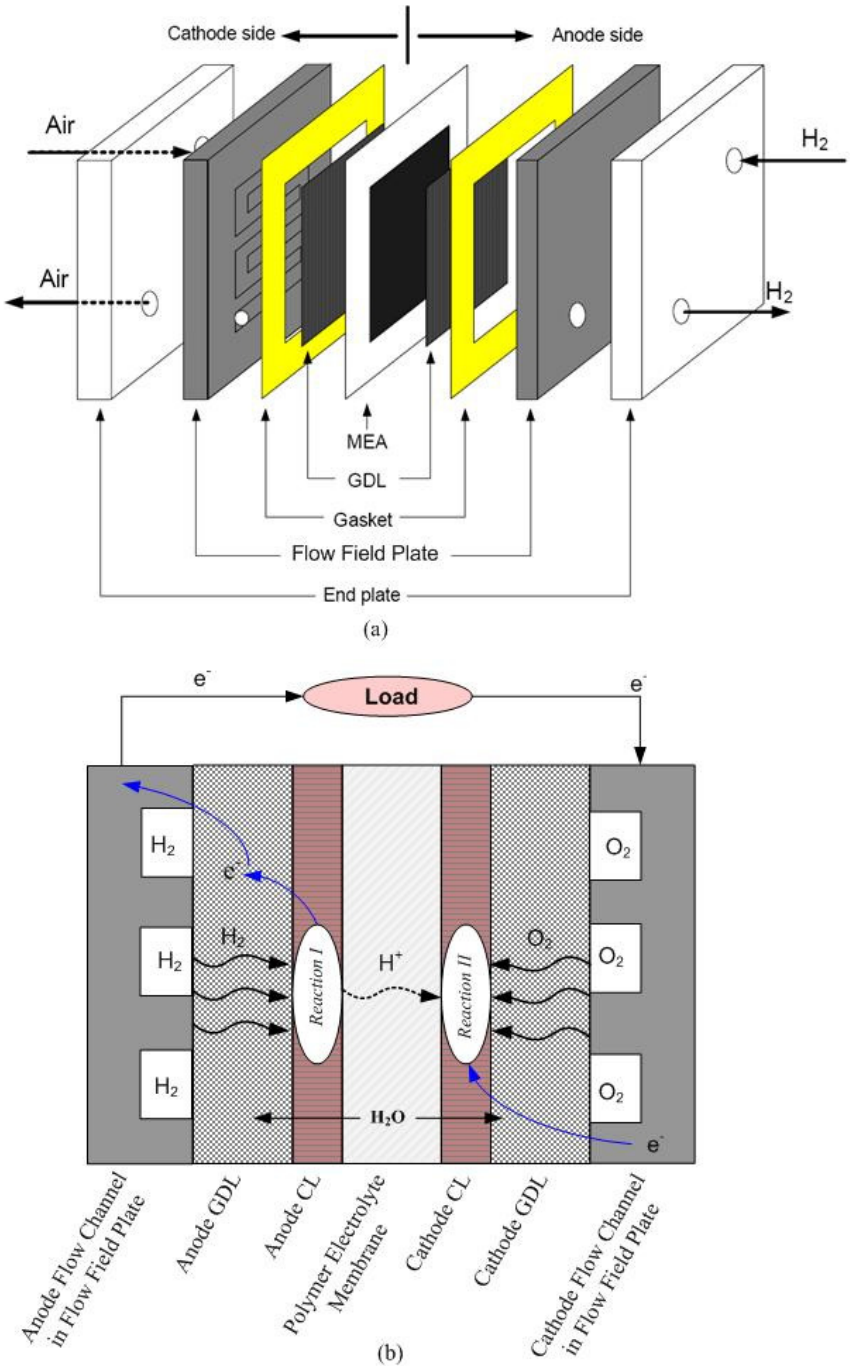

Figure 1.1: (a) main fuel cell components [5] and (b) basic operating principles a PEMFC.

1.3 Main Components of PEMFC

PEMFC obtained its name from the special plastic material used as the electrolyte. The anode, cathode, and electrolyte layers are bonded together into one piece, which is known as the membrane electrode assembly (MEA) and is just few hundred microns in thickness. This MEA is sandwiched between a pair of current collector plates, which have a machined flow field for supplying the reactants (the fuel and oxygen) to the electrodes.

1.3.1 Proton Exchange Membrane (PEM)

Polymer electrolyte membrane fuel cell (PEMFC) plays a crucial role in the operation of a fuel cell. It must have the special physical and chemical properties that make it a proton conductor between the anode and the cathode, while forcing the electron to flow through the external circuit to produce useful power output [1, 6]. The membrane should be chemically and thermally stable in the reducing environment at the cathode, as well as in the harsh oxidative environment of the anode [7]. The membrane also functions as a physical barrier between the anode and the cathode regions by preventing fuel from penetrating to the cathode side and oxygen to the anode side. Air and hydrogen crossover to the opposite sides of the membrane has been demonstrated to be very slow and responsible for only 1-3% of the losses in fuel efficiency in PEMFCs. However, exothermal direct combustion between the hydrogen and oxygen leads to local hotspots, resulting in pinholes in the membrane, and destroying the MEA itself [6, 7]. The most commonly used and studied membranes for PEMFCs are perfluorosulfonic acid (PFSA) membranes such as Nafion, which is produced by Dupont [1]. The main properties of the membrane are proton conductivity, water diffusion, gas permeability, and physical stability. All of these properties are strongly influenced by the water content. Low water content causes the anode side of the membrane to dry out, resulting in enormous performance losses. On the other hand, too much water content results in flooding of the cathode region, which prevents the reactant gases from reaching the catalyst layer leading to large amount of concentration polarization. Therefore, water management is a key element in PEMFC operation, and the amount of water must be balanced in order to achieve sufficient membrane hydration in the PEMFC without flooding.

The primary membrane material in the laboratory to be used for this present research is Nafion, which is available in three forms, classified according to their thickness [8]. Dry membranes Nafion 112, 115, and 117 have thicknesses of 50 µm, 127 µm, 177.8 µm, respectively. Experimental observations, along with numerical investigations indicated that a thicker membrane provides better insulation and physical stability along with higher proton transport resistance. In contrast, a thinner membrane provides low insulation, low physical and chemical stability, and low proton transport resistance. The appropriate choice is based on the optimal parameters for specific applications.

1.3.2 Catalyst Layers (CL)

Catalyst layers are thin layers located between the ionomer membrane and porous the electrodes at both sides of the membrane. The electrochemical reactions actually take place on the surface of the catalyst layers. Three kinds of species participate in the electrochemical reactions, namely gases, electrons, and protons. The most common catalyst used in PEMPFs for both oxygen reduction and hydrogen oxidation reactions is platinum (Pt), which thus far, is the only catalyst that provides sufficient stability and that can withstand thousands of hours of operation in a PEMFC electrode environment. The cost of PEMFCs can be drastically reduced by optimizing the amount of Pt in the electrodes. In the last two decades the Pt loading on the surface of the electrodes has been reduced from 4 mg/cm^2 to 0.2–0.4 mg/cm^2 [9]. The CLs should be reasonably thin (around 10µm) in order to minimize the overpotential of the cell due to proton resistance. Moreover, to avoid water flooding and to provide better mechanical properties, polytetrafluoroethylene (PTFE) can be added to the catalyst to give the CL hydrophobic properties. Current research is investigating better and cheaper catalyst materials to replace the platinum in a PEMFC.

1.3.3 Gas Diffusion Layers (GDLs)

The gas diffusion layer (GDL) is composed of a dual-layer carbon-based porous material. The main part of the GDL is available in two forms; macroporous carbon fiber paper and carbon cloth. The second layer is a thinner microporous layer (MPL) consisting of carbon

black powder and polyterafluoroethlene (PTEF), which changes the GDL properties from hydrophilic to hydrophobic. GDLs serve as a structural support for the catalyst layer and as an electrical conductor between the carbons supported catalyst and current collector plates. The GDL also acts as a physical barrier between the reactant gases in the flow channels and the surface of the thin membrane. The reactant gases should be distributed homogenously from the flow field to the catalyst layer through the GDLs in order to complete the electrochemical reaction. The GDL also should have the ability to remove the heat and excess water from the electrode in order to avoid hotspots and catalyst flooding.

GDLs can be selected based on their thickness, gas permeability, and electrical conductivity [10]. TORAY carbon paper is the most commonly used GDL due to its low cost, and range of thicknesses varying between 100 μm and 400 μm. Thin gas diffusion layers with less resistance to electricity are preferable; however, GDLs that are too thin cannot provide the required high level of electrical contact between the current collector plates and the catalyst layer [11].

1.3.4 Flow Field Plates

The flow field plate is the backbone and a multifunctional component in a single PEMFC or a fuel cell stack. The roles of flow field plate are to; i) supply and distribute the reactant gases toward GDL, ii) facilitate water management within the cell, iii) act as the electrical connector, and iv) remove heat and water from the active areas. The flow field consists of the flow channels and their land areas (ribs) as illustrated in Figure 1.2. Experimental results have indicated that higher width ratio between the flow channel and its rib leads to a significant improvement the cell performance, especially at low cell voltages [12]. The material most commonly used for flow field plate fabrication in the laboratory to be used for current research is graphite due to its desirable properties such as high thermal and electrical conductivities, high chemical stability, and superior resistance to corrosion [13]. However, the machining cost is still quite expensive, low mechanical strength (brittleness), and high porosity. The low mechanical strength limits the minimum thickness of the graphite plates

about 5-6 mm which leads to a large volume and weight for the required plate size [14]. Different layout designs are used in PEMFC applications, and the most common flow field designs discussed in the literature include [13, 15] straight or parallel gas channels, a pin-type flow field, a serpentine flow field, and an interdigitated flow field. Since straight and serpentine flow fields will be used in the present work, the characteristics, advantages, and disadvantages of each design are described.

1.3.4.1 Parallel Gas Channel Flow Field

A straight gas channel flow field consists of number of separate parallel channels arranging in same direction and are connected to the two edge channels, as shown in Figure 1.2 (a). Although this design is simple, the reactants flowing through such flow fields tend to follow the path of least resistance across the flow field, which may lead to the formation of stagnant areas. In addition, since the channel lengths are typically short, the pressure drop along these channels is very small. These two factors result in an uneven distribution of the reactant on the MEA surface and inadequate product water removal, both of which lead to poor fuel cell performance. On the other hand, this flow field design result in a small pressure drop along the flow channels, hence, minimum compression power requires in order to push the reactants to flow through the channels.

1.3.4.2 Serpentine Flow Field

In an attempt to overcome the drawbacks associated with straight flow channels, a new type of flow field channel has been developed which is commonly known as the serpentine flow field. The main idea of this design is a continuous fluid flow channel with an inlet at one end and an outlet at the other, which typically follows a serpentine path, as shown in Figure 1.3 (b). The main advantage of the new design is to provide better water management inside the cell and reduce the effect of the blockage caused by by-product water in the channels, especially adjacent to the cathode. However, this channel layout results in a relatively long reactant flow path, leading to both a significant pressure drop and concentration gradients from the flow inlet to the outlet.

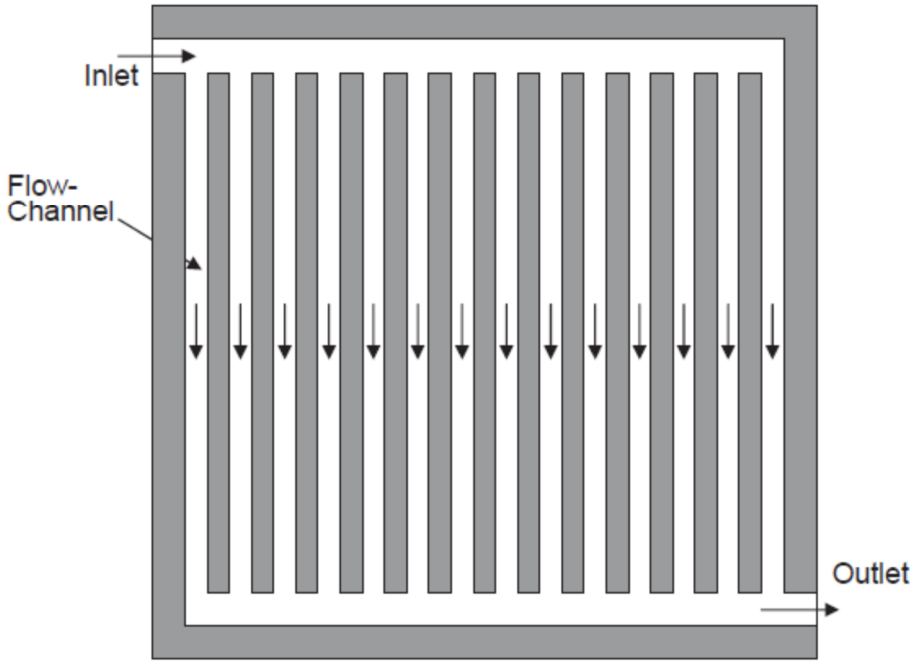

(a)

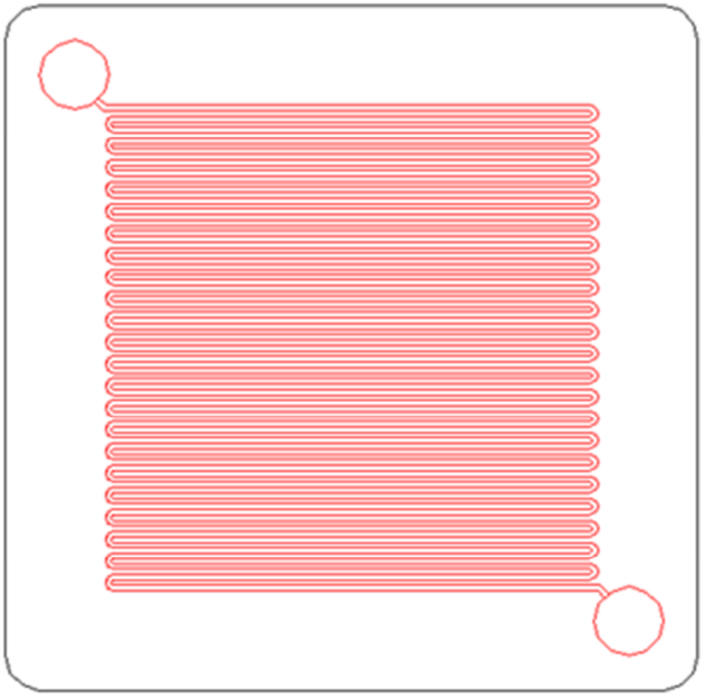

(b)

Figure 1.2: (a) straight or parallel flow field layout [16] and (b) serpentine flow field layout.

1.4 Fuel Cell Performance

The most ordinary indicator of fuel cell performance is the current-voltage (*I-V)* curve, or polarization curve. An example of a typical polarization curve for a PEMFC is illustrated in Figure 1.3. This curve plots the cell potential (*V*) against the current density (A/cm^2).

The usual first evaluation method of validating any numerical simulation result is to compare its polarization curve with the polarization curve generated from experimental data for the same operating conditions. The polarization curve also provides a clear picture of the different types of losses (overpotentials) that occur inside the fuel cell. An ideally operating fuel cell should provide a constant potential (voltage) as long as the reactants are supplied. However, the actual cell potential (*V*) is always less than the reversible thermodynamic potential (V_{rev}) due to irreversible voltage losses, which is known as the cell overpotential (η_{Cell}).

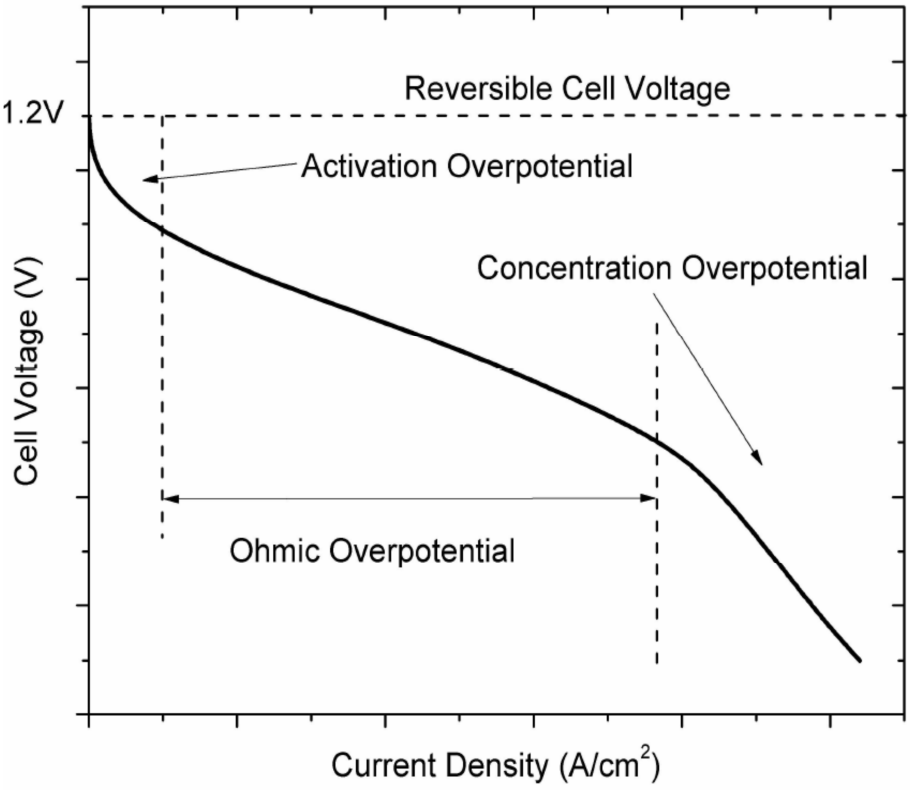

Figure 1.3: Polarization curve of single PEMFC [17].

The relationship between the actual cell potential, the reversible cell potential, and the total overpotential (losses) in the fuel cell is expressed as:

$$V = V_{rev} - \eta_{cell} \tag{1.4}$$

where

$$\eta_{cell} = \eta_{act.} + \eta_{omh.} + \eta_{conc.} \tag{1.5}$$

and η_{act}, η_{omh}, and η_{conc} are the activation, ohmic, and concentration overpotentials, respectively. The fuel cell potential decreases as the current drawn is increased because of three different types of irreversible losses. For simplicity, the polarization curve is divided into three regions: activation, ohmic, and concentration polarizations, as shown in Figure 1.3. This division does not mean that each type of polarization occurs separately at different specific regions.

The first region of the polarization curve is known as the activation polarization region. It is dominant at a low current density due to the slow rate of the electrochemical reaction. This is because a considerable amount of the energy is lost through driving up the rate of the electrochemical reaction. It is obvious that the cell potential in this region is high and the current density is very low. As a result, the power density is low since it is equal to the cell potential value multiplied by the current density.

$$Power = I \times V \tag{1.6}$$

The second region of the curve is called the Ohmic polarization region. In this region, the relationship between the current density and the cell potential is almost linear. The Ohmic polarization is caused by the electronic and ionic resistances. Electronic resistances occur in various components of the fuel cell, such as the electrode substrates, and the two catalyst layers. Ionic proton resistances occur inside the membrane electrolyte and the catalyst layers.

The third region is known as the concentration polarization region. It occurs at a high current density with a very low cell potential that may reach zero (Maximum Current Density). As the current drawn from the cell is increased, the rate of the electrochemical

reaction at the electrodes increases to meet the current demand. Thus, the electrochemical reaction consumes the reactants to meet the current demand until it reaches the point at which the reactants can no longer be supplied to the active sites because of several limitation processes. These processes may contribute to the concentration of polarization, which includes slow diffusion in the gas phase in the electrode pores, reduced partial pressure of oxygen in the air, and blockage of gas access because of water flooding, especially on the cathode side. At practical current densities, slow product removal from the electrochemical reaction site is a major contributor to concentration polarization.

1.5 Objectives of the Thesis

Enhancing the reliability and durability of PEMFC requires a good understanding of important issues related to operating fuel cells, such as the actual local current density and temperature distributions over the electrode surface and their dynamic characteristics as well as water/heat generations within a PEMFC. This is because the local current density and temperature distributions are closely related to various phenomena that occur inside the cell along with operating conditions, assembly procedures, and flow arrangements. The local current density and temperature gradient inside the PEMFC could be considerably high, especially for a large cell operating at low cell potential. Furthermore, it is well known that the sophisticated multidimensional and two-phase numerical models are capable of predicating many phenomena occurring inside an operational fuel cell but only to a certain limit due to the complexity and the high computational cost. The vast majority of numerical models' validations are limited to the overall polarization (I-V) curve, which is an insufficient approach for the comprehensive assessment of PEMFC models [18]. Thus, in order to improve the integrity of the numerical models, it is highly recommended to validate/compare each phenomenon under investigation by the numerical model with experimental results obtained under similar operating conditions for the same phenomenon. However, the local current density and temperature distributions within a single PEMFC as well as between the fuel cells in a fuel cell stack still require more attention in both the experimental and numerical investigations for better understanding. Therefore, the overall

goal of the present thesis is to conduct an experimental analysis, with emphasis on both current and temperature distributions inside a PEMFC with different flow arrangement scenarios and operating conditions. Specifically, the main objectives of this thesis research are to:

- Measure the local current density distribution over the electrode surface in a single PEMFC for different flow arrangements between the anode and cathode reactant flow streams including co-, counter-, and cross-flow arrangements,
- Investigate the effect of different operating conditions on the local current density in a single PEMFC with each type of flow arrangement,
- Determine the effect of each individual operating parameter on the local current density distribution in order to identify the dominant or limiting factors on the PEMFC performance,
- Investigate the dynamic characteristics of the local current distribution in a single PEMFC at different locations and under various operating conditions,
- Determine the actual temperature distribution within operational PEMFCs,
- Identify the relationship between the local current density and temperature distributions inside PEMFC, and
- Establish benchmark data base of experimental measurements for local current density and temperature distributions for numerical models assessment and industrial fuel cell applications.

To accomplish these objectives, the local current density and temperature profile inside a single PEMFC are investigated experimentally in order to obtain the actual current and temperature distributions (maps) on the surface of the MEA for PEMFCs. Therefore, segmented of both the flow field and current collector plates' technique is used to measure the local current distribution in a PEMFC. While in situ, nondestructive temperature measurements are also conducted to measure the local temperature distribution for the same purpose. The effect of various physical and operating conditions such as flow arrangement

configurations (between inlets and outlets), reactant pressure, air and fuel stoichiometry ratios, and reactant relative humidity is investigated.

This thesis is arranged as follows: Following the introduction, Chapter 2 provides a review of the findings of recent experimental work undertaken to provide an understanding of the local current density and temperature distributions inside operational PEMFCs. The experimental setup and procedures for measuring the local current and temperature profiles within a PEMPFC are explained in Chapter 3. Experimental results are presented and discussed in Chapter 4. In Chapter 5 includes summary of the present experimental work that has been conducted and suggestions for future work.

Chapter 2
Literature Review

A significant progress has already been made in a PEMFC research and development towards its wide commercialization. Significant effort for both experimental and numerical investigations was carried out in the past decade to understand different phenomena occurring inside an operational PEMFC. However, the experimental investigations related to local current density and temperature distributions over the MEA surface of PEMFCs are still requiring further attention because it is critically important. In this chapter, detailed summary of previous experimental effort is summarized and reviewed.

2.1 Current Distribution in PEMFCs

In the last decade, many studies have been conducted to develop and using a variety of novel methods to measure and understand the local current distribution inside PEMFC. The performed studies aimed at accelerating the slow transition from R&D to full scale commercialization of PEMFCs [19]. The uniformity of the current density over the entire active area in operational PEMFC is vital for optimizing the cell performance. Non-uniform current distribution, accompanied with non-uniform water production in the cathode, has significant negative impact on the durability, and reliability of PEMFCs [20]. It is well documented that the overall PEMFC performance is strongly affected by sophisticated interaction of the assembly method, component design, operating conditions as well as the properties and microstructure of fuel cell components [21]. The design and assembly processes include: flow field geometry, reactant flow arrangement, and clamping pressure. Operating conditions include: reactant pressure, cell temperature, relative humidity, and reactant flow rate. However, it has been observed by many studies that the most crucial implication of this complex interaction is an uneven electrochemical reaction rate, which takes place on the surface of the membrane electrode assembly (MEA) active area. As a result, this may lead to low/poor reactions and electro-catalyst utilization, which reduces the overall performance, and accelerates cell aging [22-24]. One of the techniques used to

measure the current distributions in PEMFC is segmented cell. Segmented PEMFCs have been widely adopted as in-situ diagnostic method to study the factors that lead to uneven electrochemical response of the MEA active area. The most commonly used invasive segmented techniques to measure the current distribution in PEMFCs can be classified into three types: (i) printed circuit board (PCB), (ii) resistors network, and (iii) Hall effect sensors.

These three techniques have been used with different MEA active areas and number of segments. The active area is related to the overall cell performance (power density); whereas the number of segments is related to the resolution required for the measurements. Segmented fuel cell technique has been implemented in a PEMFC with various active areas from 1 cm^2 [25], 3 cm^2[26], 5 [27] cm^2, to as large as 370 cm^2 [23] or 578 cm^2 [28]. The number of segments are varied between 3 [29] and 196 [30]. Segmented fuel cell is similar to a conventional fuel cell with the exception that one of the flow fields is divided into identical smaller cells (segments) and separated from each other by electrical insulation materials. Segmentation allows for the current, voltage or impedance to be measured independently of each other. Cleghorn *et al.* [22] made the first attempt to measure the current distribution in a PEMFC by using a printed circuit board (PCB) technique. This method requires segmenting one of the flow field and one current collector plates. In the same year, Stumper *et al*. [31] examined various segmentation methods: partial MEA approach, sub-cells, and current mapping. The partial MEA method employed a partially catalyzed membrane that limited electrochemical reaction to specific areas within the fuel cell plane. Several MEAs with progressively more area catalyzed were used to construct the spatially resolved current distribution. This method gives a rough indication about the electrochemical reaction activity on the MEA surface. Applying the PCB technique requires at least one of current collector plates (between the flow field and end plates) to be replaced by a PCB plate. The PCB substrates are made from epoxy-fiber glass [32] or polytetrafluroethylene PTFE [33]. The segments of the PCB are usually coated by a thin layer of gold to avoid corrosion and reduce

contact resistance [34]. This technique can be used to measure the local current density in PEMFC with a single straight [35] as well as multiple serpentine flow field channels [36].

Using the same principles described in Ref. [23], Brett *et al.* [35] measured the current distribution along the length of a single flow channel in a PEMFC with higher spatial and time-resolution, and the time delay of local currents was observed after inlet reactant gas changes due to the mass transport of gas through gas diffusion layer (GDL). Noponen *et al.*[37, 38] and Hottinen *et al.* [39] embedded gold-plated stainless steel ribs into an insulating plastic slab to create a segmented flow field and studied current distributions under various operating conditions in free-breathing PEMFCs. Noponen *et al.*[40] also used the same technique of segmented flow field/current collector to measure current distribution in a PEMFC. The segmenting flow field approach was also adopted by Mench *et al.* [41, 42], Dong *et al.*[43] and Yang *et al.*[44], simultaneous measurements were made for both the species distribution and current distribution. Also, Ghosh *et al.*[45] developed a semi-segmented current collector method that has an advantage of measuring the current distributions in a single cell as well as in a stack at any desired position. Freunberger *et al.* [25, 46] measured the potential distribution at the interface between GDL and catalyst layer (CL), and realized sub-millimeter resolution of current distribution measurement. Their research provided useful insight into mass transport issues in land and channel areas of the flow field plate. The current distribution by PCB technique has been measured on both the anode [22, 47] and the cathode sides [48, 49] in PEMFCs.

The sub-cell method involves creating one or more small electrically isolated islands within the cell. The processes of this technique start by punching out several circular pieces of GDL, and replacing them with smaller ones electrically insulated from each other. Thus, the local current density can be measured independently at specific regions of the cell. The sub-cell method can provide valuable information about the current density at very small areas. But the manufacturing of the special MEA and flow field plate is complex, and care should be taken during the assembly of the cell. The sub-cell approach was then modified and used by Rajalakshmi *et al.*[23], Wu *et al.* [50] and Liu *et al.* [51], with more complicated

cell designs to study current distributions in PEMFCs. Bender *et al.* [52] refined the cell segmentation technique by segmenting the entire anode side of a PEMFC including the electrode, flow field, and current collector plate. Care was taken to calibrate contact resistances between the cell components, and Hall sensors were used for low impedance ex-situ current measurements. In the current-mapping technique, a network of passive graphite resistors is placed between the flow-field plate and the current collector plate in order to measure the local current distribution. This technique does not require a major modification for the MEA or flow field plate. Also it can be used to monitor time dependent phenomena such as response to a sudden change in operating conditions. However, it is not easy to be implementing in fuel cell assembly since the resistance would be subjected to high compression force. Another technique to measure the current distribution is based on magnetic effects. Wieser *et al.*[28] was the first to implement this technique using a magnetic loop array embedded in the current collector plate to measure current distribution in PEMFC. A Hall effect sensor is a current transducer with four identical terminals: two of them for connections to a source of current and two for the measurement of voltage across each terminal [53]. When a Hall effect senor is used, the density of the magnetic field (flux) flow through the Hall element determines the output voltage of the sensor. The output voltage is proportional to the current collected by the segment. Two Hall effect sensors are used for current measurement purpose namely open loop [52] and closed loop [54]. Geiger *et al.* [55] described a new magnetic loop array with closed-loop hall effect current sensors to measure current distribution in a PEMFC. The same authors indicted that the closed loop Hall effect sensors are more accurate and linear as well as easier to calibrate due to their lower sensitivity to temperature.

Wilkinson *et al.*[56] attempted to determine the current distribution indirectly by measuring temperature distributions based on the correlation of local temperature with local current density. Hakenjos *et al.* [57, 58] and Hogarth *et al.* [59] designed a PEMFC allowing simultaneous evaluation of current, temperature and water distribution in the cell under various operating conditions. The cell had a segmented anode flow field for current

distribution measurements. The endplate of the cathode flow field was made of an optical window, which allowed infrared thermography and optical surveillance of water droplets and flow field flooding. Wang and Liu [60] developed a simple approach to directly measure the current densities under the channel and under the land separately in PEMFCs with a parallel flow field. The cathode catalyst layer was designed to have either the area under the land or the area under the channel loaded with catalyst. Such a design produced separate measurements of current densities under the land and the channel. Higier and Liu [61] conducted an optimization study of the current density distribution under the land and channel areas on a variety of serpentine flow field geometries and operating conditions. Sun *et al.* [62] established the current measurement gasket technique. The gasket is made from an epoxy resin and glass cloth substrate where 23 gold-plated copper rectangles placed in direct contact with 23 single channel flow field ribs of the cathode side. The main advantage of this technique is that no major modification is required to the fuel cell construction. The authors examined the effect of the dynamic characteristics of different parameters, including humidification temperature of the reactant gases, operating temperature, and operating backpressure, on the local dynamic responses. However, the current density profile values were not obtained instantaneously, rather recorded for one or two minutes for each current values. Hsieh and Huang [27] conducted time-dependent in-situ measurements of local current and water distributions for micro-PEMFCs (5 cm^2) with four different flow channels (mesh, parallel, serpentine, and interdigitated) using the segmented flow field plate approach. This work mainly examined the effect of membrane water content on current distribution. The author studied the dynamic response of the cell based on changing the load whereas the other main operating conditions were fixed. Natarajan and Nguyen [63, 64] investigated the effect of air flow rate and cell operating temperature on the spatial and temporal current density distribution along a single gas channel PEMFC using a segmented electrode/current collector. Strickland *et al.* [47] examined the local (I-V) curves along the flow channel in parallel flow field at steady-state conditions. Further, the authors also briefly discussed the transit power distribution at four instances of time with and without the presence of an

electro-osmotic (EO) pump for water removal. Meng *et al.* [65] conducted a brief investigation about the dynamic phenomena of the local current density response with various air volume flow rate.

Several non-invasive techniques to measure the local current density in operating PEMFCs have been introduced, such that no physical modifications are made to any of the fuel cell components. Basically, it requires sophisticated magnetic field measurement apparatus. Hauer *et al.* [66] introduced a magnetic inducted tomography approach to indirectly measure the current density. 2D and 3D magnetic field sensors are used for this purpose. A sensor scanned the upper section while the other one scanned the lower part of the cell. The experimental set-up allowed four-axis scan measurements that lead to obtain a map for the current distribution in the fuel cell.

2.2 Temperature Distribution in PEMFCs

PEMFC generates waste heat and useful electrical power output. Around 50% of the chemical energy available in the fuel is converted to electrical power, and the rest is waste heat [4]. The main sources of heat generation in a PEMFC are the entropic heat of the reactions, the irreversibility of the electrochemical reactions, water evaporation /condensation, and ohmic resistance. The polymer membrane is very sensitive to temperature variations, and the hydration of the membrane depends strongly on the temperature of the cell because the water vapor saturation pressure is an exponentially function of temperature [67]. Thus, understanding distribution of the temperature inside the fuel cell is essential to the development of proper heat management, which would improve the reliability and durability of the fuel cell.

To date, a limited work has been described in the literature with respect to the experimental field related to temperature distribution and heat generation in a PEMFC. Most of the existing numerical models have ignored the temperature gradient across the fuel cell. Vie *et al.* [68] were the first group to measure the temperature profile close to the electrodes and perpendicular to the membrane surface in a PEMFC. The results showed that the

temperature gradient at the interface between each set of two layers, such as the membrane and backing diffusion layers, is high enough to be considered. Mench and Davis [69] attempted to measure the temperature distribution at different positions in a multilayered membrane by embedding eight micro-thermocouples. This kind of experiment is complex to be conducted due to the PEMFC assembly configuration. It is also difficult to prevent the destruction of the thermocouple when the fuel cell is clamped. Therefore, only three thermocouples provided reliable temperature values. Aziz and Alkasab [70] monitored the temperature distribution along the cooling flow channel of a phosphoric acid fuel cell stack (PAFC) by arranging the thermocouples in multi-locations at the end plates. The experimental results were used to derive a mathematical model for the overall heat transfer coefficient. Adzic *et al.* [71] developed a technique for designing a thin, flat micro-thermocouple for measuring temperature at the cathode side of a planar solid oxide fuel cell. The main benefit of this experimental work is that in addition to the mapping the temperature at the cathode, hot spots were also located.

In recent years, imaging (visualization) techniques have been used to measure the temperature distribution along the active area at the anode side of a PEMFC. An infrared (IR) camera is used in this technique. Wang *et al.* [72] developed a fuel cell with an optical window fabricated from barium fluoride, which is transparent to the IR light at the anode side. The IR imaging allows the temperature at specific points along the flow channel to be measured. Shimoi *et al.* [73] applied the thermography technique for visualizing an operating test cell in a manner similar to that explained by Wang *et al.* [72]. In their experiment, they visualized the two-dimensional membrane temperature field of a PEMFC under different operating conditions. Part of the cell separator was replaced with an optical window for the thermography measurement. The visualization results are helpful for understanding the physics of several transport phenomena that occur in the PEMFC, including water flooding and local hot spots. A novel method was used by Chi-Yuan *et al*. [74] to measure the temperature inside the fuel cell. An array of micro-temperature sensors was set up on the rib of a channel in the stainless steel substrate. However, the authors focused on the fabrication

processes of the array of sensors on the metallic flow field plate rather than on the temperature distribution within the fuel cell. Using the same principles, a group at the Institute for Fuel Cell Innovation-Canada [56] applied 19 thermocouples to measure the temperature distribution inside the PEMFC. In this study, thermocouples were located in the shoulder (rib) of the flow channel of the flow field plate in direct contact with the GDL surface, and the temperature data was taken at different locations along the shoulder of the flow channel. The main problem with this experiment arises from the weakness of the micro-thermocouples; many thermocouples were no longer functional after integration into the anode and cathode plates. Only several thermocouples at the anode side and just one thermocouple at the cathode side were connected to the data acquisition system. Fabian *et al.* [75] also conducted micro-sensors to monitor temperature distribution, partial oxygen pressure, and relative humidity in the mass transport layer immediately above the planar, horizontal cathode of a PEMFC driven by natural convection. This work demonstrated the substantial changes in temperature distribution and reaction species concentration with increased current density. Lee *et al.* [76] conducted in situ measurement of the temperature distribution across the fuel cell. He found that the maximum temperature occur at the cathode catalysts layer. David *et al.* [77] conducted simultaneous measurements of temperature and relative humidity in an operating PEMFC using optical fiber sensors only at different cell potentials. Hakenjos *et al.* [57] applied infrared thermograph (IR) to measure the temperature and current distribution on the active cathode area of a PEMFC. A digital camera allowed optical surveillance of the condensed water within the flow field. The authors concluded that a low air flow rate results in poor water removal from the cathode flow channels. In other words, flooding can be minimized or completely eliminated with a higher stoichiometry flow ratio. The main drawback of these types of experiments is that they require major modifications to the fuel cell design and component material. Hence, the gas channels are completely broken through and replaced by a transparent window in order to visualize the gas diffusion layer.

Tuber *et al.* [78] attempted to visualize the two-phase flow in the flow channel using a transparent test cell made of Plexiglass. This experiment was performed at room temperature (23-30 °C) and low current density (300 mA/cm^2) conditions. The author concluded that the clogging of gas channels by liquid water results in a major decrease in cell performance and that, at such low operating conditions a hydrophilic GDL has a positive effect on cell performance. This conclusion can be valid only for PEMFCs operated at room temperature and a low current density. In the case of PEMFCs operated at higher temperatures and higher current densities (e.g. 1 A/cm^2), it is very challenging to a visualize two-phase flow and liquid water dynamics, due to condensation of water on the surface of the optical widow and the resulting severe fogging [57]. Experimental observations demonstrated that the maximum current density is limited by restricted limitation in the cathode mass transport attributed to excess liquid water [79].

Neutron radiography (NR) is another diagnostic technique that provides reliable images of water formation and distribution in a fuel cell [80]. The main idea of using NR in PEMFC is the neutrons, sensitivity to hydrogen-containing compounds such as water [81-83]. Bellows *et al.* [81] were the first group to attempt to measure the water content within the polymer membrane using NR. However, dry thick membranes of 500μm, which are not practical in a PEMFC, were prepared in order to overcome the limitations in spatial resolution of NR. Satija *et al.* [82] used specially designed NR imaging to monitor the water flow within the PEMFC. The neutron beam passes through the operational PEMFC and then is converted to a beam of light focused on a Charge-Coupled Camera Device CCD.

2.3 Summary of the Literature Review

It is clear that a significant effort has been spent on developing methods for current distribution measurements. Despite its importance, few systematic studies have been conducted experimentally to investigate the effect of the flow arrangement between the anode and cathode streams (co-, cross-, and counter-flow) under different operating

conditions on the local current distribution in PEMFCs. Moreover, the dynamic behavior of the local current density over the active area of PEMFC still requires further investigations.

A comprehensive review of the experimental studies focusing on PEMFCs reveals limited studies related to the non-isothermal operating of PEMFCs. In fact, most published studies have not provided a complete temperature distribution map within either a real single PEMFC or a complete fuel cell stack. Furthermore, most of the experiments have been conducted using imaging (visualization) or infrared techniques (IR). However, using these techniques is problematic because fuel cell components are not at all transparent. Major modifications to the fuel cell design and component materials are thus required, an optical window made of plexiglass or glass must be installed. These materials do not represent the real fuel cell environment since they are not conductive materials. Fogging and water condensation on the surface of the optical window are also a serious problem for visualization, especially at the cathode side. Consequently, measurement of temperature at the cathode side has been ignored in most of the literature. Experimental set-ups with the capabilities to measure the local current density and temperature distributions in PEMFCs were developed in the 20/20 Laboratory for Fuel Cell and Green Energy RD&D at the University of Waterloo by I. Alaefour *et al.* [84-92].

Chapter 3
Experimental Set-up, Apparatus, and Procedures

Detailed knowledge of both local current density and temperature distributions over the membrane electrode assembly (MEA) surface is helpful for improving the reliability, durability, and the overall performance of the cell as explained in Chapters 1 and 2. Although different techniques have been applied to measure the local current distribution under the steady operating conditions inside PEMFCs, measurements of current distributions during the dynamic loading processes are not well established. Moreover, the effect of various flow arrangements (co-, counter-, and cross-flow) under different operating conditions on cell performance requires further investigations.

In this chapter, special test cells with three serpentine flow channels and straight flow channels with active areas of 40 cm^2 and 50 cm^2, respectively, are designed and fabricated in-house. In-situ mapping of both local current density and temperature distributions is performed on the fabricated cells. First, this chapter will describe the method used to measure the local current density. This method involves segmenting both the flow field and current collector plates on one side of the PEMFC into sixteen segments. The dynamic characteristics of the local current density over the electrode surface are also investigated using the same segmented technique. Secondly, an in-situ non-destructive, temperature measurement technique for local temperature distribution inside a single PEMFC with multiple straight flow channels is described. This technique uses micro-thermocouples embedded in the arrays of blind holes along the flow channel. Temperature distribution is obtained for two directions (parallel and normal to direction of the reactant flow in the flow channel field) for both the cathode and anode sides of the cell. Finally, combined current and temperature experimental measurements are conducted to obtain the relationship between the local current density and temperature distributions in PEMFC. The local current density and temperature distributions are measured on the anode and cathode side, respectively.

This chapter describes the cell components, assembly, and test procedures. The operating principles of testing apparatuses such as a Fuel Cell Automated Test Stations (FCATS-S800 and G20) and data acquisition devices are explained. In addition to the description of the experimental procedures, the uncertainly analysis of the collected experimental data are discussed in this chapter.

3.1 Apparatus

3.1.1 Fuel Cell Testing Stations

All the experimental investigations related to the local current distributions are carried out using the Fuel Cell Automated Test Station (FCATS-S800), which is manufactured by Hydrogenics Inc [93]. However, the measurements related to the local temperature distributions in PEMFC with straight channels are conducted using FCATS^{TM} G20 Test Station manufactured by Green-Light Innovation Corp. [94]. Figure 3.1 shows the FCATS unit available in the 20/20 Laboratory for Fuel Cells and Green Energy RD & D. The FCATS is a fully integrated fuel cell test station designed to control fuel cell key operating conditions, such as temperature, pressure, relative humidity, and the stoichiometry of the reactant gases on both the anode and cathode sides [95]. The FCATS also has an onboard computer-based control and data acquisition system controlled and monitored by specially developed software for this purpose. This system also monitors and maintains safe operating conditions for the fuel cell. The oxidant air and hydrogen fuel gases are heated and humidified before they are supplied to the fuel cell. The reactants are supplied from compressed cylinders of hydrogen, air, and nitrogen. Nitrogen gas is used for purging the reactant gases from the fuel cell and cleaning up the formed products of the electrochemical reaction (water) during the start-up and shutdown processes. In the FCATS, the de-ionized (DI) water method is used to produce extremely pure water, which is needed to generate steam for humidifying the reactants. Regulating the dew point temperature with respect to inlet temperatures controls the degree of humidification of the reactant gases. The load box is

an integral part of the FCATS-S800 for measuring integrated voltage and current. It is the SDI 1043 model, which is developed and manufactured by TDI transistor Device, USA [93].

(a)

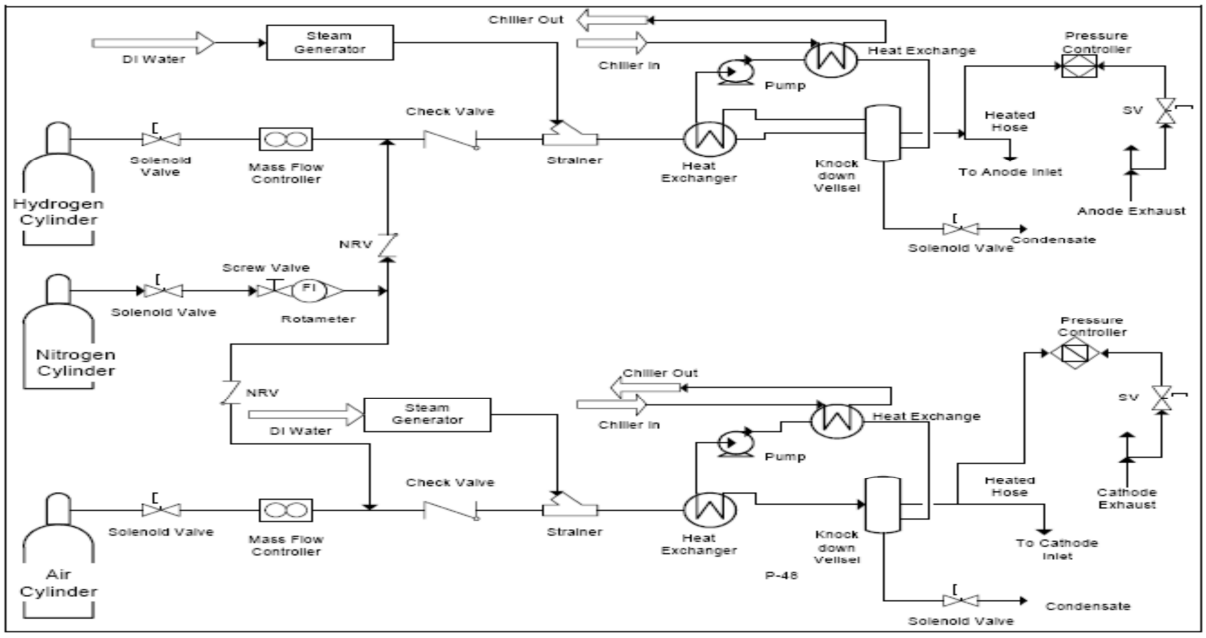

(b)

Figure 3.1: (a) Fuel cell automated test station (FCATS, S800) and (b) FCATS gas supply system schematic [93].

The loading box specifications are for 50 V, 400 A, or 2 kW. The most important function of the integrated system is the load follow and equilibrium flow modes for the cell test operation which allow for the inlet flow rate of both reactants to be controlled by the required current or voltage, respectively, according to the specified stoichiometry. The load follow mode is an ideal approach to generate consistent cell voltage values as a function of current load (I-V curve) at fixed stoichiometry of both reactants [96].

3.1.2 Data Acquisition System

A segmented technique for both flow field and current collector plates is used to measure the local current distribution inside PEMFC as well as temperature distribution with PC-based data acquisition systems (DAQ). In this experiment, National Instruments SCXI devices are used as plug-in DAQ boards. The system hardware consists of the following pieces of equipment as shown in Figure 3.2. An SCXI-1000 chassis consists of four slots house and the other modules providing the power and controlling the SCXIbus. A SCXI-1600 USB digitizer module is a high-performance plug-and-play USB device used for direct connection between the computers and the SXCI systems. It receives analog signals from other SCXI modules to acquire up to 128 analog signals from thermocouples, current sources, and voltage sources. The SCXI-1102 is a 32-channel thermocouple amplifier module. The copper wires are connected to the SCXI-1102 via the SCXI-1300 terminal block which measures the voltage drop across known resistance, while thermocouples “T- type” are connected to SCXI-1102 through SCXI-1303 terminal block.

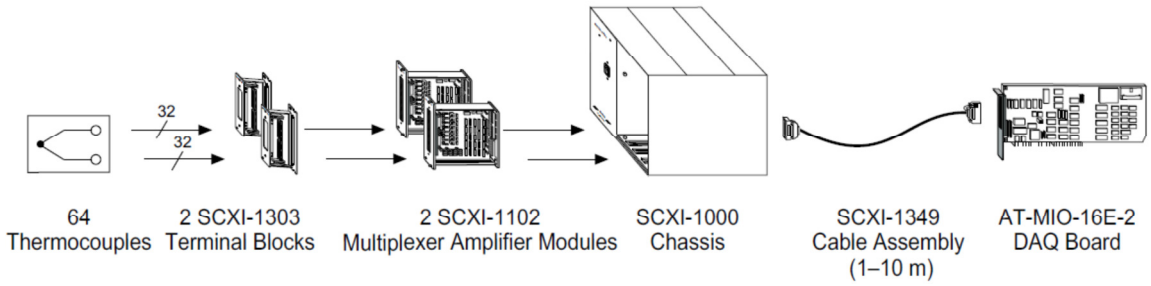

Figure 3.2: Data acquisition system [97].

3.2 Local Current Density Distribution Measurements

In this research, the segmented flow field plate and PCB technique is adapted to measure the current distribution due to its advantages over other methods mentioned in Chapter 2. The advantages include low cost, simplicity of implementation, and flexibility during assembling and dissembling of the test cells. Special test cells with three serpentine flow channels are designed in order to conduct in-situ mapping of the local current distribution over the electrode surface for various reactant flow configurations under different operating conditions.

3.2.1 Fuel Cell Components

Figure 3.3 shows a single PEMFC with an active area of 40 cm^2 used in the present study. All PEMFC components are designed and fabricated in-house except that the membrane and GDL, which are provided by SolviCore for fuel cell technologies [85]. Other main components include one conventional flow field plate, two endplates, a conventional copper current collector plate, printed circuit board (PCB) plate, and two silicon rubber gaskets. At the anode and cathode sides of each cell, the flow field and current collector plates are isolated from the aluminum endplates by thick rubber sheets. Each flow field plate for the anode/cathode has one inlet and one outlet. The cell assembly is subjected to uniform compression controlled by either hydraulic press or adjustable torque wrench.

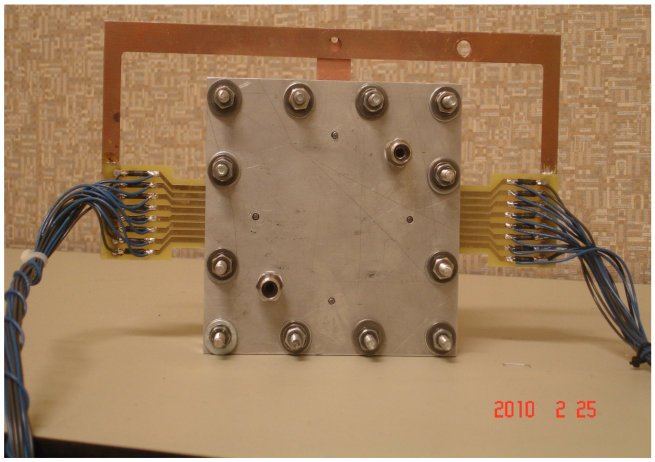

Figure 3.3: Fuel cell assembly to measure the current distribution.

3.2.2 Membrane Electrode Assembly (MEA)

The membrane-electrode assembly (MEA) used contains Nafion^{TM} 112 membrane with an approximate thickness of 53 µm, and supported catalysts with a platinum loading of 0.5 mg/cm^2 for both the anode and cathode sides as illustrated in Figure 3.4. The carbon paper gas cdiffusion layer has a thickness of 230 µm and is coated with 30% PTFE by weight as shown in Figure 3.5 (a). Scanning electron microscope (SEM) image are captured for GDL layers as illustrates in Figure 3.5 (b). Further information regarding the PEMFCs used in the present study is given in Table 3.1.

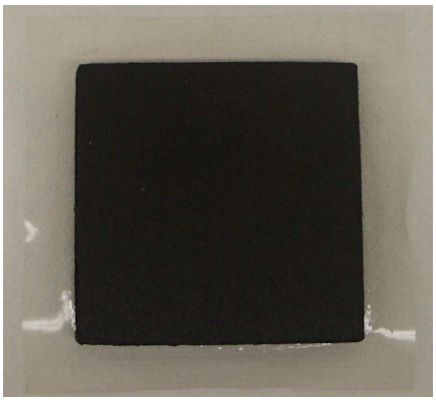

Figure 3.4: Membrane electrode assembly with 3 layers construction.

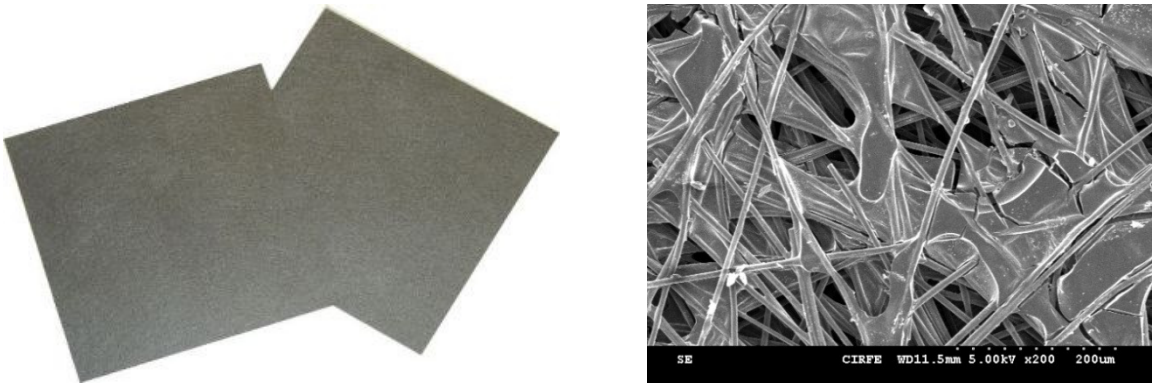

(a) (b)

Figure 3.5: (a) Gas diffusion layers (GDLs) and (b) SEM image of GDL carbon fiber layer 200 times magnification.

3.2.3 Conventional Flow Field Plate

Figure 3.6 shows the structure of conventional/original design of the flow field plate made of graphite for measuring the distribution of the local current density. Both the conventional and segmented flow field plates are machined from resin impregnated graphite sheets, (grade FU 4369 HT). The graphite material is selected due to its desirable properties even though it is brittle as discussed in the first chapter (section 1.3.4). For the local current measurements, the flow field consist of three serpentine channel layouts, which is 6 mm thick. The channel and rib dimensions are equally designed with a cross section of 1×1 mm for each. The serpentine flow channel may result in a considerable pressure drop along the flow channels that can provide a better water management inside the fuel cell. However, this improvement is usually associated with a large parasitic power load.

The serpentine flow field channel eliminates the possibility of forming areas of stagnant flow within the flow field channels. This is a common problem associated with other channel designs, such as the pin-type or parallel flow fields. The lack of flow stagnation within the flow channel reduces liquid water build-up as all water droplets are pushed along the channel to the flow field outlet [15]. Further, the noticeable pressure drop associated with the serpentine flow layout can help to remove the product water in vapour form. The correlation between the molar flow rate of water vapour and reactant gas is given in equation (3.1) [15]. This equation suggests that as total pressure increases, the capacity for vapour flow rate decreases.

$$\frac{\dot{N}_{vap}}{\dot{N}_{gas}} = \frac{P_{vap}}{P_{gas}} = \frac{P_{vap}}{P_{Total} - P_{vap}} \tag{3.1}$$

Table 3.1 summarizes the dimensions and flow parameters for the flow field channels used to measure the local current density over MEA surface of PEMFC. However, preliminary design calculations are preformed in order to estimate some important paramters related to the flow field desgin. For example the channle length and the pressure drop along the flow channeles can be estimated as follows:

In the flow channels, Reynolds number is conventionally defined as:

$$R_{eD_h} = \frac{inerial\ force}{Viscosity} = \frac{\rho U D_h}{\mu} \tag{3.2}$$

Where ρ is the density, μ is the viscosity of the gas flowing in the flow channles, and U is the flow stream velocity in the channels,wich can be determined as:

$$U = \frac{\dot{m}}{\rho A_C} \tag{3.3}$$

where $\dot{m}$ is the mass flow rate in the flow channels, and D_h is the hydraulic diameter of the flow channel. The D_h for rectangular channels is calculated as:

$$D_h = \frac{4A_C}{\mathrm{W_P}} \tag{3.4}$$

where A_C is the cross section area of flow channel, which is determined as:

$$A_C = w \times h \tag{3.5}$$

where w and h are the width and high of the flow channle, respectively.

The wetted perimeter is defend as:

$$W_P = 2 \times (w + \mathrm{h}) \tag{3.6}$$

To ensure the flow remains in the laminar regime, the maximum permissible Reynolds number for the laminar flow inside the flow channel should be maintained at 2000. However, the minimum Reynolds number to provide sufficient flow convection should be in the order of 100 or higher. In this case, the hydrodynamic entrance length is defended as:

$$L_e \approx 0.06 \times R_e \times D_h \tag{3.7}$$

Since the cross-sectional area of the flow channel is typically small compar to the length, the entrance region can be neglected. The pressure drop of flow along the flow channel length is expressed as:

$$\Delta p = f \frac{L}{D_h} \frac{\rho U^2}{2} \tag{3.8}$$

Where f is the friction factor for fully developed laminar flow in squared flow channel [4]:

$$f = \frac{56.91}{Re} \tag{3.9}$$

Condering that w=h (width = high) and substitut the equation (3.8) into equation (3.7). The pressure drop is reexpressed as:

$$\Delta p = 28.455 \left(\frac{\mu \dot{m}}{\rho}\right) \left(\frac{L}{w^4}\right) \tag{3.10}$$

Thus, the flow channel length can be determined for square cross-sectional as:

(3.11)

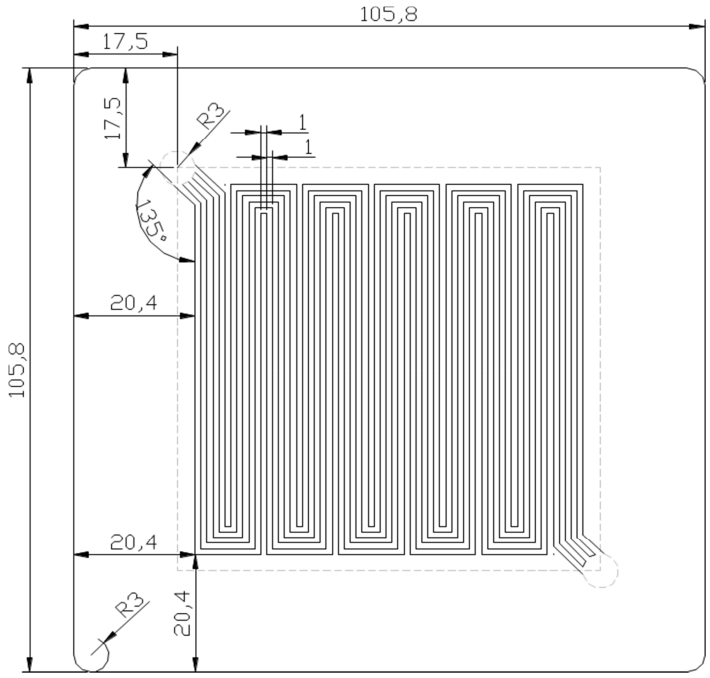

(a)

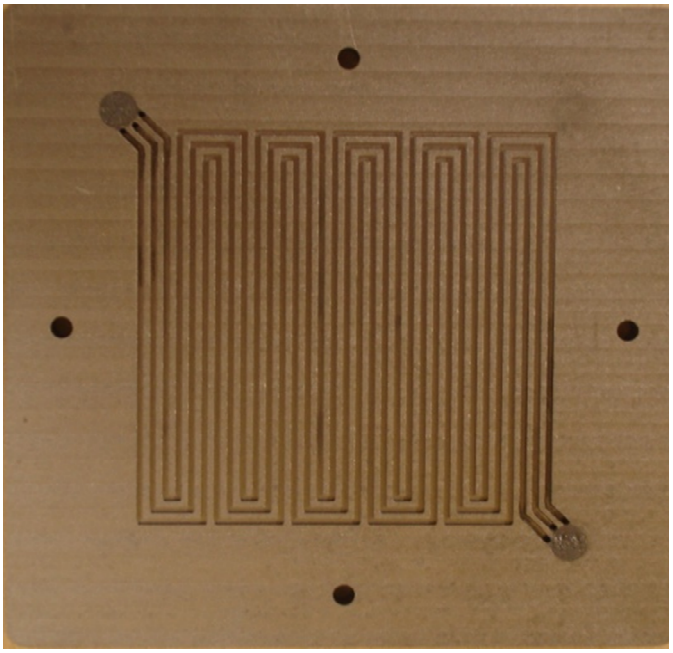

(b)

Figure 3.6: Conventional flow field plate design (a) illustration of the serpentine flow channels, and (b) picture of the designed flow channels machined on flow field plate.

3.2.4 Endplates

Figure 3.7 shows the present design of the aluminum endplate. The dimensions of the end plate are 145×145×13 mm. Four alignment holes are identical to those in flow field and electrical collector plates. Sixteen clearance holes also are machined along the four edges of the plate, four to each side, as illustrated in Figure 3.7. The thickness of the plate should be sufficient to accommodate the shear stress at the bolts without deflection because excess deflection of the end plates can result in poor sealing of the PEMFC. The desired physical properties of common materials which can be used for the end plate are as follows [98]: low density, excellent electrochemical stability, high electrical insulation, easy to machine, and high mechanical strength and stiffness. Therefore, Aluminum alloy 6061 is used to meet the functional requirements of the endplates, high strength (125 MPa tensile strength), high thermal conductivity (180 W/m.K), and it is relatively cheap compared to other aluminum alloys. The most common used materials are made of aluminum, titanium, and stainless steel alloys.

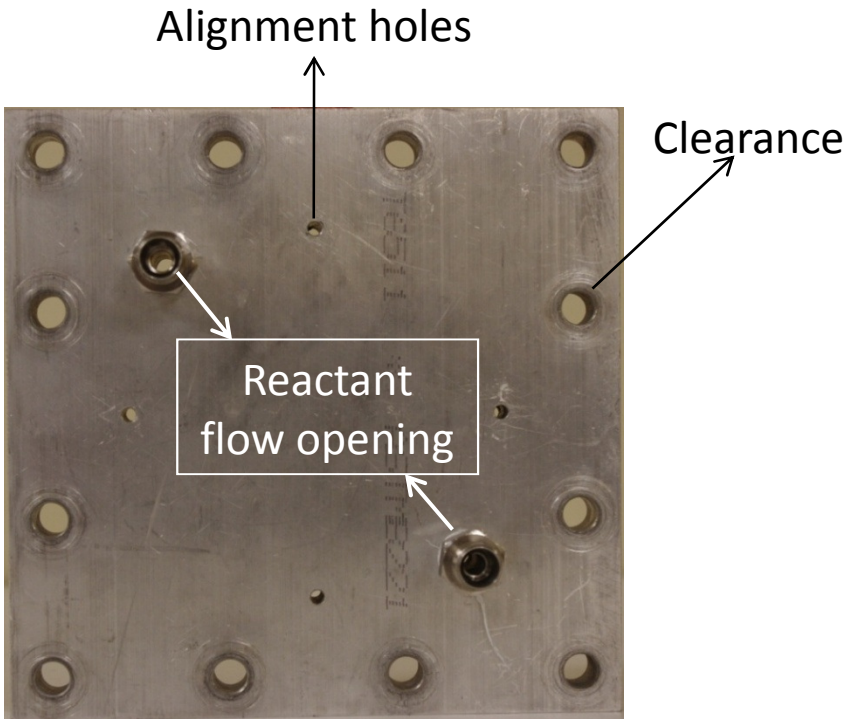

Figure 3.7: Conventional endplate.

3.2.5 Conventional Current Collector

One of the copper electrical/current collector plates is shown in Figure 3.8. The plates are designed in house and fabricated in the Engineering Machine Shop. It made from C15720 copper, which contents 99.6 wt% (weight) copper. The copper provides both excellent electrical and thermal conductivities with 89 S/m and 353 W/m.K at 20 ^{o}C, respectively. The current collector is fastened to the endplate via thick sheet of rubber. The rubber gasket is applied between these two plates to isolate the plates electrically while providing proper sealing for the inlet and outlet flow reactants. Practically, rings of silicon were usually used to seal the reactant flow between the current collector and the flow field plate. However, inserting these rings between the flow field plate and current collector usually associated with a negative impact on the overall cell performance since they increase the electrical resistance between the cell's components. To overcome this problem, a sheet of raw carbon paper is placed between the flow field channel and endplate plates to provide better contact in order to reduce the electrical resistance. The total area of the current collector is 120×120 mm; an extended terminal is made on one side for the electrical load box connection. Two holes are drilled on opposite corners for the reactant supply, and four small holes were drilled for locating dowel pins.

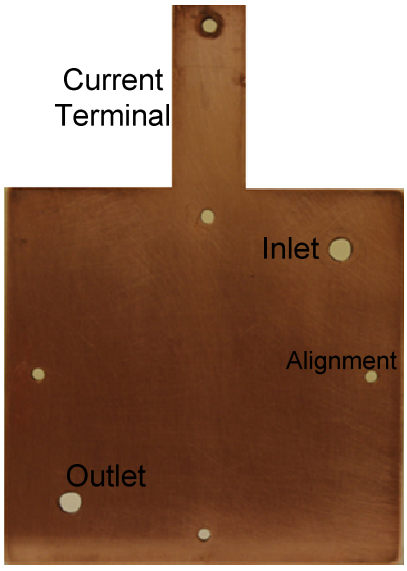

Figure 3.8: Conventional current collector plate.

3.2.6 Segmented Flow Field Plate

In the present study, one of the flow field and the current collector plates are segmented into a 4×4 squared array. The MEA is not segmented because segmenting the MEA is not only a complicated process but also is a major modification to the standard fuel cells [37]. Figure 3.9 illustrates the fabrication processes of the segmented flow field plate start with machining connected grooves of 1 mm width × 4 mm deep into a graphite block of 105 × 105 × 6.5 mm. The surface of the graphite is covered with a special plastic material to prevent contamination of the electrical insulation material by the graphite powder. Then, the grooves are filled with an electrically insulating epoxy that also has sufficiently strong mechanical strength to withstand the compression force for the cell assembly. After curing the epoxy material at room temperature for 24 hours, the surface is polished to become clean and smooth. The back side of the graphite block is milled to a thickness of 3 mm, leaving sixteen electrically isolated segments. The serpentine flow field pattern is then milled into the front of the block as shown in Figures 3.9 and 3.10. The channel and land dimensions are made equal with a cross section of 1×1 mm for each of them. Electrical resistance measurements are made before and after each test to ensure that the segments on the flow field are still insulated from each other. A digital multimeter (Agilent #34401A) from Agilent technology is used to check the electrical insulation between the sixteen segments.

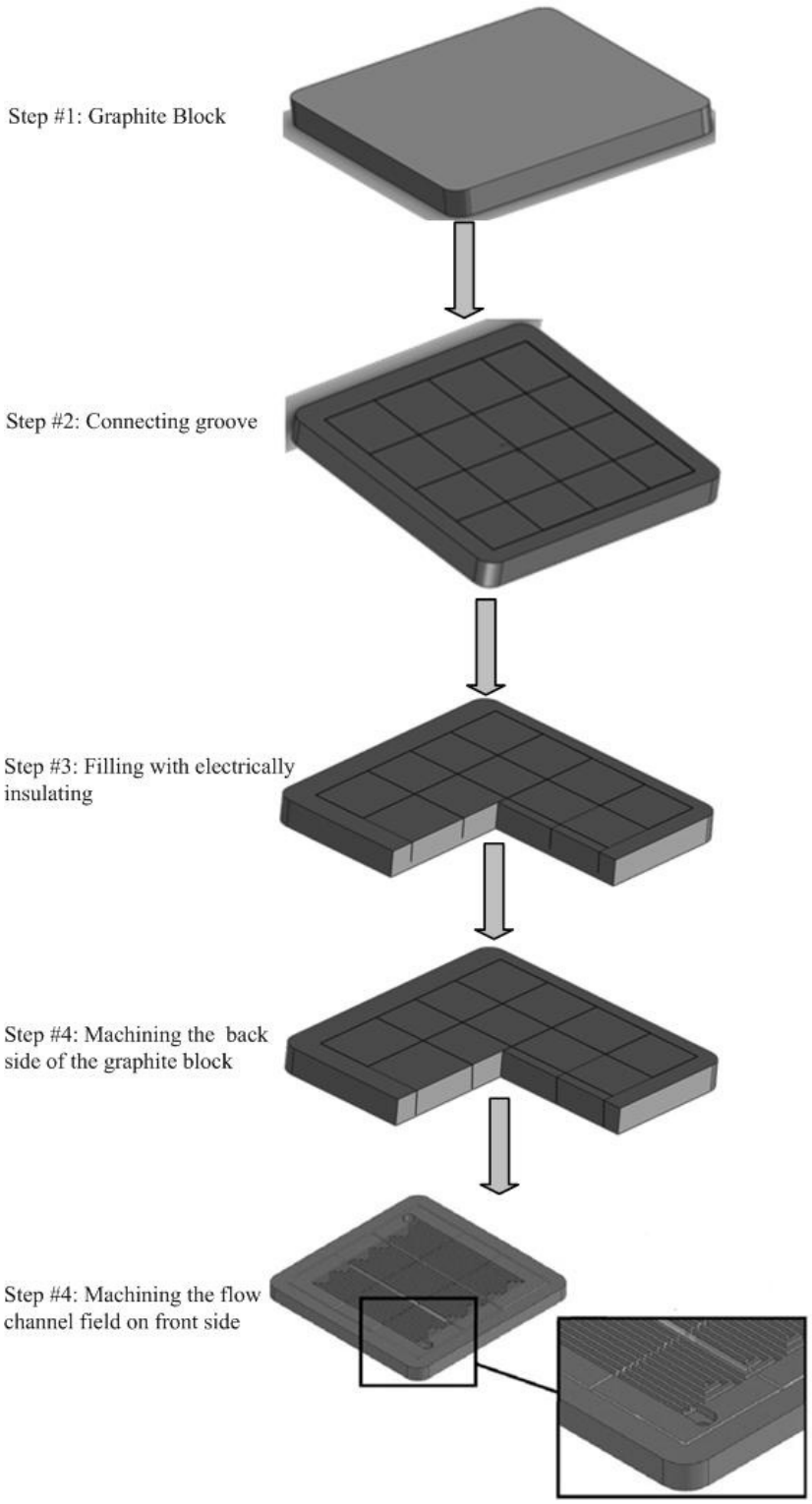

Figure 3.9: Fabrication processes of segmented flow field plate.

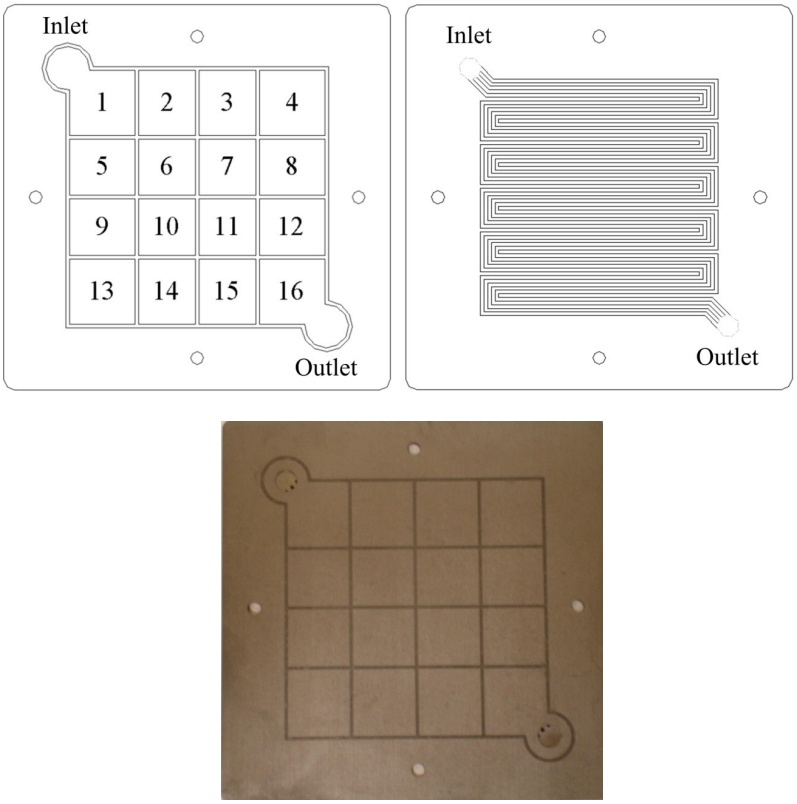

Figure 3.10: Front and back views of the segmented flow field plate with serpentine flow field channels machined on the surface.

3.2.7 Printed Circuit Board (PCB)

To collect spatial current distributions, a segmented current collector made of printed circuit board (PCB) is designed and manufactured as shown in Figure 3.11. Sixteen segments of 40µm thick copper pads with the dimension of 15.5 mm × 15.5 mm are printed in a 4×4 array on the top side of the PCB. Twenty five small through-vias connect each pad to a printed lead on the backside of the board; and these leads electrically join each segment to a connector array (header) for connection to the data acquisition system. The copper pads and leads are electroplated with nickel diffusion barrier and 1 µm gold layer to minimize the electrical contact resistances. PCB was designed in house and manufactured by AP Circuits™, Calgary, AB, Canada. PCB with the gold-plated is used in lieu of the

conventional current collector plate in direct contact with the back-side of the segmented. A silicon rubber gasket separates the current collector leads from the aluminum endplate to prevent both gas leakage and electrical short circuit. The current from the 16 measuring segments are conducted out of the fuel cell from the sides. The current collected from each segment is connected directly to a small and high-precision resistor (0.1 Ω) through a copper pad where the voltage drop across the resistance is measured; then the average current density over each of the 16 segments is determined by the measured voltage drop across the resistor of known resistance. These measurements are controlled through a special Labveiw code developed in house. Further information regarding the PEMFCs used in the present study is given in Table 3.1.

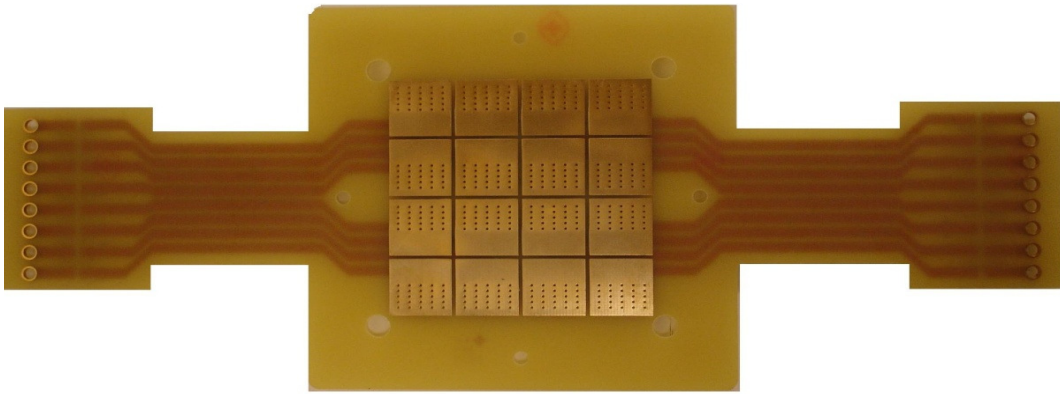

(a) Front view

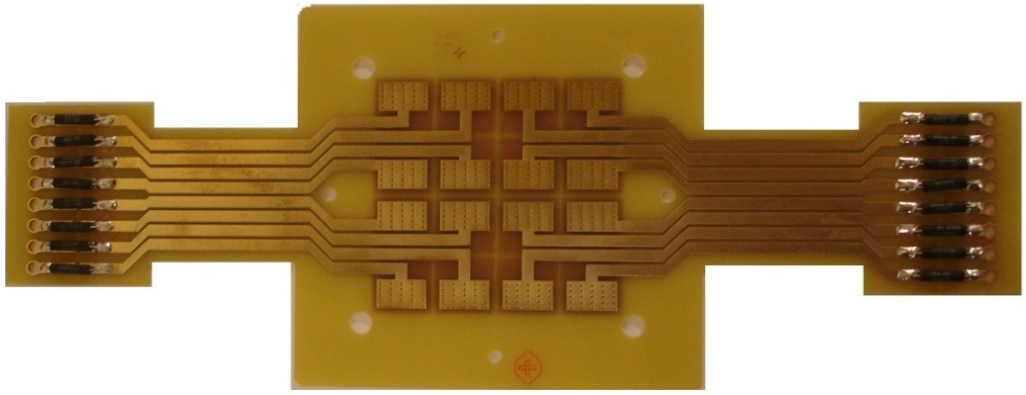

(b) Back view

Figure 3.11: Current distribution measurement device used in the present study (a) front and (b) back view of the printed circuit board (PCB) for the current measurement.

Table 3.1: Cell properties

Parameter	Values
Membrane (Nafion 112)	
Thickness	50 µm
Catalyst layer (for anode and cathode)	
Platinum loading	0.5 mg/cm^2
Active reaction area (square)	40 cm^2
Gas diffusion layer (same for anode and cathode, carbon paper, uncompressed)	
Thickness	230 µm
Porosity	0.75
Polytetrafluoroethylene (PTFE) loading by weight	30%
Gasket (silicon rubber, uncompressed)	
Thickness	254 µm
Flow channel layout (same for anode and cathode, three serpentines, co-, counter, and counter-flow arrangements)	
Number of flow channels in parallel	3
Channel width	1mm
Channel depth	1 mm
Land width	1 mm
Segmented flow field plate (graphite)	
Number of segments	16
Thickness	3 mm
Conventional Flow field plate (graphite)	
Thickness	6.5 mm
Segmented current collector (copper pads printed on both sides of circuit board)	
Number of segments	16
Thickness/in-plane area of circuit board (electrically insulating, square)	1.6 mm
Thickness of gold coating layer on copper pad	1 µm
Conventional current collector (copper, with thermocouple holes corresponding to flow field plate)	
Thickness	3.2 mm
Anode and cathode end plates (aluminum alloy, cathode plate with thermal couple holes corresponding to flow field plate)	
Thickness	13 mm
Dimensions	120×120 cm^2
Machining of cell components	
Tolerance	±25.4 µm

3.3 Temperature Distribution in PEMFC with Multiple Straight Flow Channels

Several techniques can be implemented to measure the temperature distribution in fuel cells as discussed in the literature review chapter. The most common techniques are thermocouples, infrared thermal imaging, and thermochormatic liquid crystals. However, the most accurate and practical method for measuring the temperature distribution within a PEMFC cell is thermocouples because of their desirable features, such as their simple configuration, high accuracy (0.1 °C), fast response, and wide measurement range. Thermocouples are widely used as point temperature measurement devices, which consist of two wires of different materials joined at one end. When the two junctions are placed at different temperatures, a small electrical current is generated, which leads to a small voltage drop. This voltage drop is a function of the temperature differences between the two junctions.

3.3.1 Fuel Cell Components

Generally, the fuel cell used to measure the local temperature distribution is almost identical to the cell used to measure the local current distribution. Figure 3.12 shows the structure of specially designed flow field plates made of graphite for measuring the distribution of the temperature on; i) at the top surface of MEA, ii) along the flow channel and its shoulder in two principal directions, parallel and normal to the direction of the flow channel, and iii) both the cathode and anode sides. The flow fields consist of multi-straight (parallel) channels, which are machined into a 6mm thick graphite plate. The total active area of the fuel cell is 50 cm^2. The channel and rib dimensions are equally designed with a cross section of 1×1 mm for each. In addition, 22 blind holes are made in each flow field at different positions to provide access for the thermocouples to be close as possible the reaction site. These holes are located along the center of the straight flow channels and the ribs of the flow field plates virtually at the surface of gas diffusion layer (GDL) (anode and cathode sides).

The distance between every two holes is 5 mm in the direction parallel to the flow channels and 10 mm in direction normal to the flow channels, as shown in Figure 3.12.B. To obtain a high accuracy in the temperature readings, the junction of the thermocouples is placed as close as possible to the reaction sites inside the fuel cell. Therefore, the thickness of the flow field plates at the point of measurement is 200 μm as shown in Figure 3.12.C. This is similar to or even thinner than the common GDL thickness used in the fabrication of the PEMFC.

The cell consists of two copper electrical/current collector plates. The total area of the current collector is 120×120 mm, with 22 small holes (1 mm in diameter in the channel area) to allow the thermocouples to pass through and reach the top surface of the gas diffusion layers (GDLs) at both the anode and cathode sides. An extended terminal is made on one side for the electrical load box connection. Two holes are drilled on opposite corners for the reactant supply, and four small holes are drilled for locating dowel pins. Further, the dimensions of the aluminum endplate are 160×160×13 mm. The number of the holes and their sizes are identical to those in electrical collector plate.

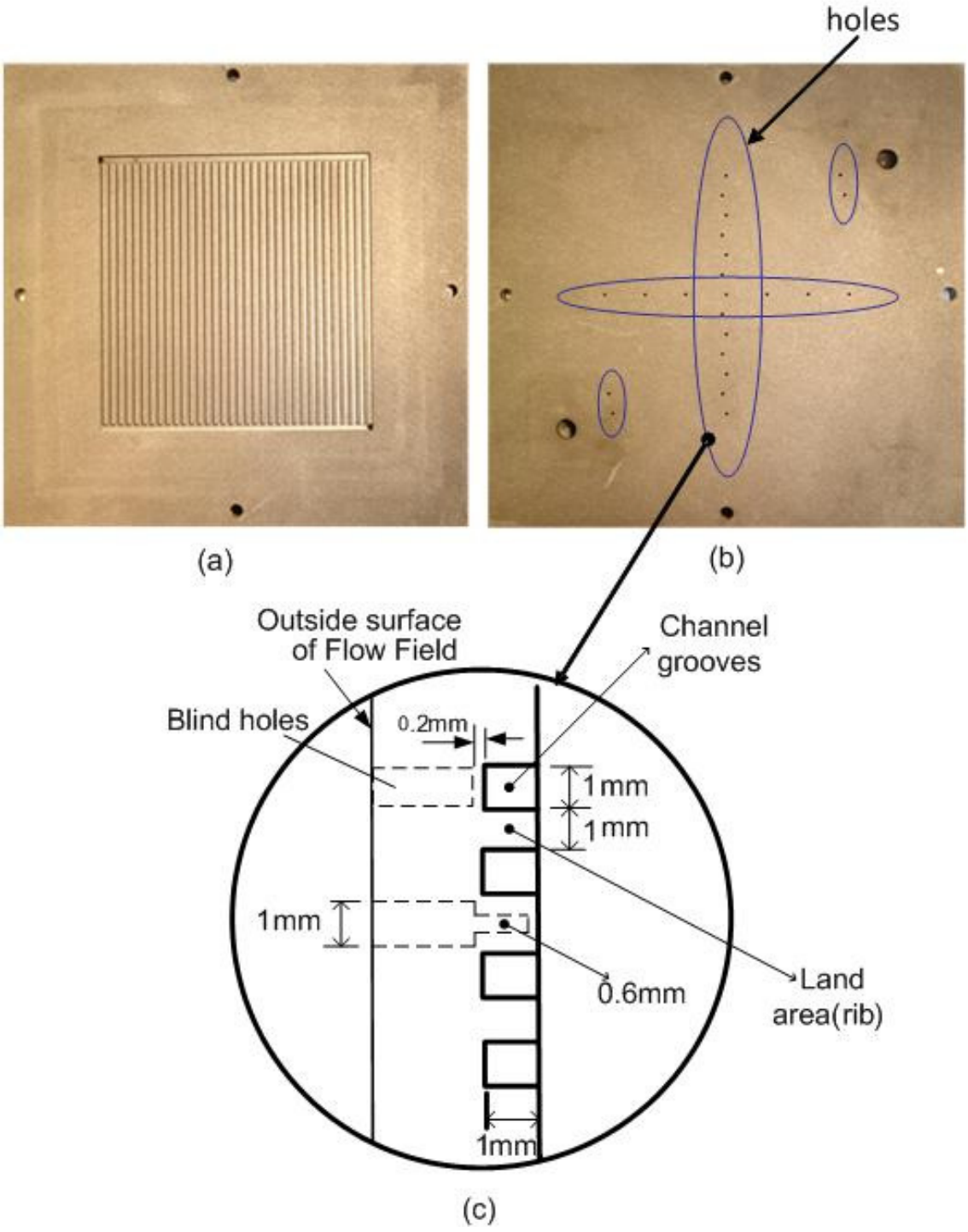

Figure 3.12: Flow field plates with parallel flow field channels machined on the surface (a) front view, (b) back view with blind holes, and (c) side view of flow field with details.

3.3.2 Thermocouple Preparation

Three main steps must be performed prior to using thermocouples for any temperature measurement as discussed below**:**

3.3.2.1 Selection and fabrication of the thermocouples

The types of thermocouples available can be classified according to the American National Standards Institute (ANSI) standard as K, J, N, R, S, B, T, or E. For example, a (T) type of thermocouple has one copper conductor that acts as a positive lead (blue insulation). The other conductor is made of constantan and acts as the negative lead (red insulation). Type (T-SLE), SLE stands for special limits of error, thermocouple is used in the present experimental work due to their; i) high resistance to corrosion in either oxidizing or reducing environments, ii) stability, especially at low temperatures, and iii) improved linear relationship between the voltage and temperature in comparison with other types as indicated in Figure 3.13 [99].

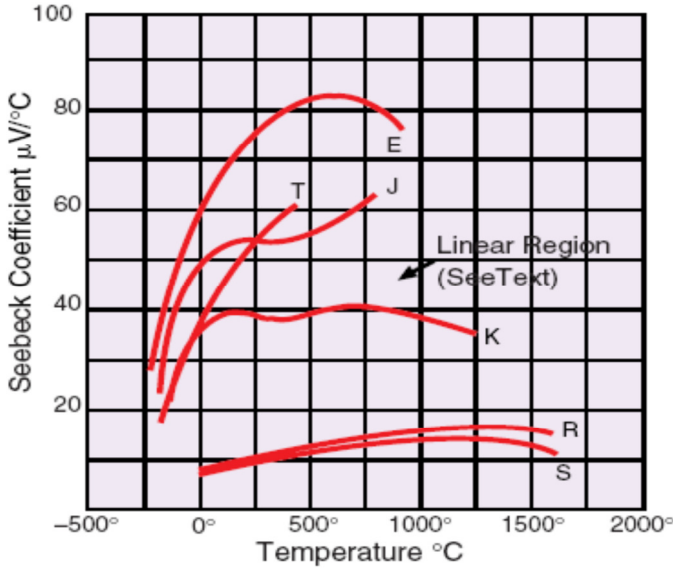

Figure 3.13: Relationship between the Seek voltage and temperature [100].

Several steps are involved in thermocouple fabrication, including checking out the "T" type thermocouple wires, removing approximately 0.5 cm of the insulation material from

both sides, twisting the two wires together (copper/constantan) at one end of the thermocouples, and welding the junction of the two wires to make sure the two wires are firmly joined together. Figure 3.14 shows the Therm-x 258B thermocouple welder used to construct the thermocouples. The Model 258B is (tungsten-inert gas) welder that works in combination of argon gas and a pressure reducing valve. The power generated from an electrical arc, flowing through two thermocouple wires, which leads to increase their temperature to their melting point. At the arc's termination, the molten wires cool down to form the final shape of the thermocouple junction. Since Therm-x 258B welder is not a gas welder, the risk of contamination is minimum. The final junction formed a homogeneous alloy that exhibits less than 0.01°C variation from one thermocouple to another for the same temperature [101].

3.3.2.2 Calibration of the Thermocouples

After the thermocouples have been constructed, they must be calibrated before usage. The type of thermocouple, the cold junction compensation, and the number of samples can be configured through the software. The common method of calibrating the thermocouples is to measure the thermocouple voltage at a variety of known temperatures. Thus, a correlation between the thermocouple's calibrated temperatures and the reference temperature is developed. In this experiment, a channel calibration wizard method is used because of its speed, accuracy and cost-effectiveness. The procedure is a fairly straightforward that uses linear interpolation to calibrate the data acquisition channel. Known temperatures are provided in the reference column values and the software calculates the differences between the known values references and the un-calibrated values in order to adjust for the offset. The minimum reference temperature used is the ice point temperature (0.01 ^{o}C), which can be determined by immersing the junction of the thermocouple in an ice bath contained in an isolated container [99]. Temperature measurements by using thermocouples are usually associated with a small error. The possible sources of error include compensation, linearization, the thermocouple wire, and experimental error. The experimental error can be minimized as much as possible by using high-precision digital temperature measurement

devices. A calibrated OMEGA HH 506RA thermometer is used to measure the ice bath temperature during the experiment. The temperature indicated by the thermometer serves as the reference temperature. In order to increase the confidence of the measurement accuracy, several water temperatures are added and the highest temperature is boiling water temperature, hence a linear correlation between the reference temperatures and the calibrated temperatures is created as illustrated in Figure 3.14.

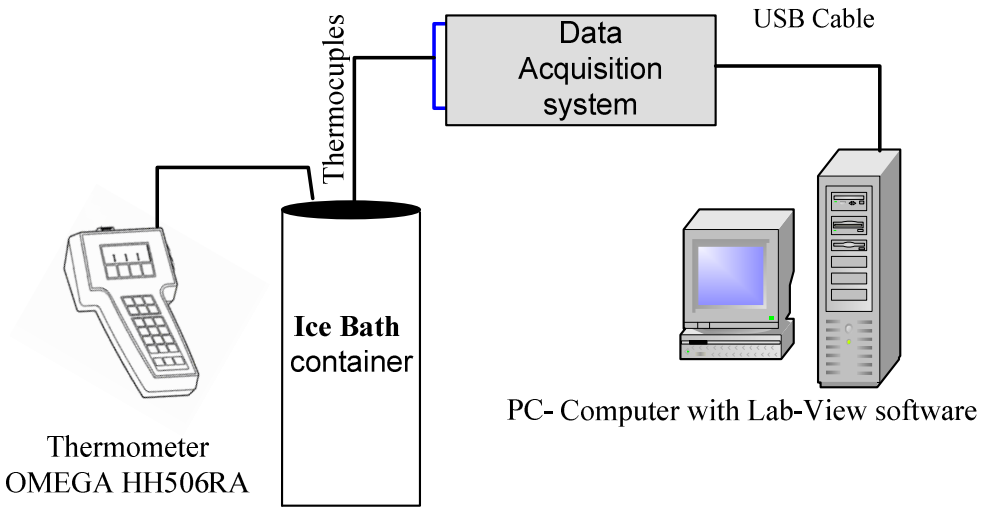

Figure 3.14: Procedures and apparatus for thermocouple calibration.

3.3.2.3 Attachment (Mounting) of Thermocouples

Thermocouples should be implanted firmly into the measurement holes located in the flow field plate in order to obtain a consistent temperature measurement as indicated in Figure 3.16. OMEGA® CC high temperature cement and Thermcoat SL are used to implant all the thermocouples in the flow field channel's back surface and acted as an electrical insulator as well. The CC high temperature cement is made from powder "Irconium Silicate", and liquid "Sodium Silicate". The two components can be mixed together to form a homogenous compound, which usually consists of 80% powder filler and 20% liquid binder by weight. This is because excess liquid can have a negative impact on the mechanical strength and

delay the curing time. The compound usually requires about 24 hours at room temperature to reach full curing [102]. Further, the data acquisition system should be connected to the computer. Each thermocouple's wire must be labeled before connected to the corresponding channel on the isothermal terminal block of the data acquisition system. The positive wire goes into the positive port, and the negative wire goes into the negative port for the terminal blocks.

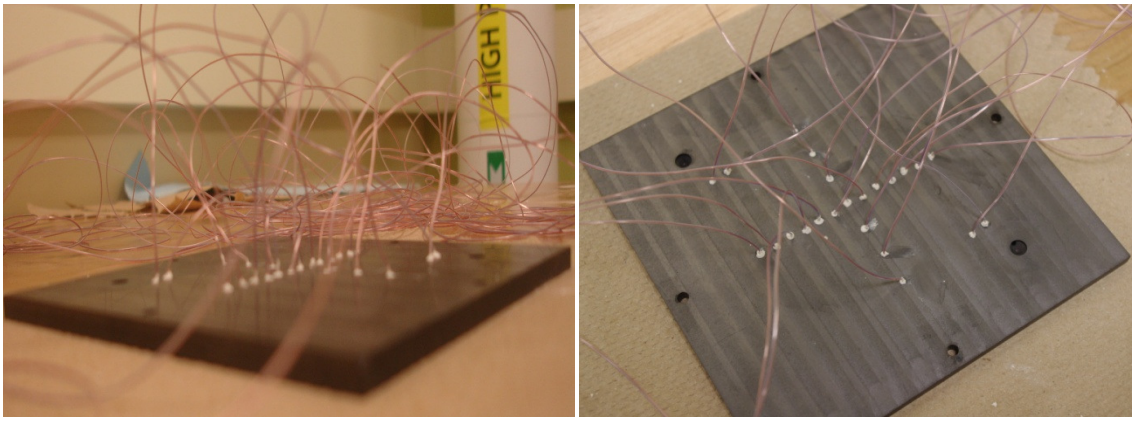

Figure 3.15: Thermocouple mounted in the back of the flow field plate.

3.4 General Fuel Cell Assembly Procedures

In order to obtain an optimum cell performance and to ensure accurate and repeatable experimental results, a consistent and deliberate cell assembly procedure is implemented. The final assembly procedure is developed as a result of number of attempts for cell assemblies and tests. The general cell assembly procedure is summarized as follows:

- The fuel cell assembly starts with preparing the main cell's components include the GDLs, gaskets, and the membrane. Templates designed by AutoCAD software and sharp knife is used are used to cut the GDLs and silicon gaskets with precise dimensions. In order to protect the membrane surface from contamination, the membrane should be kept in its protective package.

- Four identical alignment holes in each fuel cell component along with four stainless steel pins are used to ensure a proper cell assembly. These pins help the cell components to be aligned in the desired pattern as they are stacked on top of each other. These pins must be removed after the cell assembly is completed and before the real operation begins, so as to avoid any damage to the MEA as a result of electrical short circuit.
- The conventional current collector plate is placed on top of the endplate. Then, the conventional flow field plate is placed on top of the collector plate and endplate where a sheet of raw of GDL is inserted in between. The alignment pins are used to ensure a perfect alignment between the fuel cell components.
- One of the GDL layers is placed directly on top of the flow field plate such that the uncoated side is facing the flow channels, while the micro-porous layer (MPL) is exposed. To ensure complete coverage of the flow field channels including the inlet and outlet ports on the plate, the GDL area should be a little bigger than the actual active area. The silicon gasket is placed around the GDL edges. Then, the membrane is laid down gently on top of the GDL and gasket after it is removed from its protective bag.
- The second half of the cell is completed by putting the other layer of the GDL and gasket on the membrane surface. This step was the most difficult since the gaskets had to be aligned with each other, while also aligning with the GDLs and flow field gas distributors. Tweezers are always used during the assembly processes to avoid any membrane contamination.
- To align the segmented flow field plate on top of the GDL layer, stainless steel pins are also used. This ensures that both the gas flow field plates on the cathode and the anode sides are aligned with each other. The final step in the fuel cell assembly is placing the segmented current collector (PCB) and endplate on top of the flow field plate for the anode side, respectively. Again, the alignment pins allow the segments in the segmented flow field plate to match with their respective segments for the PCB.

- In the case of temperature measurements, implanted thermocouples in the flow field plate pass through the entire cell components including the current collector and endplates, respectively. The free ends of the thermocouple are connected to the DAQ through the isothermal block (SCXI-1303). Silicon material is used to fill the empty space in the holes after thermocouples are implanted in order to strengthen the measurement system.
- The washers are placed over the compression bolts, and the nuts are threaded on. Tightening is done through many steps in order to achieve even distribution of the compression force over the cell in order to avoid overloading one of the edges. (e.g the bolts are tightened to minimum value of torque 3.95 N.m, and then it is increased to final value of 7.9 N.m). It is common practice to tighten the centre bolts on each edge first, and then alternating sides after each bolt.
- The final step in this process is to visually inspect the cell assembly and perform a cell leakage test. To ensure optimal performance for fuel cell assembly, commissioning processes which include leakage and crossover tests are conducted. The commissioning processes are conducted before actual testing. Otherwise, fuel cells with internal or external leakage will not achieve the target performance and may cause a safety hazard [103]. A single PEMFC is generally composed of two independent circuit, a fuel circuits (anode side), and an oxidant circuit (cathode side). During PEMFC operation, these circuits have the potential to leak either externally or into each other (internally). There are some factors that may lead to leakage in the fuel cell, such as inappropriate component design, seal failure, membrane and electrode assembly failure, and insufficient pressure applied by the clamping force [103]. At the anode side of a PEMFC, it is preferable to use helium gas to test for fuel leakage. Since helium is not available in the Laboratory, and since nitrogen is also an inert gas, nitrogen gas is used to test for leaking from the fuel cell at both the anode and cathode sides. Two main recommendations related to testing for fuel cell leaks should be considered: hydrogen should not be used to test the leak and excessive gas pressure at one side or at both sides of a fuel cell can destroy the MEA. A variety of techniques can be used to identify the

location and source of leaks in the PEMFC. To test for leaks in the fuel cell Laboratory, FCATS-S800 is used to supply clean and dry nitrogen to both the anode and cathode sides. A pressure measurement instrument is also required in order to measure the pressure at the inlet of the fuel cell (e.g., an analog pressure gauge). The leak test procedure is summarized as follow:

- One end of the pressure gauge is connected to the inlet of the fuel cell anode and the other end is connected to the nitrogen supply line from the fuel cell testing station,
- The outlet port of the anode side of the fuel cell is plugged off,
- The fuel cell is slowly pressurized by purging the cell, while the pressure inside the cell is monitored once the inlet is closed,
- The same procedures are repeated for the cathode side of the PEMFC.

3.5 General Current and Temperature Experiment Procedures

The local current density and temperature distribution measurements are conducted experimentally by following a specific test procedure in order to achieve optimum cell performance:

- Connecting the fuel cell to test station processes. This is achieved by; i) inserting both air and hydrogen tubes for the anode and cathode to their corresponding ports in the fuel cell, ii) connecting the load box terminals to the electrical collector plates of the fuel cell, iii) clamping the heat pads to outer surface of the endplates, however, in the case of temperature measurement the fuel cell is placed inside the environment chamber.

- Fully activating the test station. This is achieved by opening all water and gas supply valves. Then the HyWare program and the LabVIEW interface should be activated.

- After the first and second steps are completed, the key operating conditions are fixed through software. (e.g the cell temperature is fixed at 65 °C, cell backpressure of 50 kPag, and stoichiometry ratios of 2 for the cathode and 1.2 for anode). The basic operating

conditions selected for the local current distribution and local temperature measurements are shown in tables 3.2 and 3.3, respectively. The oxidant and fuel gases are heated and humidified before they are supplied to the cell.

- Before data collection could begin, the fuel cell's warm-up process required to reach a steady state which would typically take 90 minutes. In order to achieve a faster warm-up process, a small load of 150-200 mA/cm^2 is applied to the cell. Applying this load to the operating cell would lead to generate heat and allow the cell to reach operational temperature faster.

- Once the target experiment requirements are conducted, the current load is removed and the data collection by the FACTS and DAQ systems are saved for post-processing purposes. The fuel cell is then purged for 1 min in order to remove the by-product water and left to cool to ambient temperature before a second experiment could be performed.

3.5.1 Local Current Density Current Distribution Measurements in PEMFC

Figure 3.16 shows the experimental system for measuring the distribution of the local current density in a single PEMFC which consists of three main components: a Fuel Cell Automated Test Station (FCATS-S800), a PEMFC, and a National Instrument (NI) data acquisition (DAQ) system. After commissioning processes including leakage tests and cell activation processes are conducted prior to testing, the anode and cathode inlets of the fuel cell are connected to the hydrogen and air supplies of the FCATS-S800. The fuel cell is connected to both the DAQ through 32 copper wires and FCATS test station in order to measure the voltage drop across precise resistance of 0.1 ohm attached to the PCB as illustrated below. Air and hydrogen gases are heated and humidified to desirable levels before being supplied to the PEMFC inlets. Table 3.2 summarizes the main operating conditions used in the present study.

Three different flow arrangements for the anode and cathode streams are investigated under steady state conditions as shown in Figure. 3.17, including co-, cross- and counter-flow configurations.

Table 3.2 : Basic operating conditions for local current density measurements*

Description	Values
Anode inlet temperature ($T_{in,a}$)	65°C
Cathode inlet temperature ($T_{in,c}$)	65°C
Anode & cathode backpressure (P_{cell})	50 kPag
Anode stoichiometry (St_a.)	1.2
Cathode stoichiometry (St_c.)	2
Relative humidity at the anode side inlet (Rh_a)	100%
Relative humidity at the cathode side inlet (Rh_c)	100%

*all operating conditions are fixed unless otherwise indicated

For the co- and counter- flow field arrangements, fuel and air flow channels are arranged in parallel, so that both streams flow in the same direction from corner (A) to (D) for the co-flow. For the counter-flow arrangement, air and fuel flow enter the cell from corners (A) and (E), and leave from corners (D) and (F), respectively. For the cross-flow arrangement, the anode and cathode flow channels are arranged perpendicular to each other so that the flow directions of the two streams are 90° apart from each other, so that the air and fuel enter the fuel cell through corners (A) and (B) and leave the cell from corners (D) and (C), respectively.

The fuel cell's temperature and other operating conditions required about 90 minutes to reach steady state as mentioned above. Each current reading is recorded by the data acquisition at 1 Hz over a period of 3 minutes. Every test is repeated five times for each operating condition for uncertainty analysis. Further, the local current density profiles with various operating conditions including: cell potential, air and fuel stoichiometry ratios, reactant backpressure, and reactant relative humidity for each flow arrangement are studied.

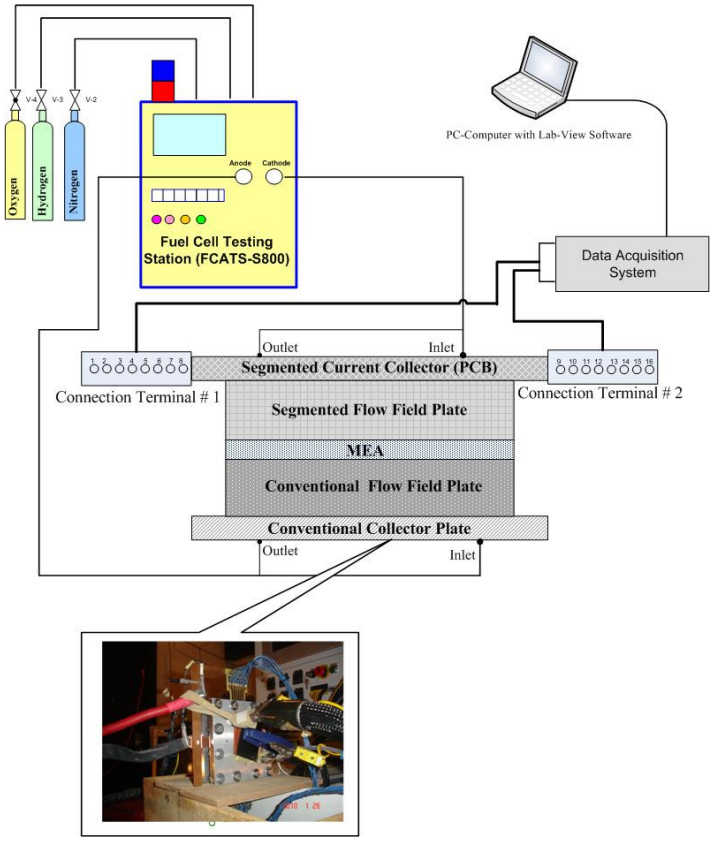

Figure 3.16: Schematic of the experimental set-up used in the present study.

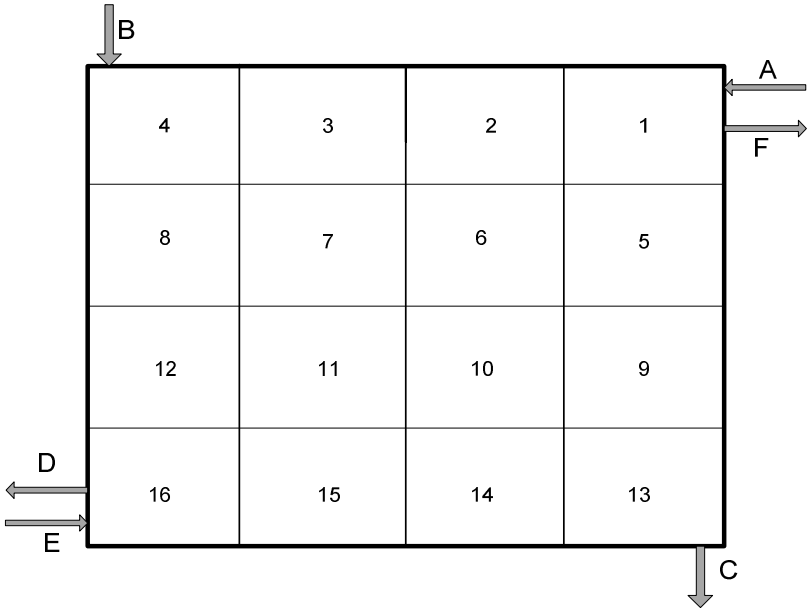

Figure 3.17 : Three common reactant flow arrangements investigated in the present study.

3.5.2 Dynamic Characteristics of the Current Distribution under Different Operating Conditions

The dynamic characteristics of the local current densities along the serpentine flow channel in PEMFC with only co-flow arrangement are investigated for various operating conditions including: cell potential, air stoichiometry ratio, reactant pressure, cell potential, and reactant relative humidity. A similar experiment set-up illustrated in Figure 3.13 is used for this purpose. In case of co-flow arrangement, both streams flow in the same direction from corner (A) to (D) as indicated in Figure 3.18. The cell temperature is fixed at 65 ^{o}C by a heating pad. Since the present experiment is designed to study the dynamic characteristic of the local current density, each individual operating condition is varied in a complete cycle; while the rest of operating conditions are fixed to values given in Table 3.2. For example, the air stoichiometry ratio is increased gradually from 2 to 5 then decreased slowly from 5 to 2 in reverse order to complete one cycle, which required at least 6000 sec for each cell potential of 0.7 V and 0.3 V. Each local current reading is recorded by the data acquisition system at 1 Hz over a period of time from the changing the experimental conditions as illustrated in Figure 3.18. It is found that several operating conditions response to the change is faster than others (e,g the cell voltage and reactant stoichiometric responded is faster than the cell backpressure and relative humidity). This procedure is repeated for other operating conditions to study their impact on the dynamic characteristic of the local current distribution in the PEMFC.

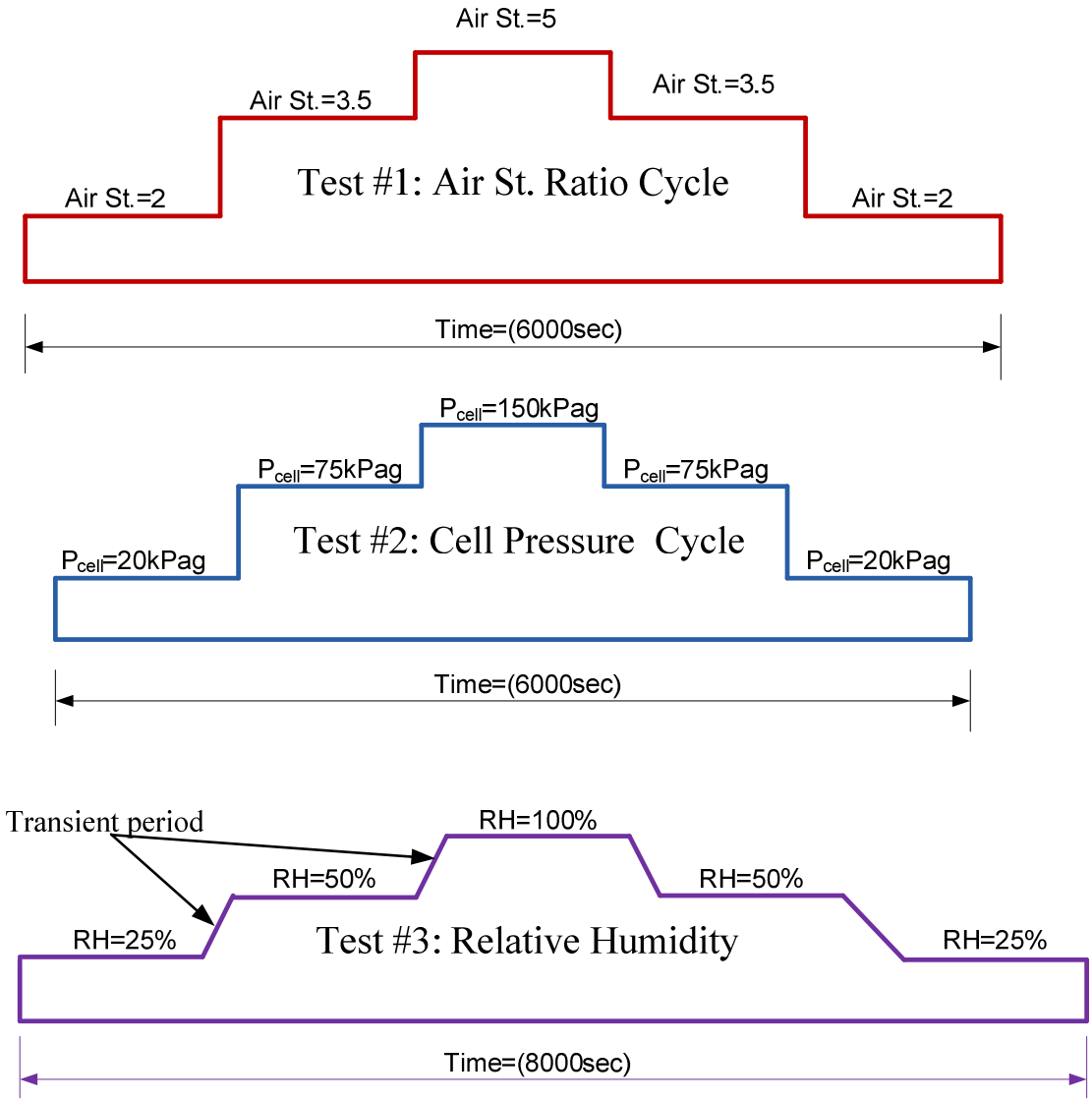

Figure 3.18: Test procedure cycles.

3.5.3 Local Temperature Distribution Measurements in a PEMFC with Multiple Straight Flow Channels under Steady State Conditions

All experimental investigations related to the local temperature distribution measurements are carried out using the Fuel Cell Automated Test Station (FCATS-G20) as shown in Figure 3.19. Micro-thermocouples, Omega T-type, are used to measure the temperature with PC-

based data acquisition systems (DAQ). OMEGA®CC high temperature cement is used to embed the 22 thermocouples in each flow field plate as explained above. Moreover, two additional thermocouples are attached to the endplates at the anode and cathode sides, along with two thermocouples placed in different locations in the environment chamber to measure its temperature during the experiment. Although the location of the measuring junction is implanted as close to the reaction site as possible by using a thin layer of the cement insulation, different methods and techniques are implemented in order to minimize the considerable errors which could affect the temperature measurements due to several factors.

(a) Probe High Velocity Effects

The measurement of temperature in gas-flow streams (especially at high velocity) can be difficult because the thermocouple probe senses the stream temperature as the total temperature, instead of the stagnation temperature. This is due to the effect of the kinetic energy of the gas when thermocouple is placed in a high-velocity gas stream, which results in slowing the velocity of the stream [104]. However, the present experiment is designed in such a way that the stagnant temperature is measured by the thermocouples in the flow field plates, close to the reaction sites; hence, the errors associated with aerodynamic effects can be ignored.

(b) Heat Transfer

Different heat transfer processes, such as conduction, convection, and radiation can have a considerable influence on the temperature measurements. However, it has been pointed out in references [105, 106] that the effect of conductive heat transfer can be minimized by using long thermocouple wires. The recommended length for thermocouple wires is at least 20 times of its diameter to ensure a distance from the probe junction. Moreover, these wires should be placed along a constant temperature (e.g inside the environment chamber) as shown in Figure 3.20 (c). The radiation effect should be considered only in high temperature measurement applications or if thermocouple is not insulated properly [107]; hence, the heat radiation is not expected to affect the current measurements.

(c) Chemical

One of the advantages of the present measurement technique; is that the thermocouple probes are not in direct contact with the reaction sites as well as the reaction by-products inside the cell. Otherwise, chemical effects by the reaction by-products such as combustion processes or catalytic reactions may lead to unexpected significant errors in the temperature measurements. In some cases, thermocouple's bead junction may require a protection from the local environment. For example, soot formation in the combustion flow may build up on the probe surface resulting in a higher temperature reading [105].

Leak testing is performed prior to actual testing. Table 3.3 summarizes the main operating conditions adopted in present study. Figure 3.20 shows the schematic diagram for measuring the temperature distribution inside a PEMFC. The anode and cathode inlets of the fuel cell should be connected to the hydrogen and air supplies of the FCATS-G20, respectively. The oxidant and fuel gases are heated and humidified before they are supplied to the cell. The current and voltage of a PEMFC can be measured by the load box through two power cables. Forty-eight calibrated micro-thermocouples are embedded in arrays of very small blind holes in the flow field plates which are connected to the DAQ. The fuel cell requires about 90 minutes reaching the steady state condition before the actual measurements begin. In the present study, each temperature measurement is collected by the data acquisition with sample rates of one reading each five seconds over period of 30 minutes from changing the experiment condition. This procedure is repeated for different current densities between 0 and 850 mA/cm^2.

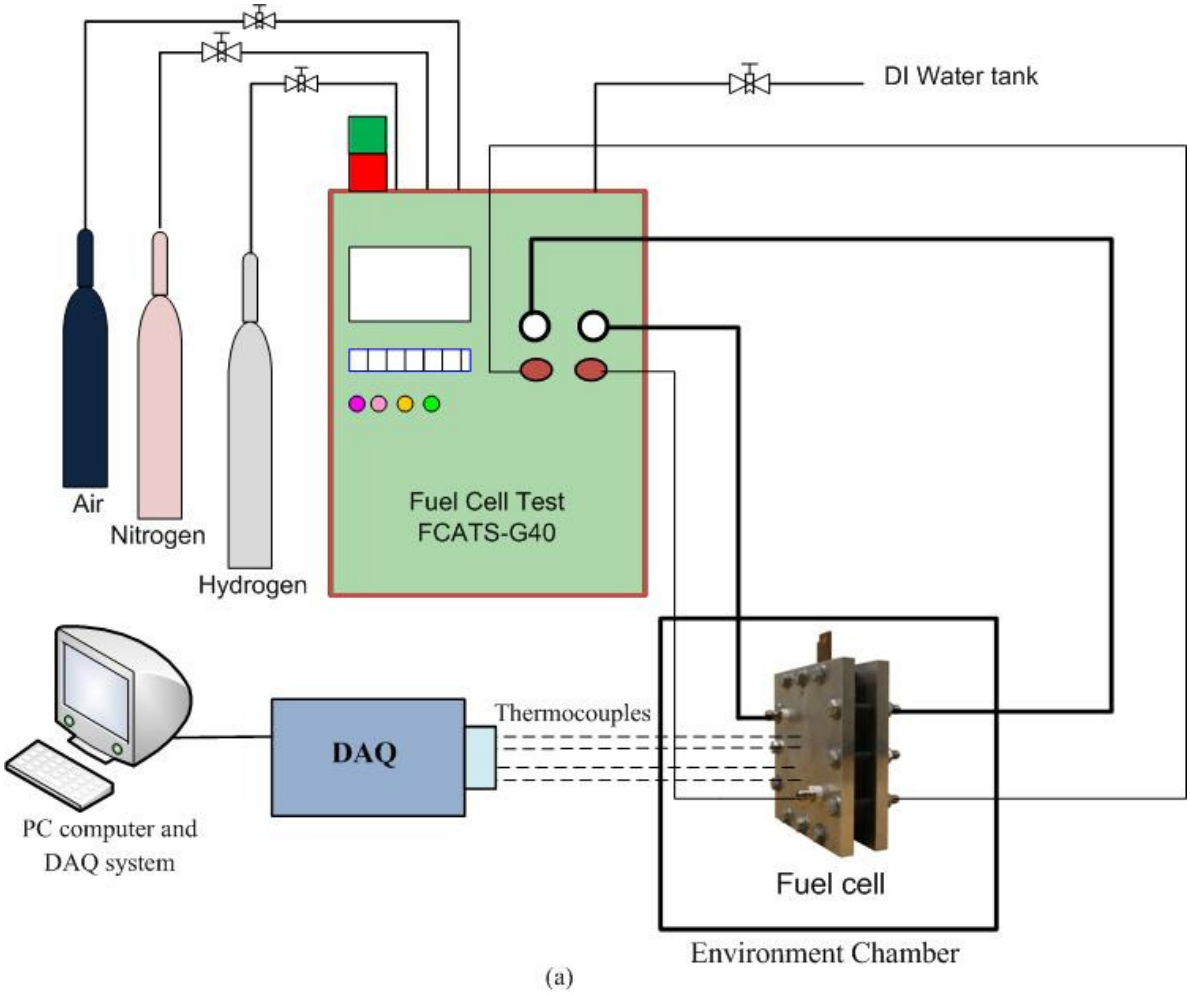

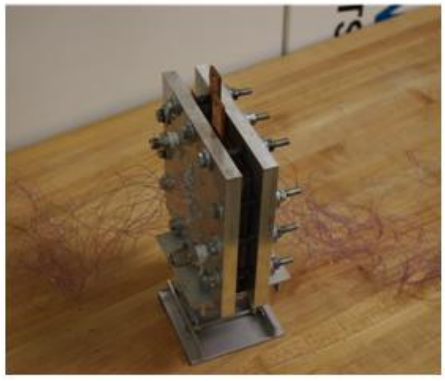

(b)

(c)

Figure 3.19: (a) Apparatus set-up required measuring the temperature distribution within PEMFC. (b) Fuel cell with thermocouples for temperature measurements, (c) Fuel cell inside the environment chamber.

Table 3.3: Basic operating conditions for local temperature distribution measurements*

Description	Values
Anode inlet temperature ($T_{in,a}$)	65°C
Cathode inlet temperature ($T_{in,c}$)	65°C
Anode & cathode backpressure (P_{cell})	Atmospheric
Anode stoichiometric (St_a.)	1.5
Cathode stoichiometric (St_c.)	3
Relative humidity at the anode side inlet (RH_a)	100%
Relative humidity at the cathode side inlet (RH_c)	100%

*all operating conditions are fixed unless otherwise indicated

3.5.4 Combined Current and Temperature Measurement Distribution in PEMFC

The combined current and temperature method is simply a combination of the two techniques presented previously. Figure 3.20 shows the used approach to conduct combined measurements of the local current density and temperature distributions for the anode and cathode sides, respectively. The local current density distribution is measured on the anode side in a similar manner described previously in section (3.5.3). A three channels serpentine flow channel layout is used for both the anode and cathode with co-flow arrangement. Since a large portion of the heat generation occurs at the cathode side, it is expected to have the most significant impact on the temperature profile in the PEMFC; hence, the local temperature distribution is measured at the cathode side by inserting 16 thermocouples (type-T) into the flow field which is corresponding to the centre of 16 segments at the anode side. These thermocouples pass through the endplate (aluminum alloy) and current collector (copper plate). The local temperature distribution is measured at a distance of 0.20 mm from the reaction site along the flow channels. The thermocouple holes have a diameter of 1 mm, and the sizes of the thermocouples with and without the plastic cover are about 0.4 mm and 0.2 mm, respectively. Sixteen thermocouples are implanted into the holes of the cathode flow field plate by using high temperature ceramic cement as explained previously. The free ends of the labelled 16 thermocouples and 32 copper wires are connected to the SXCI-1300 and

SXCI-1303 on the DAQ system for the local current density and temperature distributions, respectively. Finally, the PEMFC is placed inside an environmental chamber, which was used to control the cell and the surrounding temperature of 65 ^{o}C.

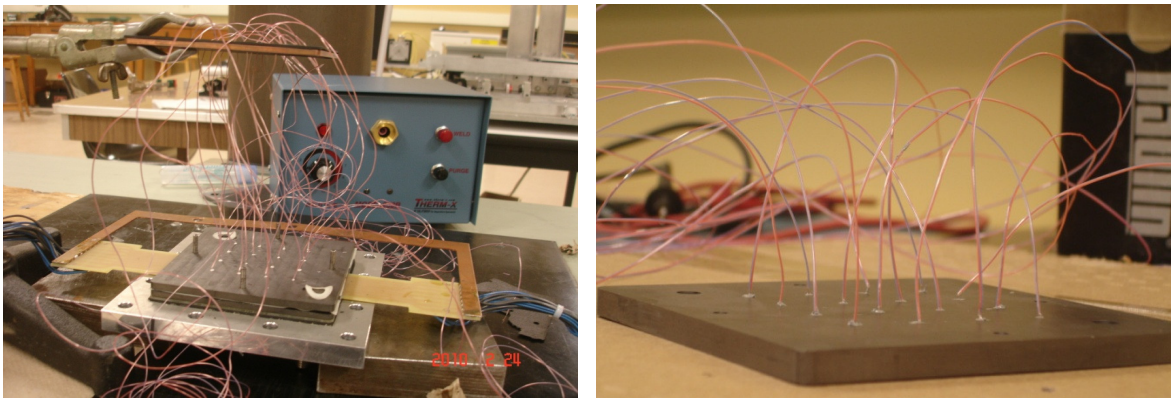

(a)

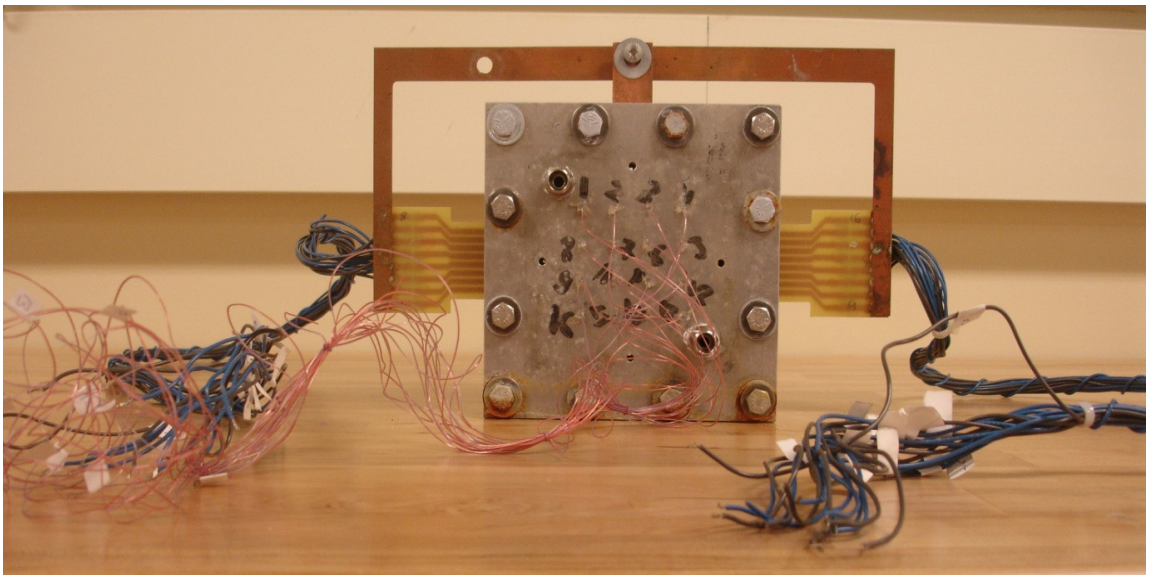

(b)

Figure 3.20: Combined current and temperature measurement distributions in PEMFC.

3.6 Measurement Uncertainty Analysis

The uncertainty of a measured property represents the interval within which the true value of property lies with a certain probability. Uncertainty can be defined as an absolute value whereby it is represented as the same units as the measured value, or uncertainty can be defined as relative value which is represented as a percentage [108]. According to the manufacturer's specification and our laboratory calibration sheets for FCATS-S800 and other measuring apparatuses, the uncertainties associated with different measured values can be summarized in Table 3.4 [93]. Further, comparison technique with different calibrated devices is implemented by the author in the laboratory to enhance the integrity of the current and temperature measurements. There are two types of errors:

1- Bias errors (fixed or systematic),

2- Precision (random errors).

Bias errors are constant during the experiment and could be positive or negative; while precision errors can be treated as random variables which require repeated measurement under the same conditions. Table 3.4 summarizes the bias errors that associated with the present measurements for the local current density and temperature distributions. Both bias (b) and precision (p) limits contribute to the total measurement uncertainty (u) determined by

$$u = \sqrt{b^2 + p^2} \tag{3.12}$$

The bias limits (b) are presented by k for different components of the measuring parameters. The total bias limit is determined as

$$b = \sqrt{\sum_{k=1}^{K} \left(\frac{\partial I}{\partial y_k} b_{yk}\right)^2} \tag{3.13}$$

where: b_{yk} refers to the individual bias limits summarized in Table 3.4.

The precision error (limit) for the values of the local current density can be reduced substantially by averaging the number of these values obtained from different repeated tests as will be explained later. Before discussion of the effect of the operating conditions on the

local current density and temperature distributions in the PEMFC for various flow arrangements, it is important to ensure that the results of the local current density and the temperature are repeatable and reproducible and the degree of agreement among repeated measurements of a particular parameter is within an acceptable level.

Therefore, every test is repeated five times (*N*) for each operating condition and each current reading (*c*) is recorded by the data acquisition system at a frequency of 1 Hz (1 reading per second) over a sufficient period of time. The average and variance (standard deviation) can be computed as follows:

Average of local current density ($\bar{C}$) value can be calculated as:

$$\bar{C} = \frac{1}{N}\sum_{i=1}^{N} c_i \tag{3.14}$$

Therefore, the standard deviation of the set of reading for the local current density can be estimated as follows:

$$\sigma = \sqrt{\frac{1}{N-1}\sum_{i=1}^{N}(c - \bar{C})^2} \tag{3.15}$$

The precision limit is determined as

$$p = \frac{\sigma}{\sqrt{N}} \tag{3.16}$$

The coefficient of variation (CV) is defined as the ratio of the standard deviation σ to the mean $\bar{C}$:

$$CV = \frac{\sigma}{\bar{C}} \tag{3.17}$$

A similar procedure is used to calculate the coefficient of variation for the local temperature distributions. Figures 3.22 and 3.23 show the coefficient of variations (*CV*) associated with the local current and temperature distribution measurements, respectively, for different flow arrangements under the same operating conditions. It is seen that the *CV* is within 5% for all local current density cases studied, while shown in Figure 3.23 is the coefficient of variation (*CV*) associated with the temperature distribution measurements for co- flow arrangement. It is seen that the *CV* for the local temperature values are within 1 %.

Table 3.4 : Summary of parameter uncertainty for test stations

Measurement Parameters	Unit	Range	Accuracy	Comments
Anode inlet temperature	°C	20-100	± 2 °C	FCATS-S800
Cathode inlet temperature	°C	20-100	± 2 °C	FCATS-S800
Anode & cathode pressure	kPa	0-350	± 2 kPa	FCATS-S800
Anode flow rate	mlpm	0-4000	± 1%	FCATS-S800
Cathode flow rate	mlpm	0-16000	± 1%	FCATS-S800
Load box-constant current	Amp	0-400	± 0.25%	FCATS-S800
Load box-constant voltage	Volt	0-50	± 0.25%	FCATS-S800
Electrical resistance	Ohm	--	5%	PCB plate
Temperature measurement	°C	-200-350	0.1 °C	NI-DAQ

Thus, the total measurement of uncertainties (u) for the local current density and temperature distributions, with considering both the bias and precision errors for a given a specific region (e.g segment #1- co-flow arrangement) in fuel cell and operating conditions are 30 mA/cm^2 and 0.1 ^{o}C, respectively.

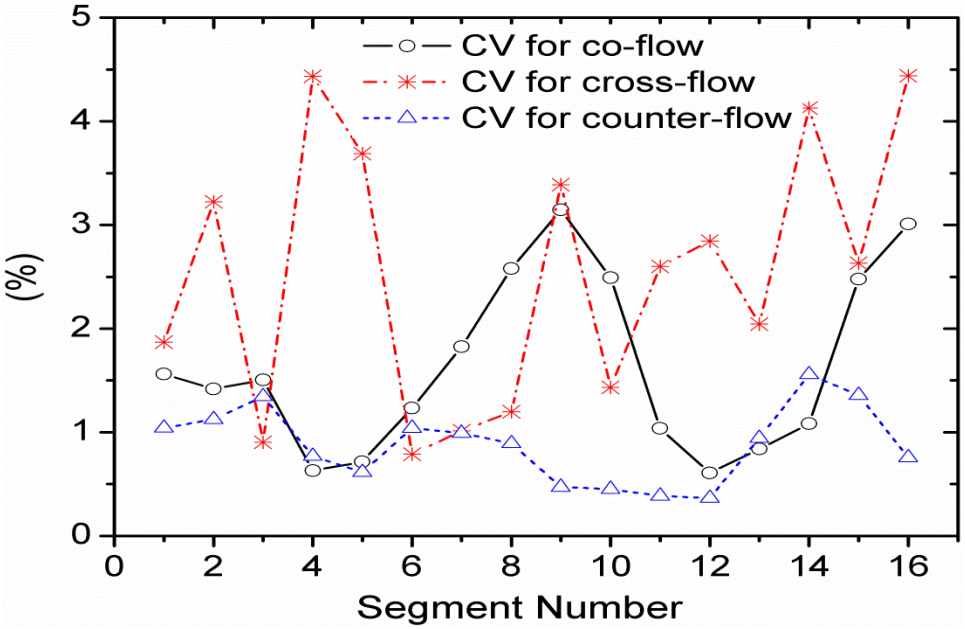

Figure 3.21: Coefficient of variations (CV) for the current density distribution for the three different flow configurations. Measurement conditions: cell potential of 0.4 V, cell backpressure of 50 kPag, cell operating temperature of 65 °C, stoichiometry of 2 for for the anode hydrogen gas, fully humidified for both cathode and anode gas stream.

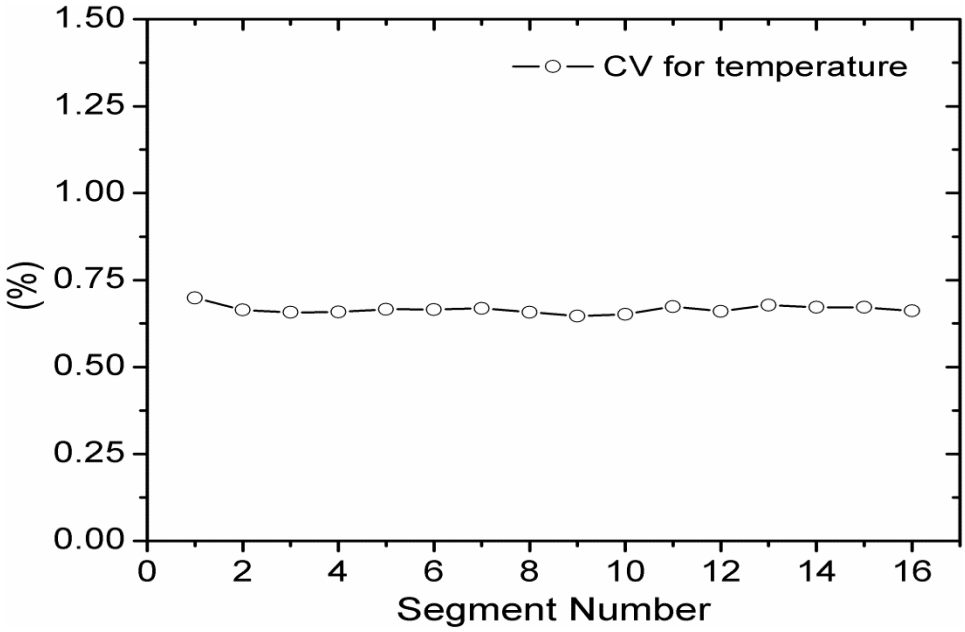

Figure 3.22: Coefficient of variations (CV) for the temperature measurement distributions for the co-flow configuration. Measurement conditions: cell potential of 0.4 V, cell backpressure of 50 kPag, cell operating temperature of 65 °C, stoichiometry of 2 for the cathode air and 1.2 for the anode hydrogen gas, fully humidified for both cathode and anode gas stream.

Chapter 4
Results and Discussion: Local Current Density and Temperature Distributions

Extensive experimental work has been conducted in order to gain a better understanding of the local current density and temperature distributions under steady-state conditions and only the dynamic characteristics for local current density in single Proton Exchange Membrane Fuel Cells (PEMFCs). The detailed experimental parameters, set-up, and procedures are discussed in chapter 3. This chapter is arranged as follows: Local current density distribution in a single PEMFC with three different flow configurations including co-, counter-, and cross-flow arrangements for the anode and cathode streams are presented. The impacts of key operating parameters under steady state conditions such as stoichiometry ratios, reactant inlet humidity, cell backpressure, and temperature on the local current density profile are examined. Dynamic characteristics of the local current distribution due to changing the cell potential or operating conditions for a PEMFC with co-flow arrangement is also studied. In-situ, nondestructive temperature measurement has been performed for a PEMFC with multiple straight flow channels virtually at the surface of gas diffusion layer (GDL) using micro-thermocouples embedded in the arrays of blind holes under the flow channel and rib area. The temperature distribution has been obtained for both the cathode and anode sides and along the flow channel. The effects of various operating conditions, such as air stoichiometry ratio, cell current density, and cell backpressure on the temperature distribution, are discussed.

Simultaneous combined measurements of the local current and temperature distributions in PEMFC with serpentine flow field and under various operational conditions are conducted. It is a combination of the previous two techniques (current and temperature measurements). The PCB and 16 embedded thermocouples are used to measure the local urrent density and temperature variations simultaneously on the anode and cathode sides, respectively.

Part (I)

Effect of Reactant Flow Arrangements on the Local Current Distribution in PEMFCs

4.1 Effect of Reactant Flow Arrangements on the Local Current Distribution in PEMFCs

It has been reported that the segmented flow field approach may lead to a noticeable reduction in the overall cell performance. Several studies [62-64, 109] investigated the local current density in a segmented PEMFC, even with considerable low overall cell performance of 250 mA/cm^2 for 0.3 V. The reduction in the cell performance can be attributed to a high electrical resistance between the fuel cell components when the segmented approach is implemented. Therefore, it is important to examine the impact of the both segmented flow field and current collector plates on the overall cell performance. Figure 4.1 shows the cell performance for the two different cell constructions. The conventional fuel cell refers to the cell construction with the standard gas flow field plates and current collection plates, while the modified fuel cell construction denotes to the conventional flow field plate that has been replaced by the segmented one, and the regular current collection plate (copper plate) that has been replaced by the segmented PCB plate, as explained in chapter 3. It is seen that the modified fuel cell arrangement has a lower performance than the conventional fuel cell, signifying that the present segmented flow plate and the current collector plate have an undesirable impact on the overall cell performance. Since the present study is focusing on the measurement of the current density distributions over the cell surface, the noticeable reduction in the cell voltage for the same current density is not expected to cause major concern in the resulting measured current distributions. Further, the fuel cell used in the present study generates a reasonable performance of 800 mA/cm^2 at 0.3 V.

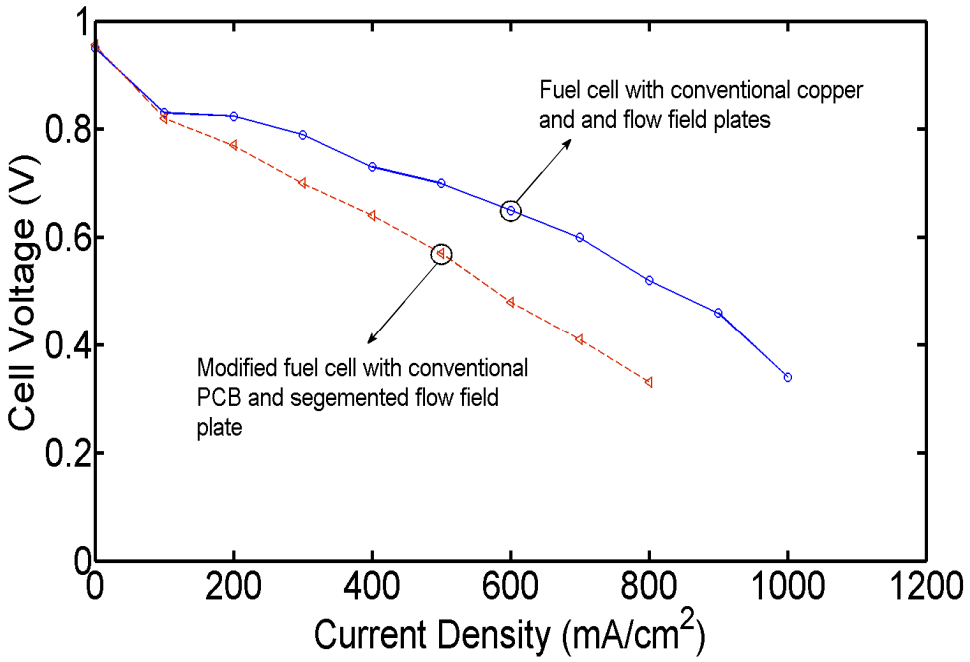

Figure 4.1: Cell polarization curves for fuel cell with and without PCB plate. Cell operating conditions: cell backpressure of 50 kPag, temperature of 60 °C, stoichiometry of 2 for the cathode air stream and 1.2 for the anode hydrogen stream, fully humidified for both cathode and anode gas streams.

4.1.1 Local Current Distribution in PEMFC for Co-flow Arrangement and Different Cell Potentials

Figure 4.2 shows the local current distributions in PEMFC for the co-flow arrangement. The current profile in this figure is obtained at three different cell potentials of 0.7 V, 0.4 V, and 0.3 V, respectively. The anode and cathode stoichiometries are fixed at 1.2 and 2, respectively. Fully humidified reactants on both the anode and cathode are set to the fuel cell operating temperature of 65 °C. It is seen in Figure 4.2 that for the co-flow arrangement for the anode and cathode streams, the local current density is the highest in the near inlet region and then decreases downstream following the flow direction and becomes the lowest in the region near the outlet. This may be attributed to the experimental conditions of the fully humidified anode and cathode streams at the cell inlet. Due to the depletion of the reactants of the reactant along the flow channels, the reactant concentration is reduced along the flow

direction, accompanied with the water formation/condensation, the local current distribution depends accordingly. At a high cell voltage of 0.7 V, the local current density variation from the cell inlet to the outlet region is relatively small, but still amount to about 15%, as shown in Figure 4.2a. It is obvious that the local current density decreases very slowly over most of the cell surface, and a steep gradient is observed close to the cell outlet. As the cell operating potential is reduced to 0.4 V and 0.3 V, as shown in Figure 4.2b and 4.2c, the local current density value increases noticeably along the flow channel with large variations from the cell inlet to the outlet. The iso-current density curves become almost aligned with the reactant stream flow arrangement (flow channel layout). This suggests that the flow arrangement may have a predominant impact on the current density distribution, especially at high current density operation in modern PEMFCs.

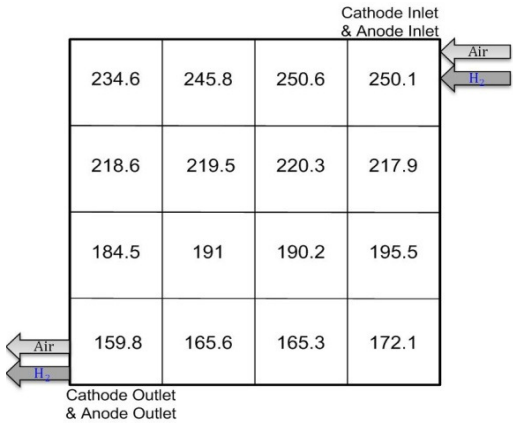

(a)

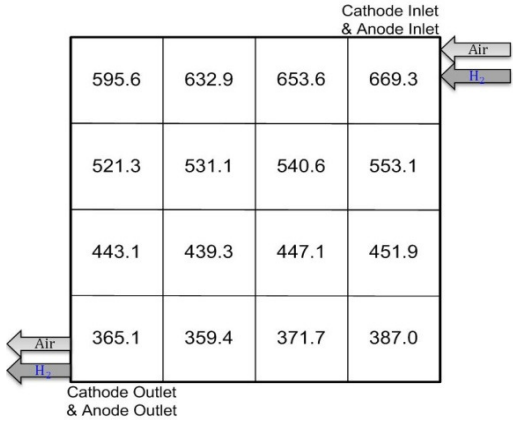

(b)

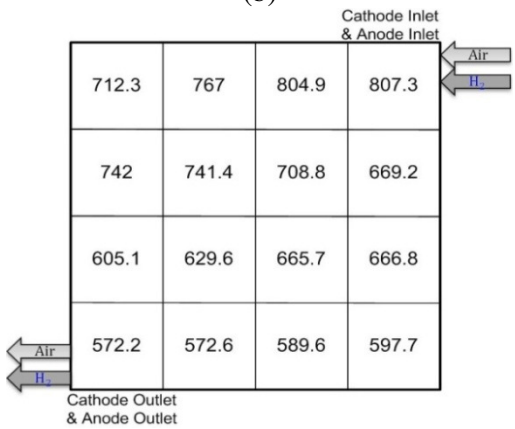

(c)

Figure 4.2: Current density distribution over the MEA surface for co-flow arrangement and different cell potentials of (a) 0.7 V, (b) 0.4 V, and (c) 0.3 V. The numbers shown in the figure are the current density value in mA/cm^2. Operating conditions: cell temperature of 65 ^{o}C, cell backpressure of 50 kPag, stoichiometry of 2 for the cathode air and 1.2 for the anode hydrogen gas, fully humidified for both anode and cathode gas streams.

4.1.2 Local Current Distribution in PEMFC for Counter-Flow Arrangement at Different Cell Potentials

Shown in Figure 4.3 is the local current density distribution for the counter-flow arrangement between the reactants; hydrogen stream enters the cell at the bottom left corner and leaves at the top right corner, while the air stream flows in the exactly opposite direction. Figure 4.3 is generated under identical operating conditions as Figure 4.2. It is seen that the current density is slightly higher near the anode inlet (on the cathode outlet) when compared to region near the anode outlet (on the cathode inlet) for the three cell potentials of 0.7 V, 0.4 V, and 0.3 V. This signifies, again, the dominance of the hydrogen fuel stream on the local current density over the MEA surface as result of its low stoichiometry value of 1.2 as compared with stoichiometry of 2 for the cathode air stream. This observation clearly purposes that anode hydrogen stream has a predominant impact on the overall cell performance due to its limiting condition for the hydrogen concentration along the flow direction, despite the fact that conventional wisdom implies that the cathode is more important due to the sluggish oxygen reduction reaction and the formation of product water that can flood the cathode electrode and is difficult to remove due to large capillary effect. Another important observation is that the counter-flow arrangement yields to the most uniform local current density distribution in PEMFC as compared to the two flow configurations investigated. This result is consistent with conventional heat exchanger performance for which the counter-flow arrangement results in optimum thermal effectiveness. Further, this observation is found to be in agreement with the work conducted at Los Alamos National Laboratory by using the neutron imaging technique [110].

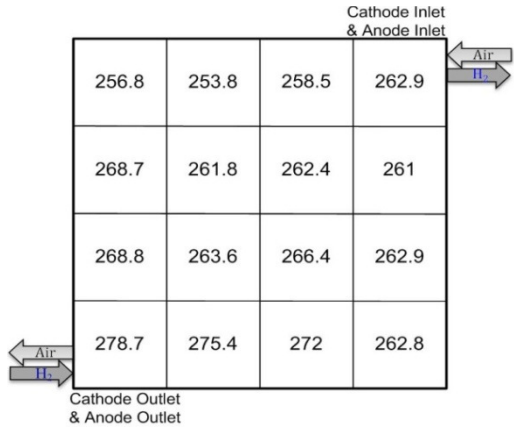

(a)

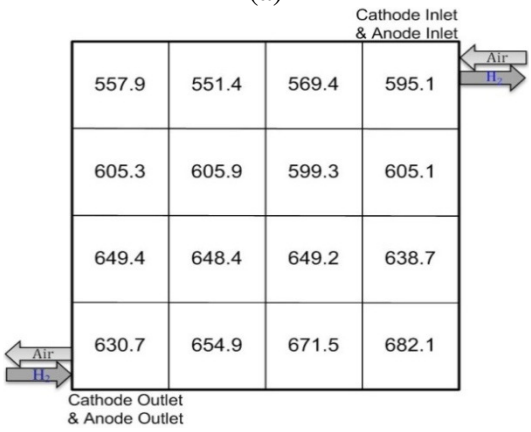

(b)

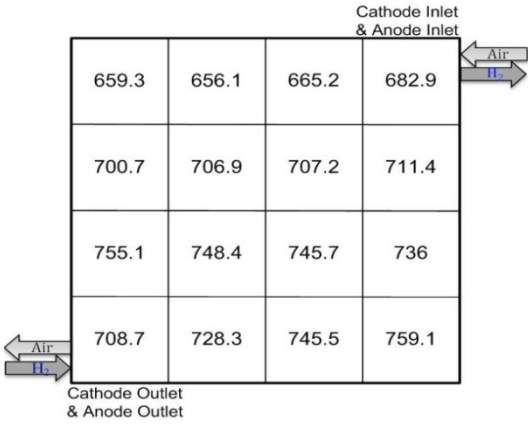

(c)

Figure 4.3 : Current density distribution over the MEA surface for counter-flow arrangement and different cell potentials of (a) 0.7 V, (b) 0.4 V and (c) 0.3 V. The numbers shown in the figure are the current density value in mA/cm^2. Operating conditions: cell temperature of 65 ^{o}C, cell backpressure of 50 kPag, stoichiometry of 2 for the cathode air and 1.2 for the anode hydrogen gas, fully humidified for both anode and cathode gas streams.

4.1.3 Local Current Distribution in PEMFC for Cross-Flow Arrangement and Different Cell Potentials

Figure 4.4 shows the local current density profile for PEMFC with a cross-flow arrangement under similar operating parameters, including temperature, pressure, cell potentials, and reactant stoichiometries as the other two flow configurations shown in Figures 4.2 and 4.3. It is seen that the highest local current density is measured in the region near the anode inlet region, whereas the minimum local current density occurred near the anode outlet region. This may be attributed to the fact that the lower stoichiometry ratio for the anode of 1.2 as compared to the cathode stoichiometry of 2, although it is well known that air reduction reaction at the cathode side is much slower than the hydrogen oxidation reaction that occurs at the anode side. It is clearly seen that the local current distribution for the cross-flow arrangement is much different from a monotonic change along the flow channel shown in Figure 4.2 for the co-flow configuration. The current density profile is much more complex for cross-flow arrangement, as shown in Figure 4.4. Since the anode stoichiometry is only 1.2 while the cathode stoichiometry is 2, it seems that the current density change is more strongly influenced by the fuel stream (the limiting reactant) than the air stream. As a result, the current density change from the anode inlet to outlet is much larger than the corresponding change from the cathode inlet to outlet. In fact, Figure 4.4 shows that the current density at the cathode gas inlet and outlet regions is almost the same. But the variation from the anode gas inlet to exit for the cross-flow configuration, shown in Figure 4.4, is larger than the corresponding change for the co-flow arrangement shown in Figure 4.2. Particularly, the current density near the anode inlet is about the same for both flow configurations, but the current density near the anode outlet is smaller for the cross-flow case.

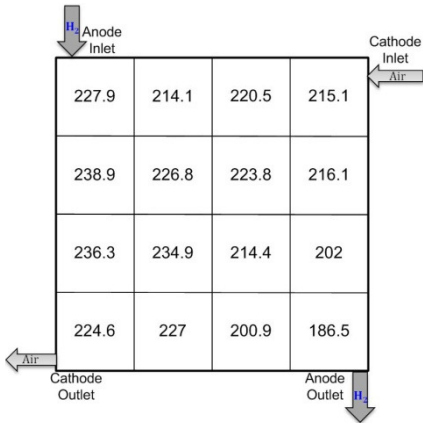

(a)

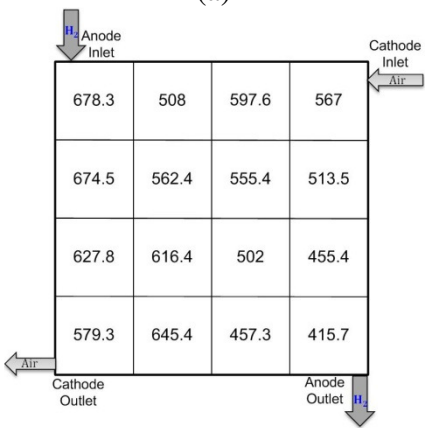

(b)

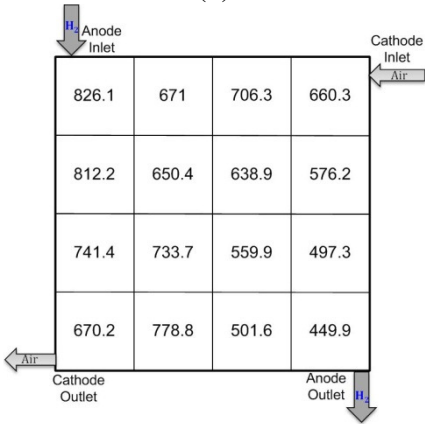

(c)

Figure 4.4: The current density distribution for cross-flow arrangement at the different cell potentials of (a) 0.7 V, (b) 0.4 V and (c) 0.3V. The numbers shown in the figure are the current density value in mA/cm^2. Cell operating conditions: cell backpressure of 50 kPag, cell temperature of 65 ^{o}C, stoichiometry of 2 for the cathode air and 1.2 for the anode hydrogen gas, fully humidified for both anode and cathode gas streams.

Part (II)

Effect of various operating conditions on the local current distribution profiles with different flow arrangements

4.2 Effect of Various Operating Conditions on Local Current Distribution Profiles with Different Flow Arrangements

In this section, the effects of key operating conditions, such as reactant stoichiometry ratios, cell pressure, cell temperature, and inlet humidity levels on the local current density distributions for co-, counter-, and cross flow arrangements will be discussed.

4.2.1 Effect of Air Stoichiometry Ratio

Figure 4.5 shows the local current distributions inside a PEMFC from the inlet to outlet and for co-flow arrangement at a fixed anode stoichiometry ratio of 1.2 and different cathode stoichiometry ratios of 2, 3.5 and 5. The anode and cathode stoichiometry is always defined relative to the real operating condition. A high stoichiometry ratio is expected to remove the product water more effectively and enhance the cross flow through the GDL [111-115]. It also reduces the performance fluctuations [111]. The current profile in this figure is obtained at the cell potential of 0.4 V. Fully humidified reactants on both the anode and cathode are set to the fuel cell operating temperature of 65 °C. As seen in Figure 4.5, local current densities are the highest in the region near the inlet, decrease along the flow direction and become the lowest in the region near the outlet. The reduction in the local current densities can be attributed to the reactant depletion and water formation (accumulation/flooding) along the flow direction. Water flooding in the region near the cathode outlet has been observed in an operating PEMFC by using visualization techniques, as described in reference [116]. Experimental results clearly show that the local current density is considerably affected by the air flow rate especially at the downstream region of the cell (near the outlet). In this region, an increase of the cathode stoichiometry ratio from 2 to 5 can improve the local current density by about 20%. This is because of higher air flow rate always results in a better water removal capability as well as increasing the oxygen concentration. At the region near the inlet, an increase of the cathode stoichiometry ratio from 2 to 5 results in a negligible change in the local current density because of the availability of the oxygen regardless of the air stoichiometry ratio.

Shown in Figure 4.6 are the local current density distributions for counter-flow arrangement under the same operating conditions as Figure 4.5. For this case, hydrogen stream enters at the lower left corner and leaves at the top right corner, as illustrated in Figure 3.18, while the air stream flows in the opposite direction. It is seen that the current density for the counter-flow arrangement is almost uniform along the flow channels, as opposed to the distributions obtained for co-flow arrangement, shown in Figure 4.5, where the current density is shown to change dramatically [85]. As air stoichimetry ratio is increased from 2 to 5, a noticeable improvement in the local current density is observed in the region near the anode inlet. This implies the dominant influence of the hydrogen stream due to its low stoichiometry ratio of 1.2, as compared to the cathode air stream.

The local current density distribution is shown in Figure 4.7 for the cross-flow arrangement under the identical operating conditions as the other two flow configurations shown in Figures 4.5 and 4.6. In this arrangement and referring to Figure 3.18, the hydrogen stream enters at the top left corner and leaves at the lower right corner; while the air stream enters at the top right corner and leaves at the lower left corner. It is seen that the local current density and hence the overall cell performance is improved significantly as air stoichiometry is increased from 2 to 5, and the local current density variations for the cross-flow arrangement are more complex than those obtained for co- and counter-flow arrangements. The local current density increases from the cathode inlet region towards the anode inlet region where the maximum local current density is observed. Once again experimental data indicates that the region near the anode outlet presents the lowest current density, which can be due to the hydrogen (the limiting reactant) depletion along the flow channels due to its low stoichiometry ratio.

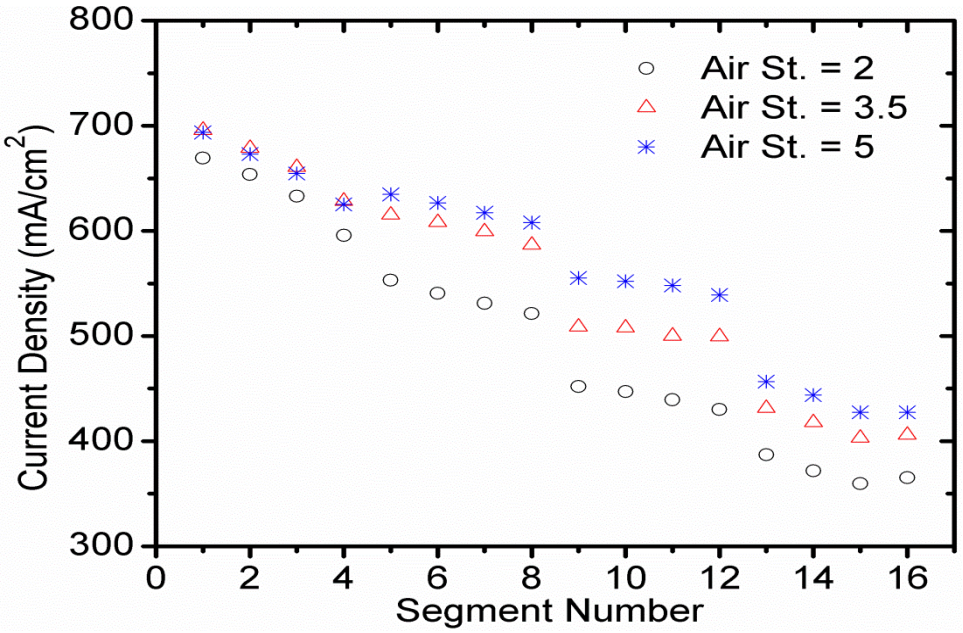

Figure 4.5: Effect of the air stoichiometry ratio on the current density distribution for co-flow configuration. Measurement conditions: cell potential of 0.4 V, cell backpressure of 50 kPag, cell operating temperature of 65 °C, stoichiometry of 1.2 for the anode hydrogen gas, fully humidified for both cathode and anode gas stream.

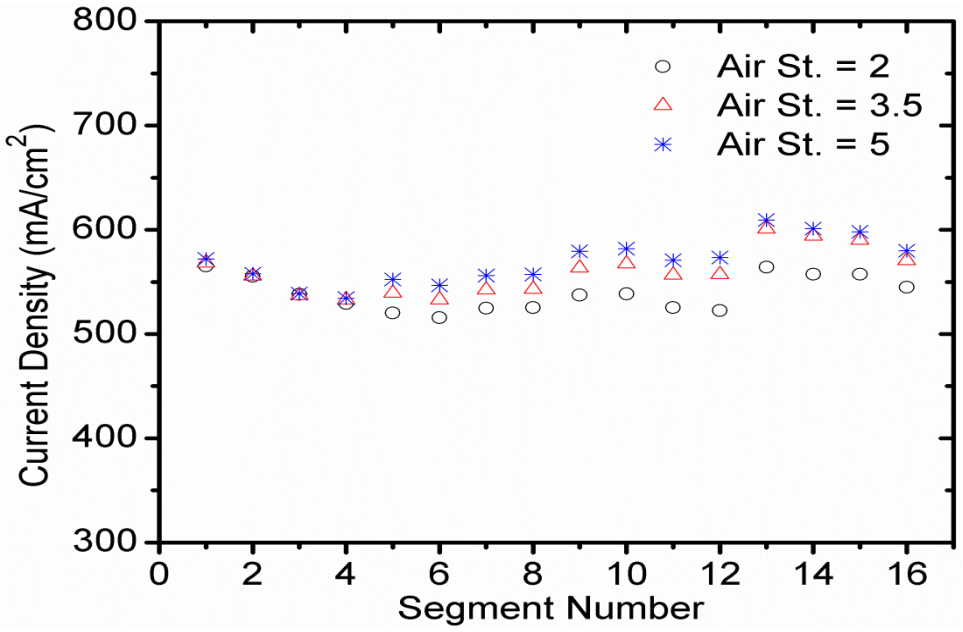

Figure 4.6: Effect of the air stoichiometry ratio on the current density distributions for counter-flow configuration. Measurement conditions: cell potential of 0.4 V, cell backpressure of 50 kPag, cell operating temperature of 65 °C, stoichiometry of 1.2 for the anode hydrogen gas, fully humidified for both cathode and anode gas stream.

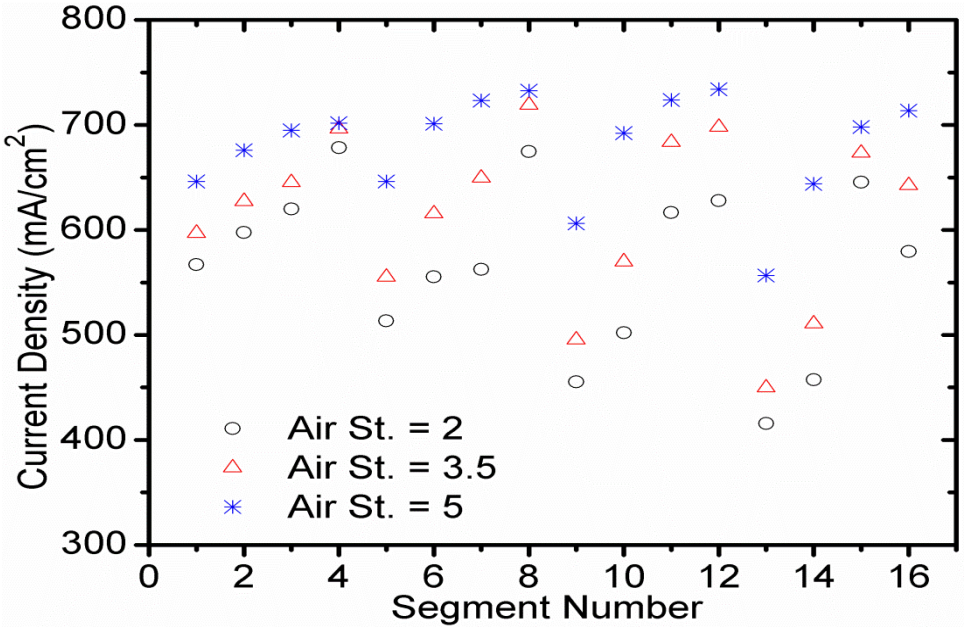

Figure 4.7: Effect of the air stoichiometry ratio on the current density distribution for cross-flow configuration. Measurement conditions: cell potential of 0.4 V, cell backpressure of 50 kPag, cell operating temperature of 65 °C, stoichiometry of 1.2 for the anode hydrogen gas, fully humidified for both cathode and anode gas stream.

It is obvious that the co-flow arrangement shows the largest variations in the local current density between the inlet and outlet with a monotonic decrease along the flow channel; hence, three regions along the flow channel are selected to demonstrate the effect of air stoichimetry ratio on the local polarization curves. Figure 4.8 (a, b, c) is the polarization curves (I-V curves) which are generated under similar operating conditions as Figure 4.5, except for different cell potentials. It shows that the local polarization curves of current versus cell voltage for three regions including: near inlet, middle, and near outlet regions, respectively. It is seen in Figure 4.8 that the performance of local areas from the inlet to the outlet decrease for the same reasons discussed earlier. It indicates that the limiting current density is quite different from one region to another inside the cell even under same operating conditions. It is obvious that the local current density in the region near the inlet is 850 mA/cm^2 for 0.3 V and air stoichiometry ratio of 2, while the value of the local current density is 620 mA/cm^2 and 450 mA/cm^2 near the middle and outlet regions, respectively.

Another observation is that a higher air flow rate will result in a noticeable impact only on the local polarization profile near the outlet region as compared to others. It hypothesizes that a higher anode and cathode stoichiometry ratio can reduce the variation of the local current density between the cell inlet and outlet dramatically. This may suggest that a higher value of both air and hydrogen stoichiometry ratios may lead to better water management as well as higher reactant concentration over the reaction site.

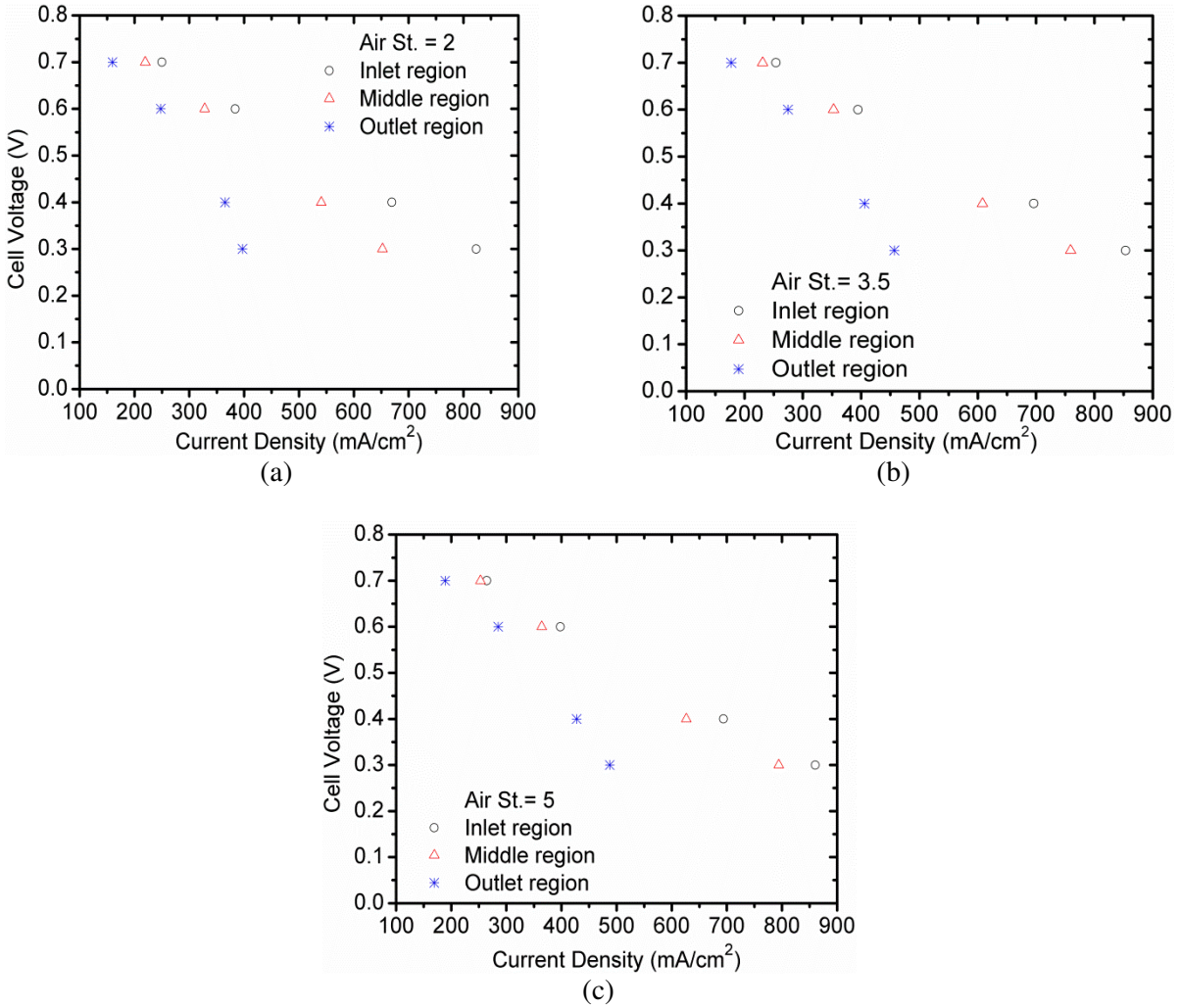

Figure 4.8: Effect of air stoichiometry ratios on the current density distribution for co-flow configuration at different regions and air stoichiometry ratio of 2 (a), 3.5 (b), and 5 (c), respectively. Measurement conditions: cell potential of 0.3 V, cell backpressure of 50 kPag, cell operating temperature of 65 °C, stoichiometry of 1.2 for the anode hydrogen gas, fully humidified for both cathode and anode gas stream.

4.2.2 Effect of Hydrogen Stoichiometry Ratio

Variations of local current density for the co-flow arrangement are shown in Figure 4.9 as a function of anode stoichiometry ratio of 1.2, 1.8 and 2.4. Fully humidified reactants are fed into the PEMFC operating at 65 °C and the air stoichiometry ratio is fixed at 2. Figure 4.9 indicates that for all anode stoichiometry ratios, the current densities are higher near the cell inlet and degrade toward the outlet. At the middle and near the outlet regions of the cell, it is seen that the local current density and the cell performance are improved significantly when the hydrogen stoichiometry ratio is increased from 1.2 to 1.8, but the improvement is much less noticeable when the hydrogen stoichiometry changes from 1.8 to 2.4. At the cell potential of 0.4 V, it is found that 19% and 7% increases in the local current density value is achieved when the hydrogen stoichiometry is increased from 1.2 to 1.8 and from 1.8 to 2.4, respectively. Since the air stoichiometry ratio is fixed at a value of 2, a higher hydrogen flow rate in the anode side cannot lead to uniform current distribution along the flow channel in a PEMFC with the co-flow arrangement due to the oxygen depletion and water formation, especially in the region near the outlet. Further, it is observed that the anode stoichiometry ratio does not have a significant effect on the region near the inlet due to the high hydrogen concentration (fuel) there.

The effect of anode stoichiometry ratio on the local current distribution in a PEMFC for the counter-flow arrangement is shown in Figure 4.10. Current density profiles are generated under the identical operating conditions as the co-flow arrangement shown in Figure 4.9. Comparing Figure 4.9 and 4.10, it is seen that the current distribution profiles of the two flow arrangements are very different since the current distribution in a PEMFC with the counter-flow is much more uniform than that with co-flow arrangement. It is also found that the local current density in Figures 4.9 and 4.10 can be only improved with increasing the hydrogen stoichiometry ratio from 1.2 to 1.8 and a further increase in the hydrogen stoichiometry ratio will not lead to a considerable improvement in cell performance. Further, it can be seen that the results reported in Figures 4.6 and 4.10 are measured at different lifetimes of the cell. The difference for the current density measured under the same operating conditions of 1.2 for anode stoichiometry and 2 for the cathode air gas is due to the ageing effect that has caused a decrease in the overall current density.

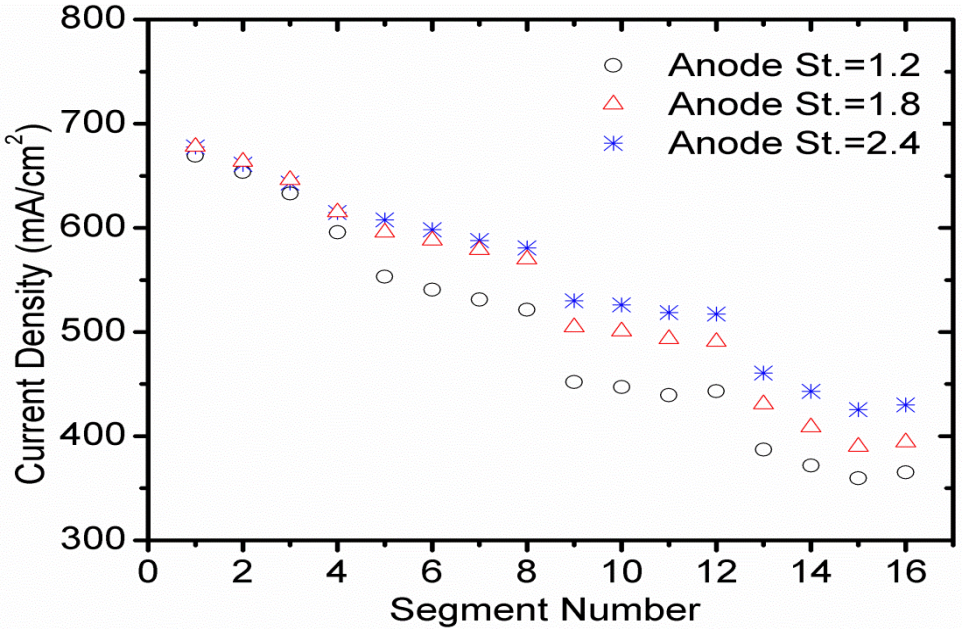

Figure 4.9: Effect of hydrogen stoichiometry ratio on the current density distribution for co-flow configuration. Measurement conditions: cell potential of 0.4 V, cell backpressure of 50 kPag, cell operating temperature of 65 °C, stoichiometry of 2 for the cathode air, fully humidified for both cathode and anode gas stream.

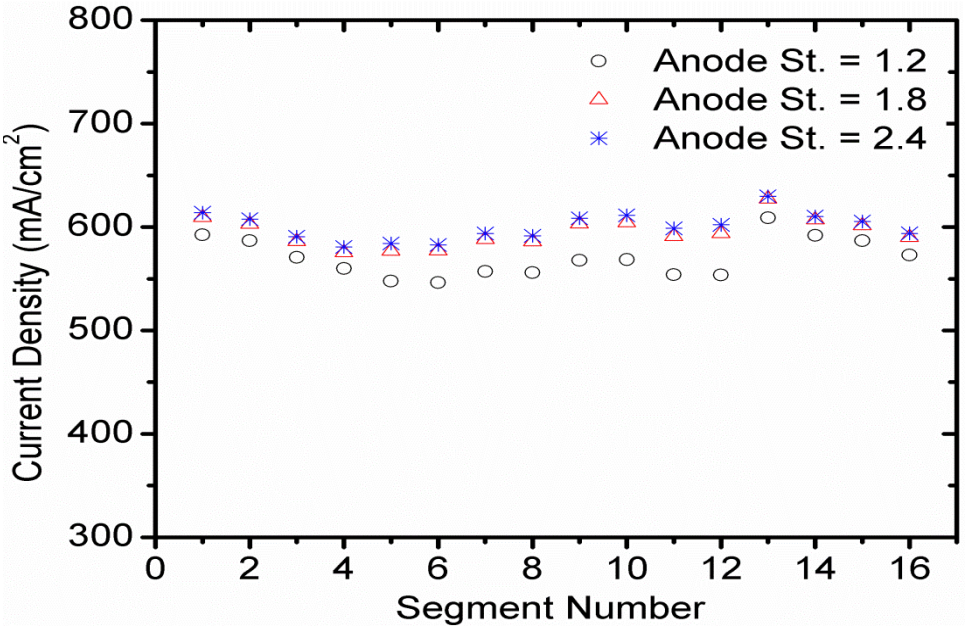

Figure 4.10: Effect of the hydrogen stoichiometry ratio on the current density distribution for counter-flow configuration. Measurement conditions: cell potential of 0.4 V, cell backpressure of 50 kPag, cell operating temperature of 65 °C, stoichiometry of 2 for the cathode, fully humidified for both cathode and anode gas stream.

4.2.3 Effect of the Cell Backpressure

The effect of hydrogen and air stream pressures on the distribution of current density in a PEMFC is investigated for three different cell backpressures of 0, 75, and 150 kPa (gauge), and the results are shown for co-, counter-, and cross-flow arrangements in Figures 4.11,4.13 and 4.14, respectively. These three figures are generated for the same operating conditions and cell potential of 0.4 V. Experimental data indicate that the PEMFC performance is enhanced at higher operating pressures. This can be attributed to higher reactant concentrations in the cell which prevails at higher cell pressures. Figures 4.11 and 4.12 clearly show that although the local current density decreases along the flow channels with the co-flow configuration, the cell overall performance enhances considerably at higher pressures. Quantitatively, the average current densities are increased by 21% and 11% as the backpressure is increased from 0 to 75 kPa and from 75 kPa to 150 kPa (gauge), respectively.

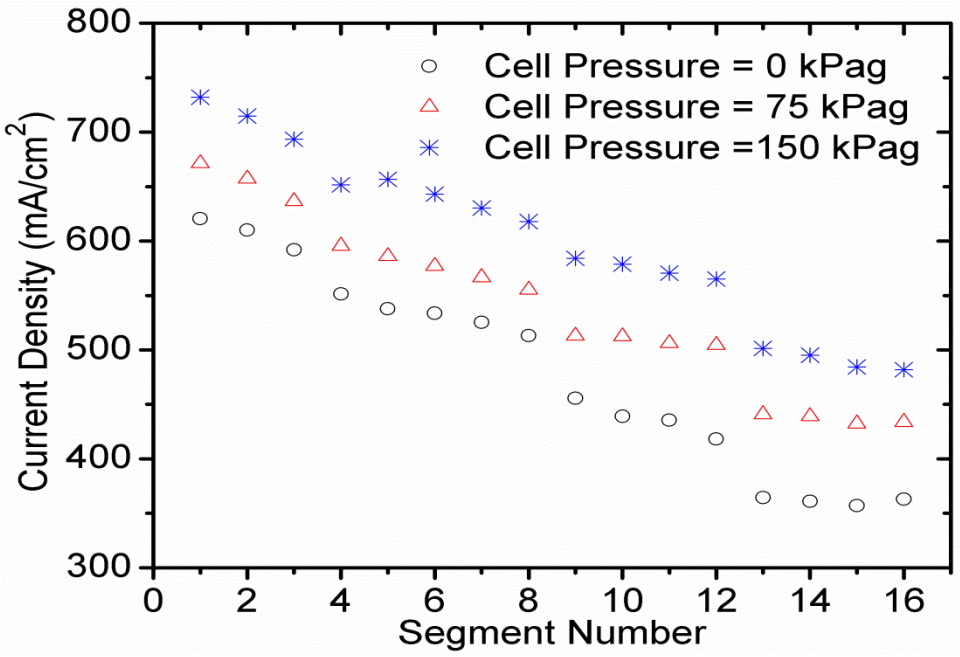

Figure 4.11: Effect of the cell backpressure on the current density distribution for the co-flow configuration. Measurement conditions: cell potential of 0.4 V, cell operating temperature of 65 °C, stoichiometry of 1.2 for the anode and air stoichiometry of 2 for the cathode, fully humidified for both cathode and anode gas stream.

Figure 4.12 presents the polarization curves for two selected regions (near the inlet and outlet) and three different cell backpressures under investigation. It shows that the magnitude of the local current density near the inlet region is higher than the outlet region for the same cell potential. Further, it indicates that the difference in the local current between the two regions became more noticeable at high current density.

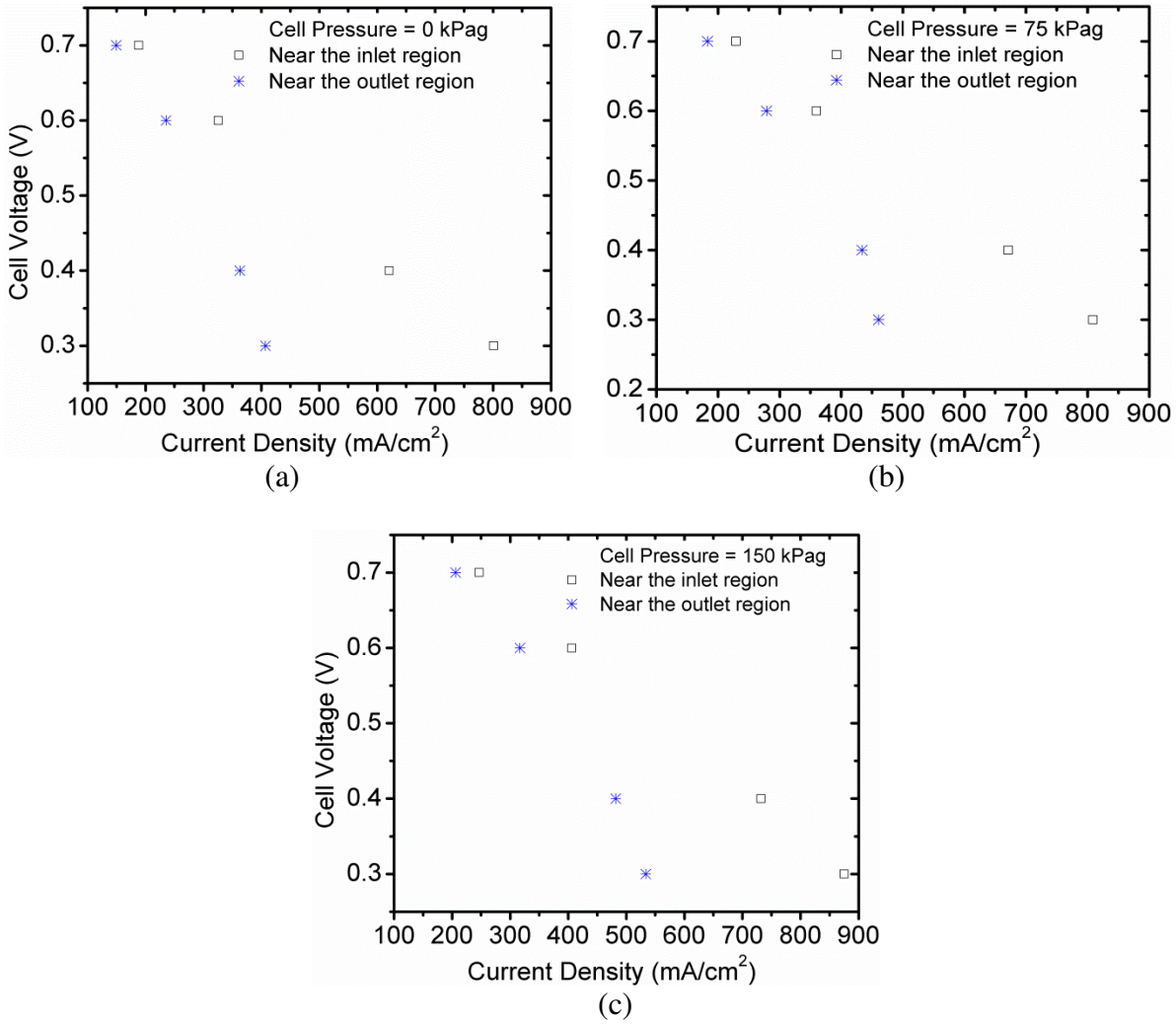

Figure 4.12: Effect of cell backpressure on the current density distribution for co-flow configuration and different regions and cell backpressure of (a) 0, (b) 75, and (c) 150 kPag, respectively. Measurement conditions: stoichiometry of 2 for the cathode, cell operating temperature of 65 °C, stoichiometry of 1.2 for the anode hydrogen gas and 2 for cathode, fully humidified for both cathode and anode gas stream.

Figure 4.13 shows that the local current density increases significantly in the region near the anode outlet (cathode inlet) for the counter-flow arrangement. It is observed from Figure 4.14 that the effect of the operating backpressure for the cross-flow is very different from those obtained from those in Figures 4.11 and 4.13. The improvement in the local current density values can be attributed to the increased electrochemical activities as a result of higher reactant concentration. Figure 4.14.b shows that the local current density distribution along the flow channel follows the H_2 flow direction. It signifies again the dominate impact of the H_2 stoichiometry ratio on the current distribution along the flow channels in a PEMFC.

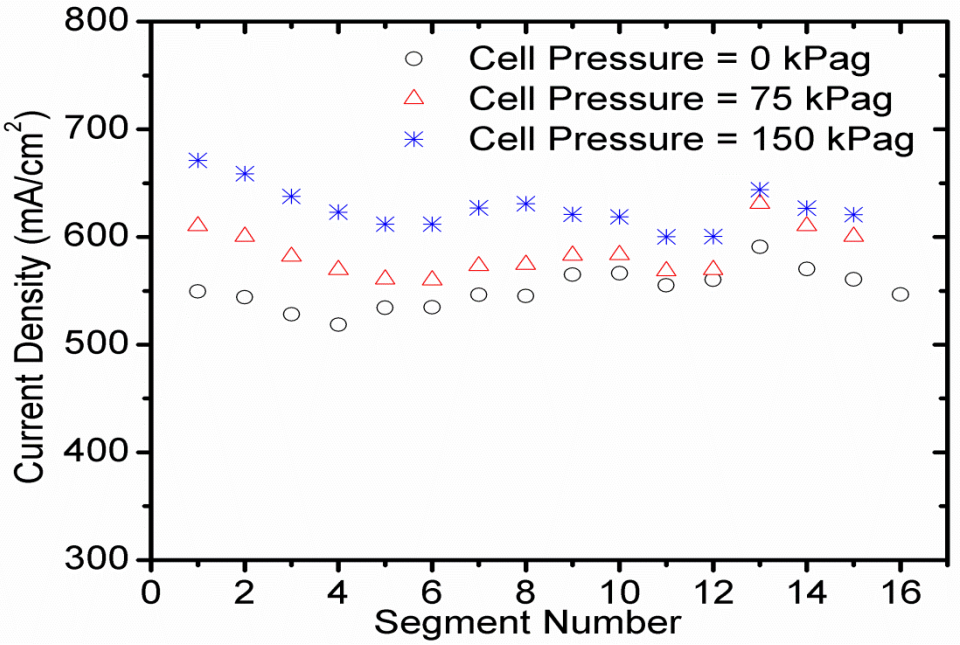

Figure 4.13: Effect of cell backpressure on the current density distribution for the counter-flow configuration. Measurement conditions: cell potential of 0.4 V, cell operating temperature of 65 °C, stoichiometry of 1.2 for the anode and air stoichiometry of 2 for the cathode, fully humidified for both cathode and anode gas stream.

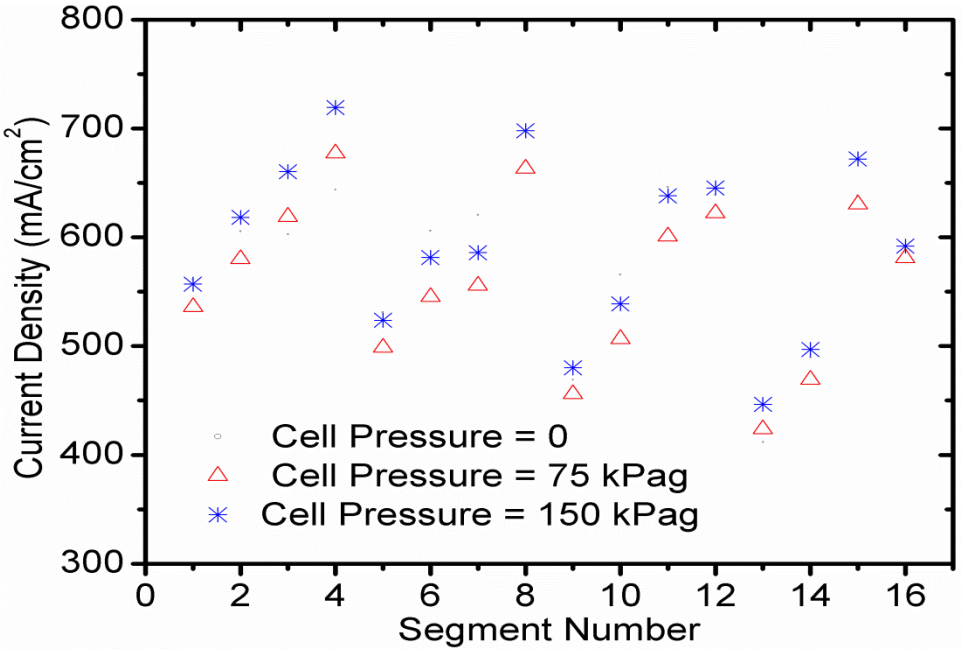

(a)

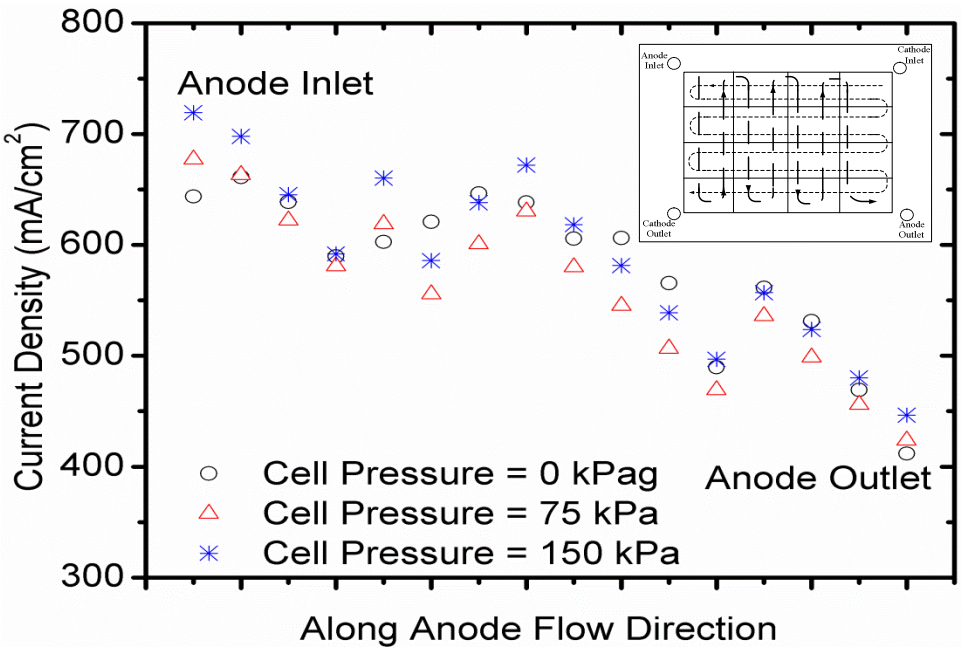

(b)

Figure 4.14: Effect of cell backpressure on the current density distribution for the cross-flow configuration. Measurement conditions: cell potential of 0.4 V, cell operating temperature of 65 °C, stoichiometry of 1.2 for the anode and air stoichiometry of 2 for the cathode, fully humidified for both cathode and anode gas stream. (a) Results plotted following the air flow direction, and (b) results plotted following the H2 flow direction.

4.2.4 Effect of Cell Temperature

Figures 4.15, 4.16, and 4.17 show the local current distributions at different cell temperatures for co-, counter-, and cross-flow arrangements, respectively. Fully humidified reactants are supplied at the same cell temperatures of 40 °C, 55 °C, and 70 °C, with the cell potential of 0.4 V. The anode and cathode stoichiometry ratios are fixed at 1.2 and 2, respectively. It is seen from Figure 4.15 that raising the cell temperature from 40 °C to 55 °C will only cause a very small increase in the local current density over most of the electrode surface; however, when the cell temperature is increased from 55 °C to 70 °C, the local current densities are enhanced significantly, particularly in the region near the inlet. The local current density can be improved by 5 % in the region near the inlet when the temperature increases from 40 ^{o}C to 55 ^{o}C, whereas an increase in the local current density of 15% is achieved when the cell temperature increased from 55 ^{o}C to 70 ^{o}C, indicating a significant increase in the local current density as well as the overall cell performance from 55 ^{o}C to 70 ^{o}C. Similar to Figure 4.15, the effect of increasing the cell temperature with the counter- or cross-flow arrangements can be seen in Figures 4.16 and 4.17, respectively. The general trends of current distribution profiles in these three figures are different from each other, but they show similar responses to the cell temperature. This is because of the catalytic activity and mass diffusion coefficient increase with the cell temperature; hence, a decrease in the activation polarization for both the oxygen reduction reaction and hydrogen oxidation reactions. That is, the local current density as well as the overall cell performance is strongly affected by the cell temperature.

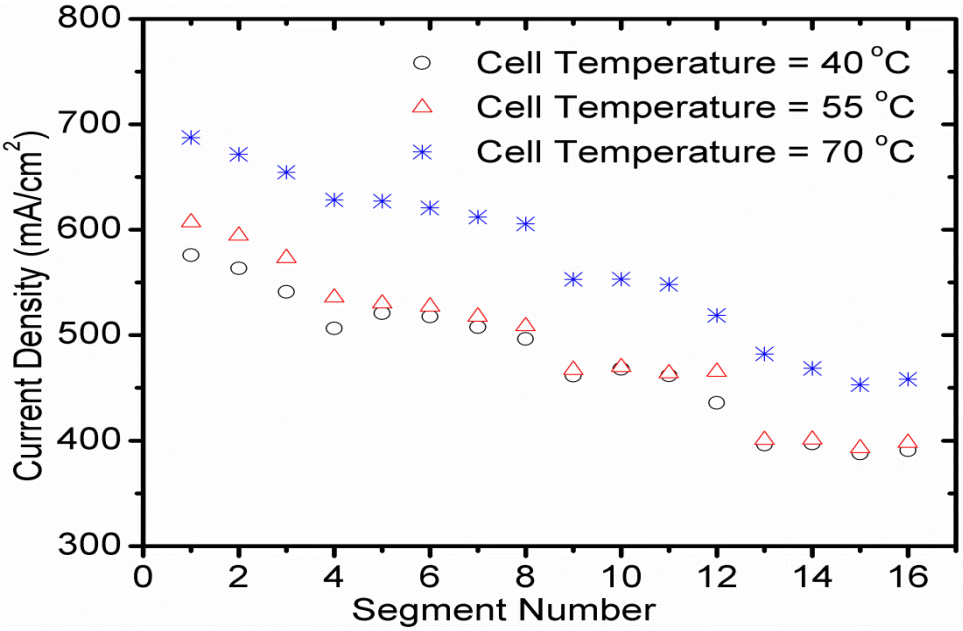

Figure 4.15: Effect of cell temperature on the current density distribution for the co-flow configuration. Measurement conditions: cell potential of 0.4 V, cell backpressure of 50 kPag, stoichiometry of 1.2 for the anode and air stoichiometry of 2 for the cathode, fully humidified for both cathode and anode gas stream.

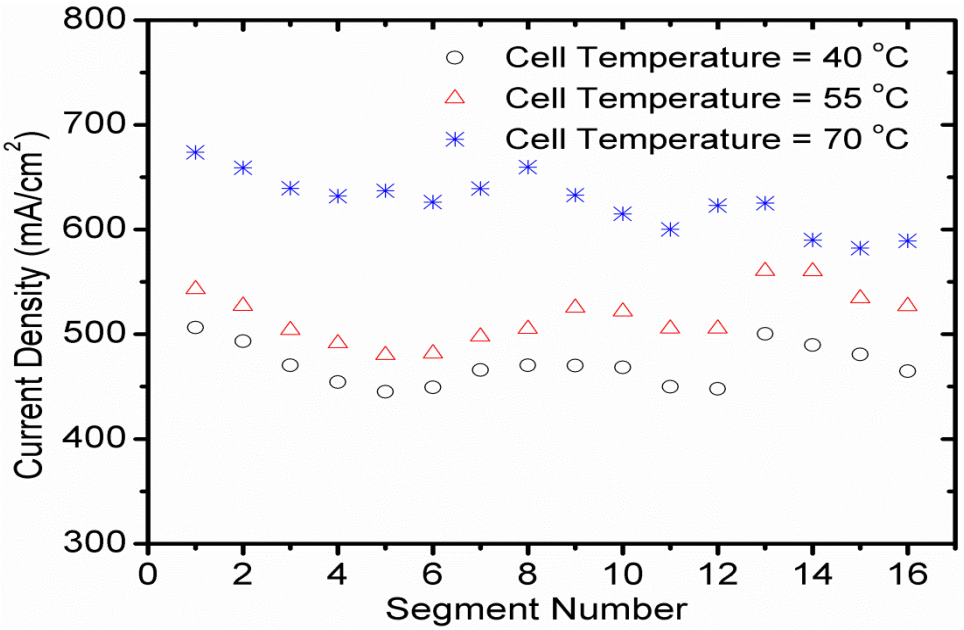

Figure 4.16: Effect of cell temperature on the current density distribution for the counter-flow configuration. Measurement conditions: cell potential of 0.4 V, cell backpressure of 50 kPag, stoichiometry of 1.2 for the anode and air stoichiometry of 2 for the cathode, fully humidified for both cathode and anode gas stream.

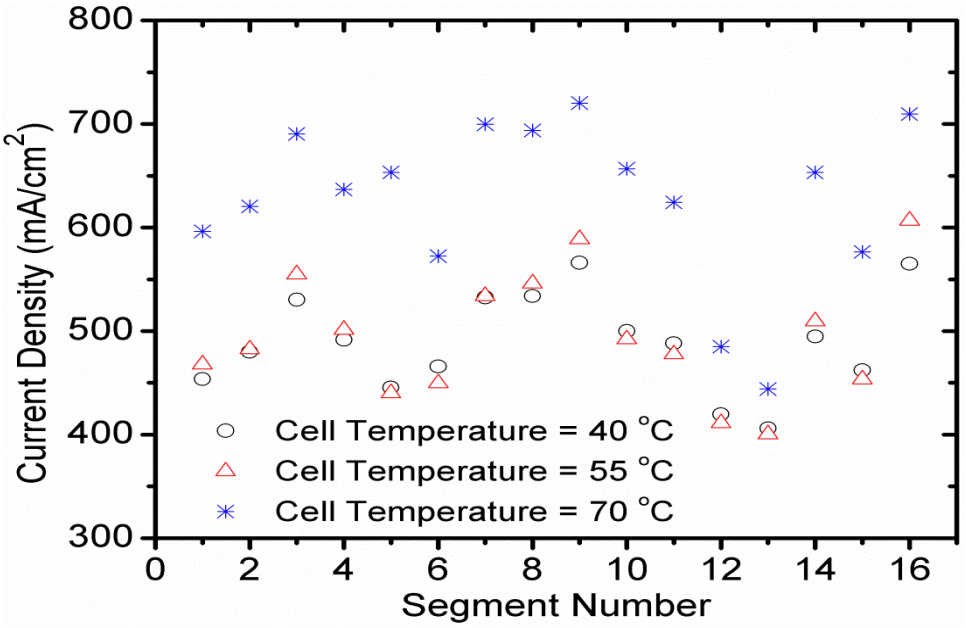

Figure 4.17: Effect of cell temperature on the current density distribution for cross-flow configuration. Measurement conditions: cell potential of 0.4 V, cell backpressure of 50 kPag, stoichiometry of 1.2 for the anode and air stoichiometry of 2 for the cathode, fully humidified for both cathode and anode gas stream.

4.2.5 Effect of Inlet Relative Humidity (Rh)

It is expected that there exits an optimum reactant humidity for better cell performance [117]. In the present study, the FCATS-S800 fuel cell test station is employed for the control and conditioning of the reactant gas streams [118]; specifically, the reactant gases are humidified by a steam injection method, with de-ionized (DI) water is used for steam generation. The effects of the relative humidity on the local current distribution in a PEMFC for co-, counter-, and cross-flow arrangements are shown in Figures 4.18, 4.19, and 4.20, respectively. The fuel cell temperature is fixed at 65 °C; the cathode and anode stoichiometry ratios are fixed at 2 and 1.2, respectively; and the reactant relative humidity at the cell inlet is 25%, 50%, and 100%, respectively. For the relative humidity of 25% and 50%, Figure 4.18 shows that local current density is low near the inlet, increases along the flow channels towards the channel midpoints, and decreases in the region near the outlet. Local current

densities are higher at the relative humidity of 50% near the inlet region and lower near the outlet when compared with the relative humidity of 25%. The higher cell performance in the inlet region can be attributed to better membrane hydration and proton conductivity (and hence lower Ohmic overpotential) at higher inlet humidities. The lower cell performance near the outlet could be due to water flooding in the cathode at higher inlet humidities [119]. As the inlet humidity is increased to 100%, the overall cell performance is degraded, as shown in Figure 4.18. Under such conditions, the local current density is the highest in the region near the inlet then decreases sharply along the flow channels and became the lowest in the region near the outlet. This signifies the generation of a sufficient amount of water from the electrochemical reaction for the membrane self-hydration; hence, this observation may suggest that the water flooding issue in the cathode can be minimized by avoiding the high degree of relative humidity in the reactant streams, which is consistent with other experimental results reported [120-122].

The local current density distribution for the counter-flow arrangement is shown in Figure 4.19. It is seen that the local current density is almost uniform over the cell surface, and that relative humidity in the reactant streams has little impact on the local current profile compared to Figure 4.18. This seems to suggest that water can transport between anode and cathode stream to even out its distribution in such a manner that membrane humidification and water flooding phenomena are balanced out to produce fairly uniform current distribution.

The local current density distribution inside the PEMFC for a cross-flow arrangement is shown in Figure 4.20. It is seen that a reactant with 50% relative humidity can lead to the most uniform distribution for the local current in a PEMFC, when compared to 25% and 100%. As a result, the overall cell performance is improved as well. However, the local current density in the anode inlet region with the reactant relative humidity of 25% and 50% is slightly lower than that with 100% relative humidity. This might be attributed to the membrane dehydration as a result of a lower degree of reactant stream humidification in the inlet region.

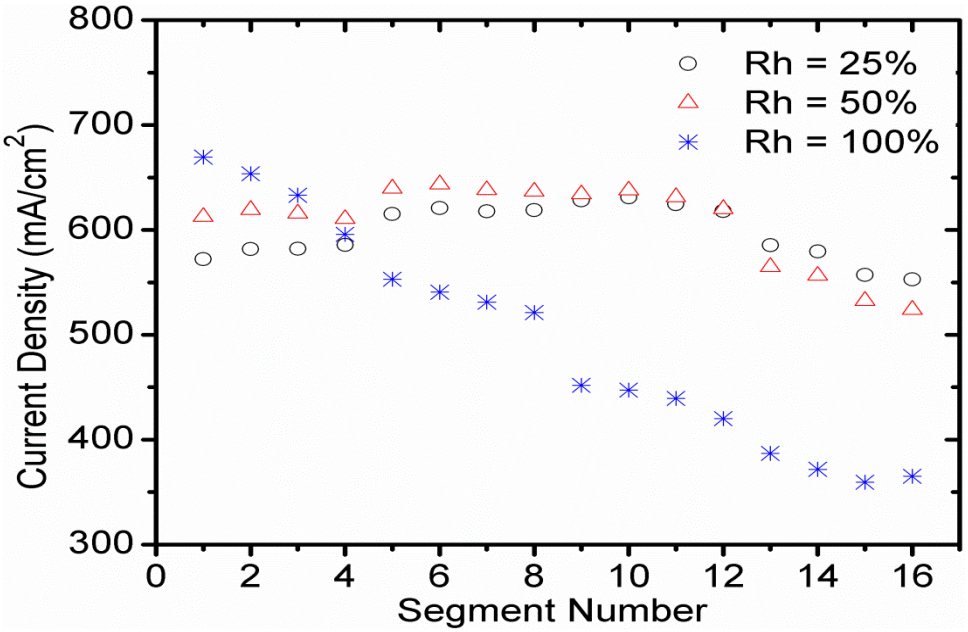

Figure 4.18: Effect of reactant relative humidity (Rh) on the current density distribution for the co-flow configuration. Measurement conditions: cell potential of 0.4 V, cell temperature of 65 ^{o}C, cell backpressure of 50 kPag, stoichiometry of 1.2 for the anode and air stoichiometry of 2 for the cathode.

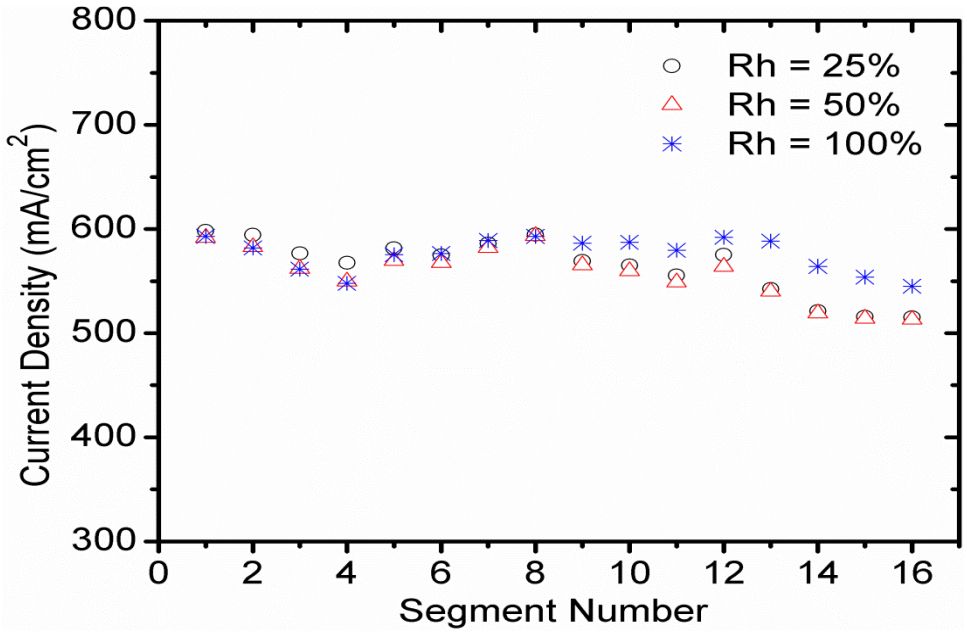

Figure 4.19: Effect of reactant relative humidity (Rh) on the current density distribution for the counter-flow configuration. Measurement conditions: cell potential of 0.4 V, cell temperature of 65 ^{o}C, cell backpressure of 50 kPag, stoichiometry of 1.2 for the anode and air stoichiometry of 2 for the cathode.

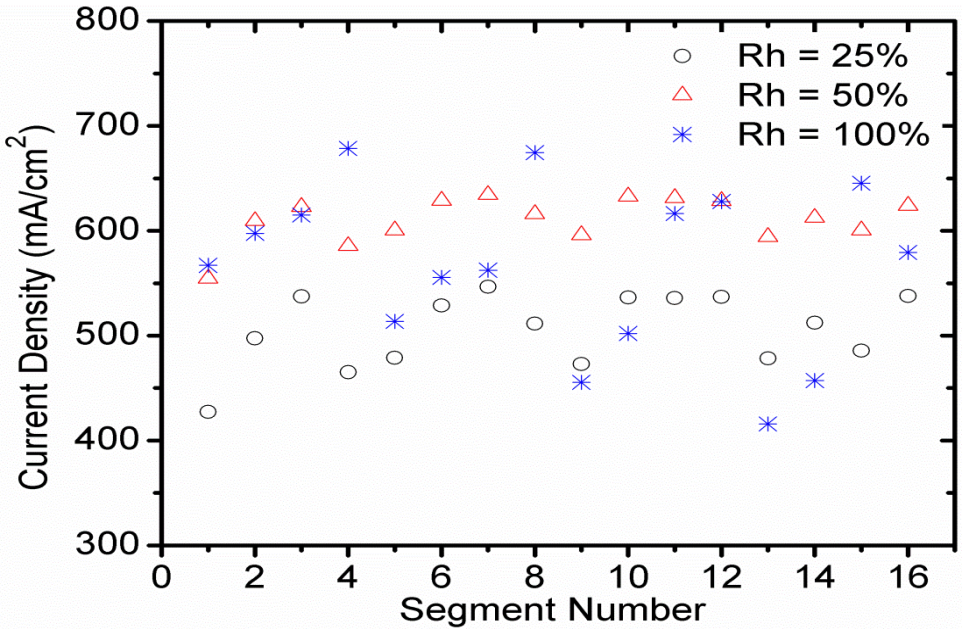

Figure 4.20: Effect of reactant relative humidity (Rh) on the current density distribution for the cross-flow configuration. Measurement conditions: cell potential of 0.4 V, cell temperature of 65 ^{o}C, cell backpressure of 50 kPag, stoichiometry of 1.2 for the anode and air stoichiometry of 2 for the cathode.

Part (III)

Dynamic characteristics of the Local Current Density in a PEMFC with Different Operating Conditions

4.3 Dynamic Characteristics of the Local Current Density in Proton Exchange Membrane Fuel Cells with Different Operating Conditions

The continuous change in load of the automotive engines necessities the investigation of the dynamic performance of PEMFC. Since the PEMFC with co-flow arrangement results in large variations in magnitude of the local current density between different regions in the cell (especially between the inlet and outlet), it is worthwhile to investigate the dynamic characteristics of the local current density along the flow channels for the PEMFC with co-flow arrangement. The investigation of the dynamic characteristics can highlight the correlations between the crucial operating conditions and local current density behavior inside the fuel cell. It is expected that the general trend of the local current density profiles for the other two arrangements (counter- and cross-) under dynamic conditions will be similar to those under steady state conditions presented previously. However, the difference in the dynamic behavior of the local current density along the flow channel with cross- and counter-flow over the co-flow arrangement is the degree of fluctuation. This is because the degree of fluctuation is directly influenced by the water generation/accumulation, reactant concentrations, and the input operating conditions. Thus, the effect of various operating conditions, including air stoichiometry ratio, cell pressure, and relative humidity on the dynamic characteristics of local current density in a PEMFC with co-flow arrangement only, will be discussed in this part of thesis.

To approve the repeatability, selected tests are repeated three times for each operating condition and each current measurement is recorded at a frequency of 1 Hz over a sufficient period of time from the changing in the experiment condition. Shown in Figure 4.21 are three measurements of the transient characteristic of the local current density near the inlet region that were taken at three different times. All relevant operating conditions are maintained constant as given in Table 3.2 except that the cell voltage is varied in a complete cycle between 0.7 V and 0.3 V. It is seen in Figures 4.20 and 4.21 that the results of the three repeated tests agree fairly well with each other since they show identical magnitudes and trends of the average current density especially in the time domain, suggesting that

repeatability of the measurements is achieved in the present study. As shown in Figure 4.21, the fluctuations in the local current density measured are minimal for the high cell voltage of 0.7 V, corresponding to an average cell current density of about 200 mA/cm^2. However, the local current density fluctuates considerably when the cell voltage is lowered to 0.3 V, corresponding to a much higher average cell current density of nearly 700 mA/cm^2. Figure 4.22 shows the results from the fast Fourier transform (FFT) analysis for the time domain shown in Figure 4.21 with the cell voltage of 0.3 V. It is seen in Figure 4.22 that there is a lack of dominant frequency under these given operating conditions for the three tests conducted.

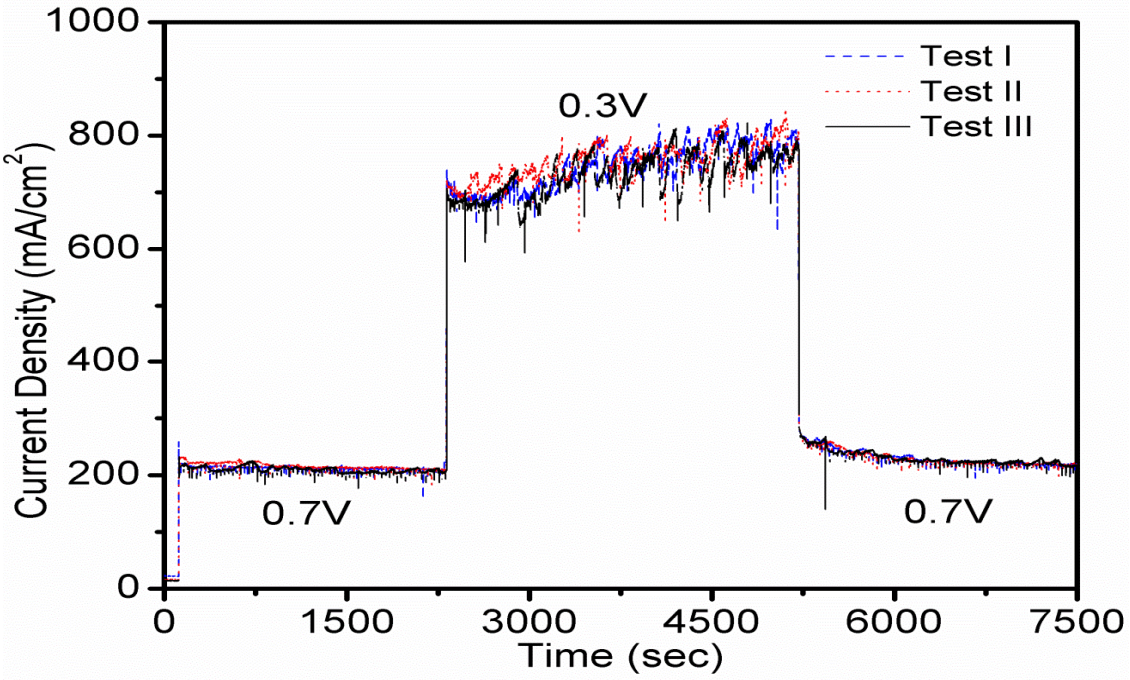

Figure 4.21: Dynamic characteristics of the local current density near the inlet region of a tested cell (Segment #1 shown in Fig. 3.18). Measurement conditions conducted at three different times: cell potential varied between 0.7 V and 0.3 V, cell backpressure of 50 kPag, stoichiometry of 2 for the cathode air and 1.2 for the anode hydrogen gas, fully humidified for both cathode and anode gas stream.

In the following sections, the effect of various operating conditions on the transient local current density will be presented only for segments with even numbers, as illustrated in

Figure 3.18. Presenting the dynamic characteristic of the local current density for eight segments instead of sixteen can be sufficient to extrapolate useful information for the entire cell. This is because the above results for the local current density distribution in PEMFC with co-flow arrangement showed that the local current density decreases monotonically along the flow channels and become almost aligned with the reactant stream flow arrangement (flow channel layout) [85, 92]. Therefore, all the results presented in this study are for the co-flow arrangement of the anode and cathode reactant gas streams.

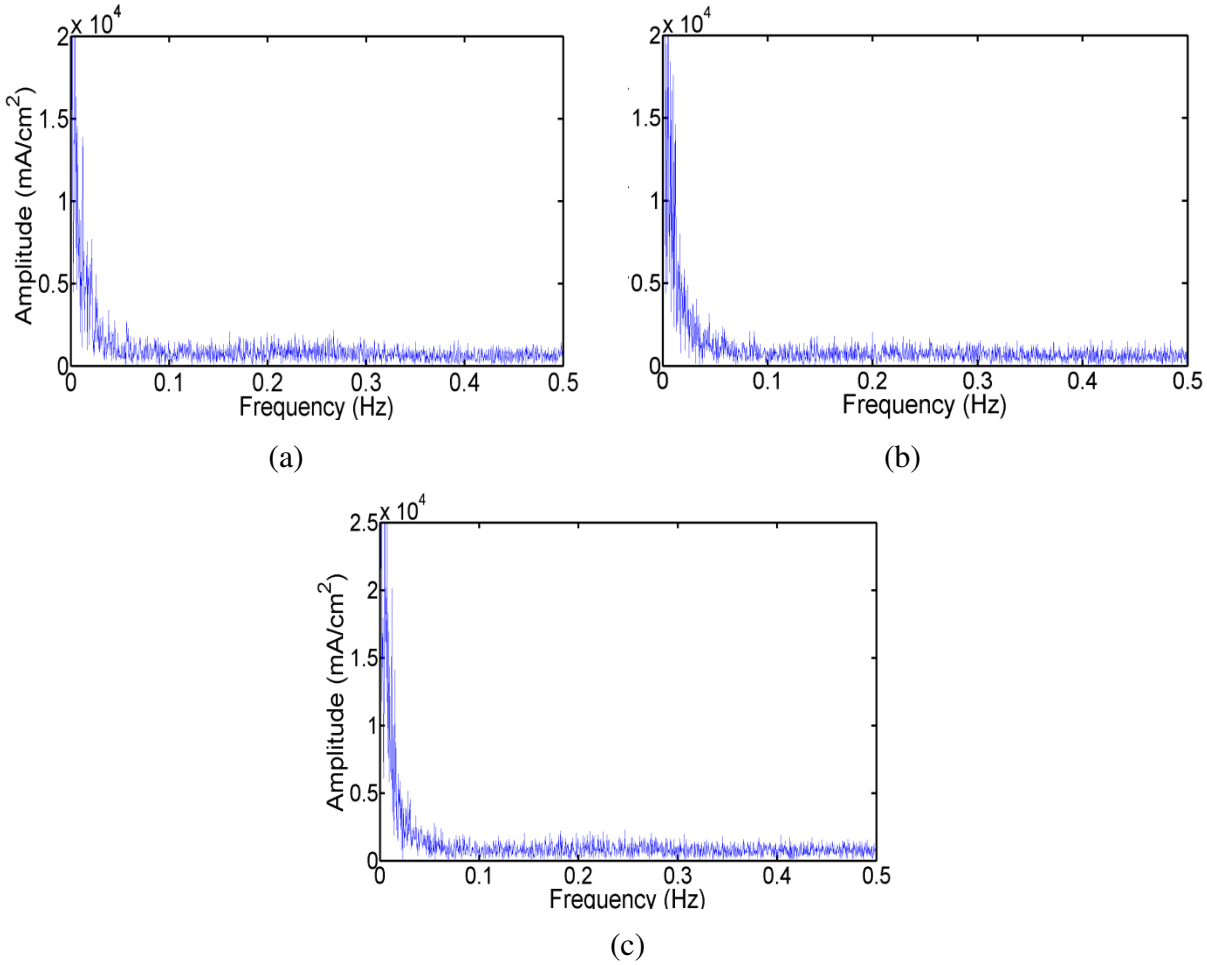

Figure 4.22: Results for the Fast Fourier transform (FFT) analysis for the three tests shown in Fig. 4.21 conducted at the nominally identical operation conditions: cell potential of 0.3 V, cell backpressure of 50 kPag, stoichiometry of 2 for the cathode air and 1.2 for the anode hydrogen gas, fully humidified for both cathode and anode gas stream.

4.3.1 Effect of the Air Stoichiometry Ratio

Figure 4.23 shows the effect of air stoichiometry ratio on the dynamic characteristic of the local current density at different regions in the cell (near the flow channel inlet and outlet, corresponding to Segment #1 and #16 in Figure 3.18, respectively). The results are measured for the cell potential of 0.7 V, cell temperature of 65 ^{o}C, and anode (hydrogen) stoichiometry of 1.2. All the operating conditions are maintained constant, as given in Table 3.2, except the air stoichiometry ratio. The air stoichiometry ratio is increased from a minimum value of 2 to 3.5 and then to the maximum value of 5. Subsequently, the air stiochiometry is then decreased from the maximum value of 5 to 3.5 and then back to the initial value of 2. Each complete cycle takes about 6000 sec, as illustrated in Figure 4.23. It is seen that the average current density near the inlet region is larger than its counterpart near the outlet region because the reactant oxygen concentration decreases from the flow channel inlet to the outlet as a result of cell reaction. Also, the average current density remains virtually the same as the air stoichiometry is varied. However, the fluctuation is reduced for higher stoichiometry values. The current density near the outlet region has a larger fluctuation than its counterpart near the inlet region, attributed to the higher water content near the outlet region.

Presented in Figure 4.24 are the corresponding transient characteristics of the local current density along the flow channels at eight segments under the same experimental conditions as those shown in Figure 4.23. It is seen that the local current densities are the highest in the region near the flow channel inlet (i.e., Segment #1 in Figure 4.23 and Segment #2 in Figure 4.24), decrease along the flow direction, and become lowest in the region near the outlet (i.e., Segment #16), similar to the steady state results [84, 85]. The reduction in the local current densities may be attributed to the reactant depletion along the flow direction. It is also observed that the local current density is very sensitive to the air flow rate. The local current density experiences severe fluctuation (unstable performance) at the low air stoichiometry ratio of 2, especially in the region near the cell outlet. However, an increase in the air stoichiometry ratio from 2 to 3.5 and then to 5 reduces the degree of the fluctuation dramatically.

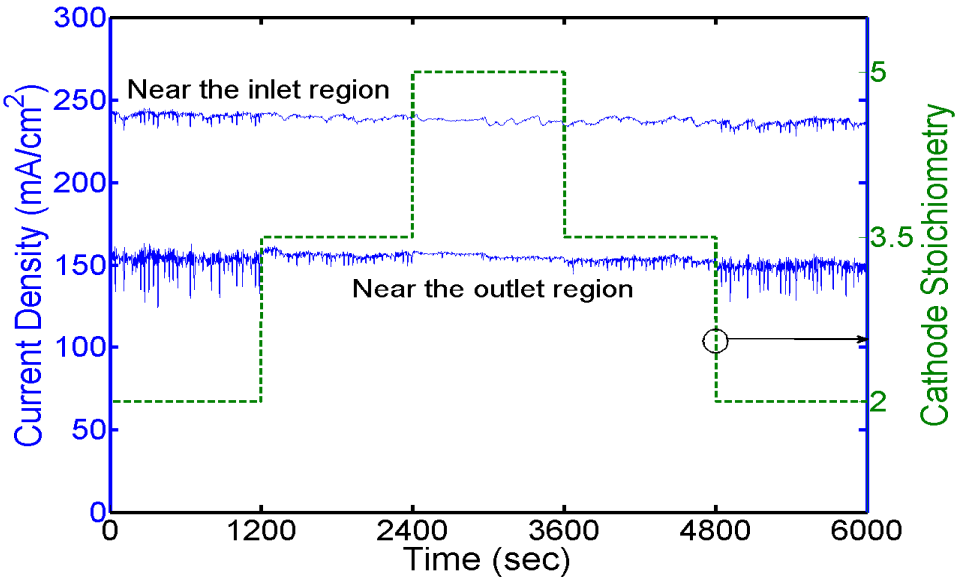

Figure 4.23: Dynamic characteristics of the local current density near the inlet and outlet regions of the tested PEMFC for different air stoichiometry ratios. Measurement conditions: cell potential of 0.7 V, cell backpressure of 50 kPag, cell operating temperature of 65 °C, stoichiometry of 1.2 for the anode hydrogen gas, fully humidified for both cathode and anode gas stream.

In the absence of a sufficient air flow rate for a given air flow condition, it is seen that the fluctuations in the local current density increase along the flow channel and becomes severest near the flow exit, especially for the low air stoichiometry value of 2 tested. It is expected that the local current fluctuation will increase its intensity as the air stoichiometry is further reduced below 2. It might be hypothesized that the local current becomes more sensitive or affected as the local air concentration is reduced while water concentration is increased along the flow channel. Since the air stoichiometry of 2 is often considered as an "industry standard" for the air flow rate in the cathode, the conventional operating condition might be subject to significant performance fluctuations, especially for higher backpressure operation when the fluctuations intensifies as will be shown later. Therefore, for a cell operating in a transient loading condition, increasing air stoichiometry might be considered appropriate, although this will incur an additional parasitic power loss associated with providing higher air flow.

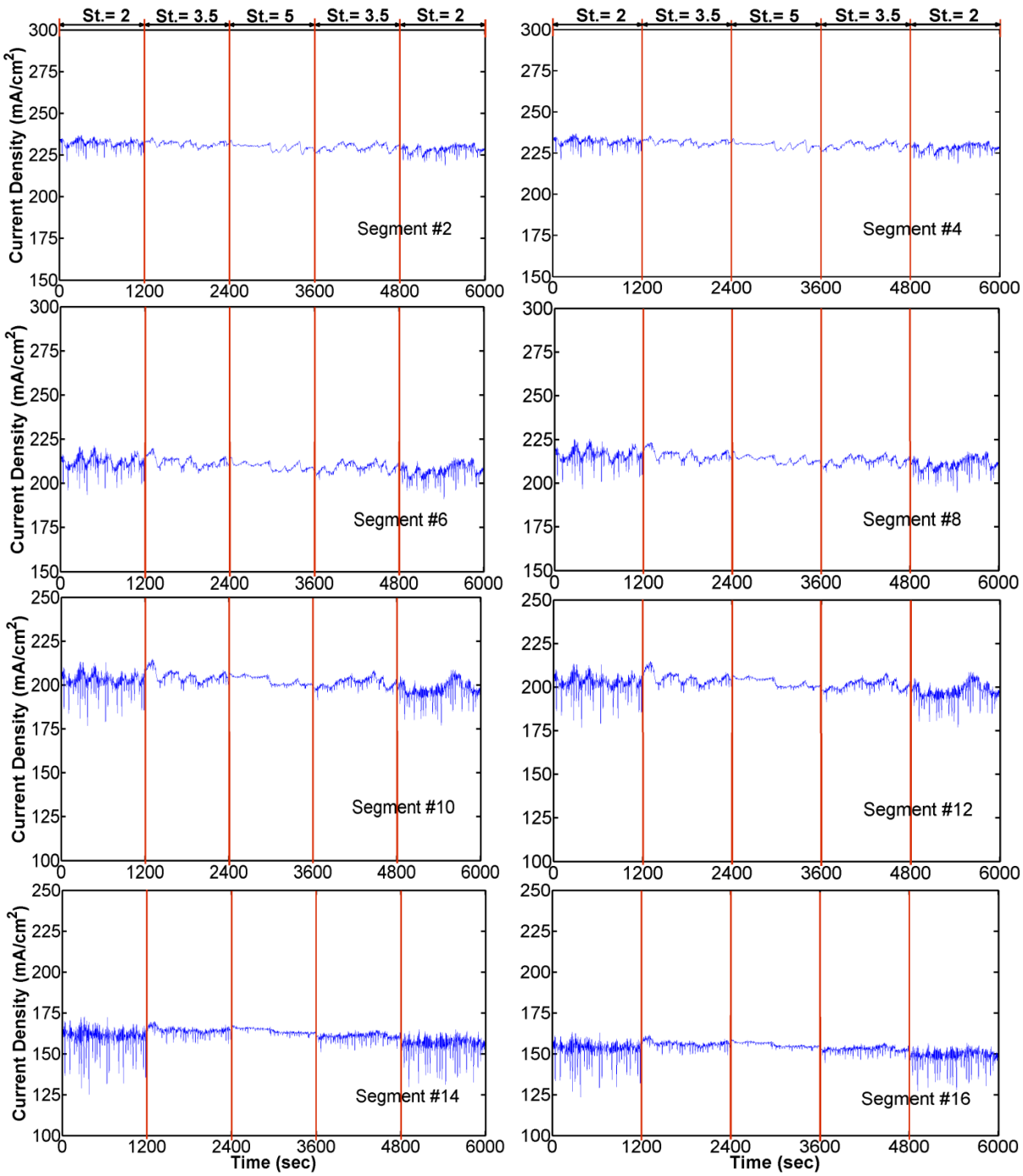

Figure 4.24: Dynamic characteristics of the local current density for all the segments with even numbers along the flow channels for different air stoichiometry ratios. Measurement conditions: cell potential of 0.7 V, cell backpressure of 50 kPag, cell operating temperature of 65 °C, stoichiometry of 1.2 for the anode hydrogen gas, fully humidified for both cathode and anode gas stream.

Figures 4.25 and 4.26 show the effect of air stoichiometry ratio on the dynamic characteristic of the local current density for low cell potential of 0.3 V, corresponding to a high value of the average cell current density (or the cell loading); while all other operating conditions are maintained the same as those for Figures 4.23 and 4.24.

Figure 4.25 shows only the dynamic characteristics of the local current density at regions near the inlet and outlet, respectively, whereas Figure 4.26 shows the dynamic characteristic of the local current density along the flow channels for segments with even numbers. It is seen that at this low cell potential of 0.3 V, the local current density is much larger compared to the results shown in Figures 4.23 and 4.24, which is for the cell potential of 0.7 V and otherwise identical operating conditions. With the much larger current density values, the air flow rate is increased several times, even though the stoichiometry remains the same for both cases. Figure 4.25 shows that the local current density is higher in the inlet region than in the outlet region; the fluctuation is less in the inlet region than in the outlet region when the air stoichiometry is higher, similar to those observed in Figure 4.23. However, when Figure 4.25 is compared to Figure 4.23, it is clear that the difference between the local current density at the inlet and the outlet is greater for the low cell potential of 0.3 V than the corresponding value for the high cell potential of 0.7 V and that the fluctuations are also increased for the low cell potential of 0.3 V. As the air stoichiometry is increased from 2 to 3.5, and then to 5, high frequency fluctuation is suppressed, while low frequency fluctuation remains. It is also seen from Figure 4.26 that the amplitude of fluctuation is the largest near the flow channel inlet region reduces toward the flow channel exit region; and the high frequency fluctuations increase in the flow direction towards the flow channel exit. The transient response in the local current density shown in Figure 4.26 is in general qualitatively similar to that shown in Figure 4.24 for higher cell voltage; for example, the high frequency fluctuations increase in the flow direction towards the flow channel exit. However, it is seen in Figure 4.26 that the amplitude of fluctuation is the largest near the flow channel inlet region and reduces toward the flow channel exit region [123, 124]. This is perhaps because of the operating condition of low cell voltage (and high current density), the absolute air flow rate is high, even though the

air stoichiometry value is the same, and the high air flow rate might cause the excess removal of water and the membrane electrolyte to dry out in the near inlet region. Product water is formed along the flow direction, alleviating this problem along the flow channel. This is consistent with the literature that shows that excessive air stoichiometry ratio in the region near the inlet leads to a negative impact on the local current density [124].

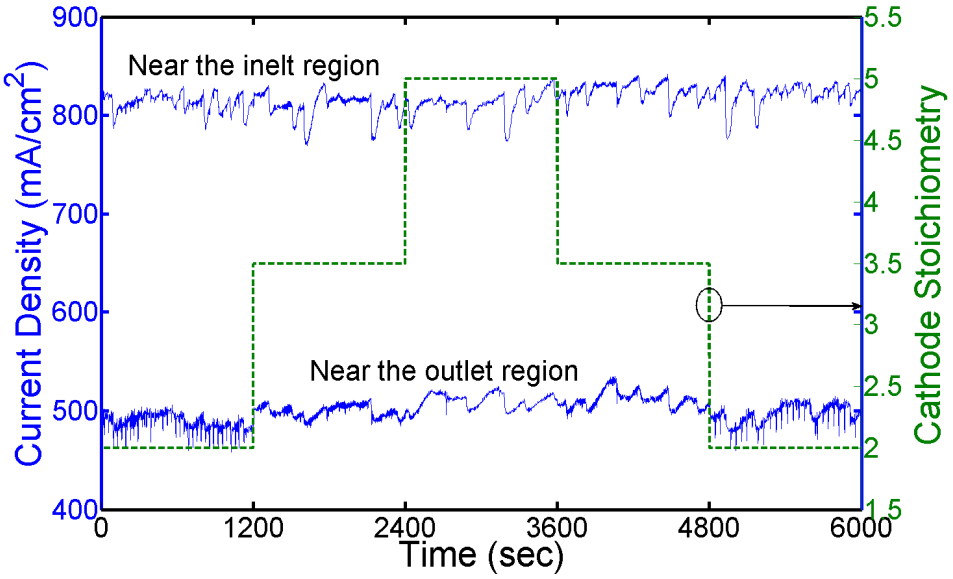

Figure 4.25: Dynamic characteristics of the local current density near the inlet and outlet regions, respectively, for the cell tested for different air stoichiometry ratios. Measurement conditions: cell potential of 0.3 V, cell backpressure of 50 kPag, cell operating temperature of 65 °C, stoichiometry of 1.2 for the anode hydrogen gas, fully humidified for both cathode and anode gas stream.

Figure 4.27 shows the dynamic characteristics of the local current density for air stoichiometry ratios of 2 and 5, and their corresponding frequency spectrum obtained through a fast Fourier transform (FFT) analysis in the region near the flow inlet (Segment #2 shown in Figure 3.18) over a period of 1200 sec, the data is a subset of those shown in Figure 4.25 earlier. A similar result is shown in Figure 4.28 for the local current density in the region near the cell outlet (Segment #16). It is seen that the dominant frequency of fluctuations is at a very low frequency, as the air stoichiometry of 2 a small peak occurs at the frequency of about 0.18 Hz for the near inlet region, and this peak values increases for the outlet region shown in Figure 4.28c.

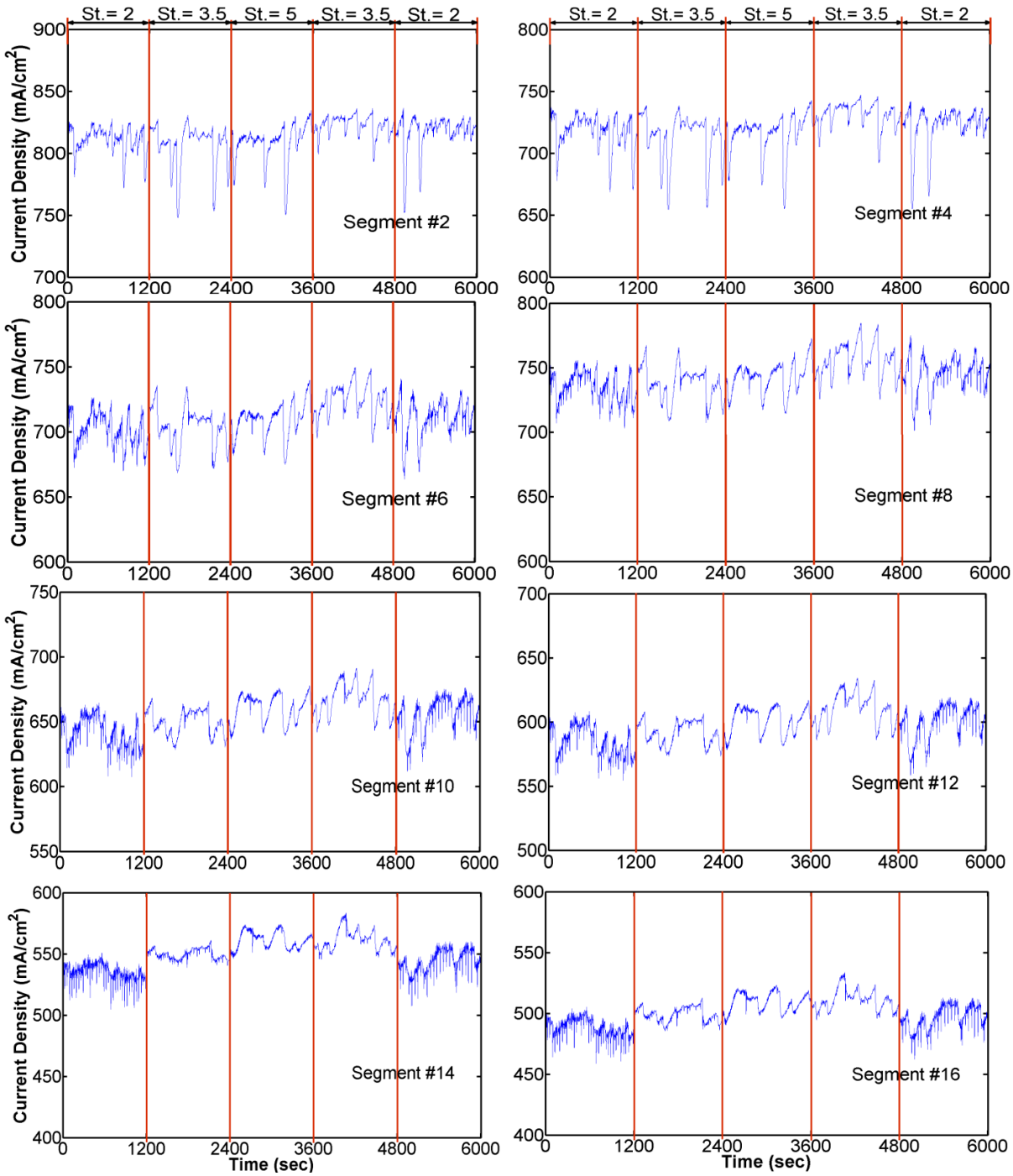

Figure 4.26: Dynamic characteristics of the local current density for all the segments with even numbers along the flow channel for different air stoichiometry ratios. Measurement conditions: cell potential of 0.3 V, cell backpressure of 50 kPag, cell operating temperature of 65 °C, stoichiometry of 1.2 for the anode hydrogen gas, fully humidified for both cathode and anode gas stream.

However, for the higher air stoichiometry of 5 the peak near 0.18 Hz disappears and only the low frequency fluctuations remain. For higher stoichiometry values, the reactant flow rate increases significantly in accordance. This will result in a higher reactant concentration over the active sites and better water removal throughout, benefiting the region downstream where product water is removed, but which might cause a problem for the inlet region causing, membrane dryout as mentioned earlier. Further, higher air stoichiometry will accompany with higher pumping power requirement, leading to decreased overall system efficiency [118]. A comparison of the results shown in Figure 4.27 a and b with those in Figure 4.28 a and b for the air stoichiometry of 2 and 5, respectively, reveals that at the low stoichiometry of 2, the fluctuations in the inlet region are less than in the outer region; and it is opposite for the high stoichiometry of 5. As mentioned earlier, this observation can be explained by the water content and distribution in the cell. Excessive water in the region near the cathode outlet has been observed in operating PEMFC [111, 116].

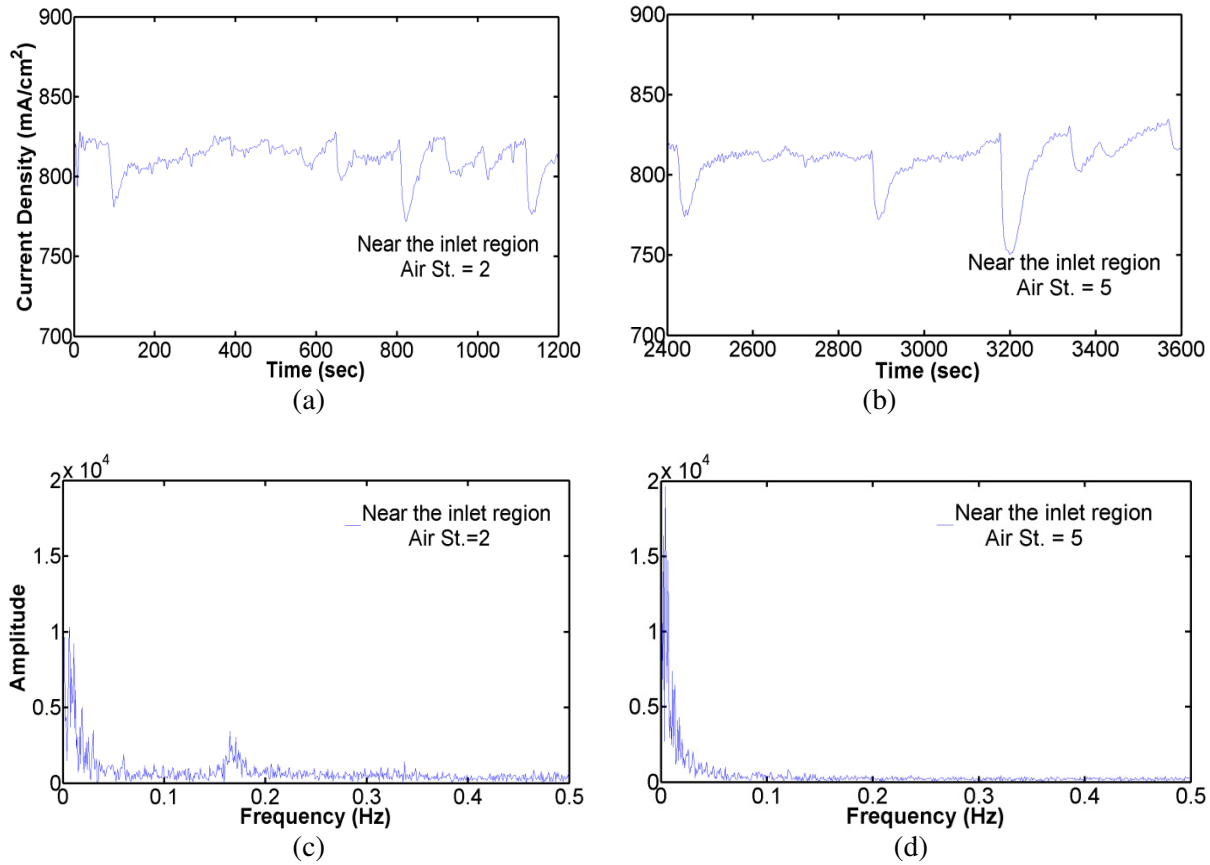

Figure 4.27: Dynamic characteristics of the local current density in region near the cell inlet for the cathode stoichiometry of 2 (a) and 5 (b), and their corresponding frequency spectrum (c) and (d), respectively. Measurement conditions: cell potential of 0.3 V, cell backpressure of 50 kPag, cell operating temperature of 65 °C, stoichiometry of 1.2 for the anode hydrogen gas, fully humidified for both cathode and anode gas stream.

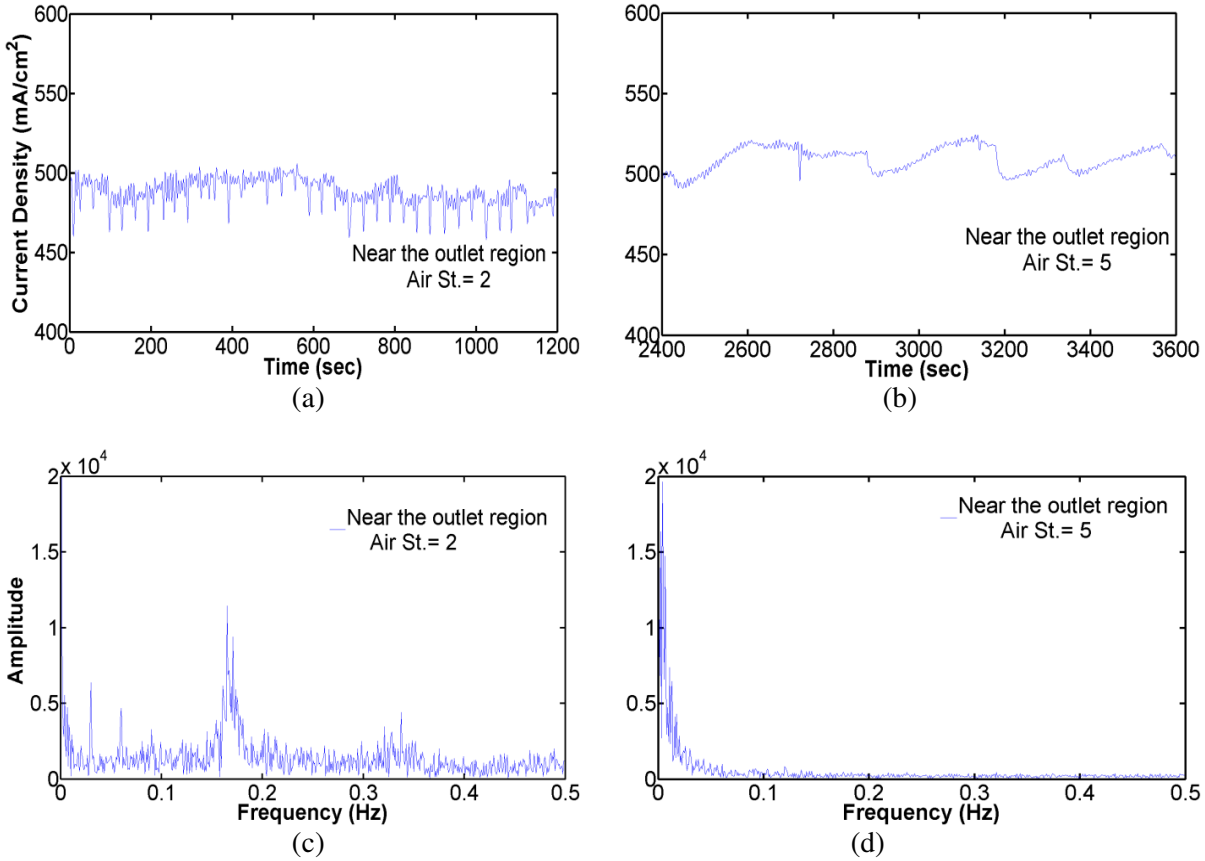

Figure 4.28: Dynamic characteristics of the local current density in region near the cell outlet for the cathode stoichiometry of 2 (a) and 5 (b), and their corresponding frequency spectrum (c) and (d), respectively. Measurement conditions: cell potential of 0.3 V, cell backpressure of 50 kPag, cell operating temperature of 65 °C, stoichiometry of 1.2 for the anode hydrogen gas, fully humidified for both cathode and anode gas stream.

4.3.2 Effect of Cell Backpressure

The dynamic characteristics of the local current density along the flow channels of the tested PEMFC are investigated for three different backpressures of 20, 75, 150 kPag for both anode and cathode side, and the results are shown in Figures 4.29 and 4.30 for different regions and cell potentials of 0.7 V and 0.3 V, respectively. It is seen in Figure 4.29 and 4.30 that as the cell operating backpressure is increased, the local current density increases as well; however, this accompanies with the significant increase in the fluctuations in the current density, especially near the cell outlet (Segment #16) at the lower cell potential of

0.3V. This is because water production in the cell is enhanced due to the higher current density at higher operating pressure, but the diffusion coefficient, being inversely proportional to pressure, reduces, resulting in water accumulation in the cell structure, especially near the cell outlet region due to the accumulation of the product water. As noticed before, the fluctuations could be associated with the water content and transport in the cell structure. This suggests that a cell operating at high backpressure would have additional problems associated with transient loading to be resolved, although the average (steady state) cell performance is improved. As mentioned earlier, providing a higher air stream flow can alleviate the cell performance fluctuations, but providing air flow at higher flow rate at higher backpressure would incur excessively high parasitic pumping power. Experience indicates that air compression for such a scenario could consume as high as over 35% of the stack power output.

It is also seen in Figure 4.29 that at the high cell potential of 0.7 V almost instantaneous increases in the average values of the local current density occurs when the cell backpressure is increased stepwise, although accompanied with more intensified fluctuations. However, at the low cell potential of 0.3 V the increase in the average values of the local current density becomes gradual, and the clear instantaneous change could not be observed, but the cell backpressure change can be identified by the changes in the fluctuations. This is even more evident in Figure 4.31 where the local current density is presented along the flow direction. It is seen that as the cell operating backpressure is changed, the changes in the average local current density levels off along the flow direction, such that for Segment #12, the average local current density is hardly changed when the cell backpressure is changed, although the fluctuations are clearly changed almost simultaneously. This observation again suggests that the benefit of operating at high cell backpressure diminishes for transient loading application.

As aforementioned, a higher cell backpressure tends to lower the water removal capability of the reactant gas streams especially in regions near the outlet, and increases the degree of the water presence inside the cell structure, which is considered responsible for the

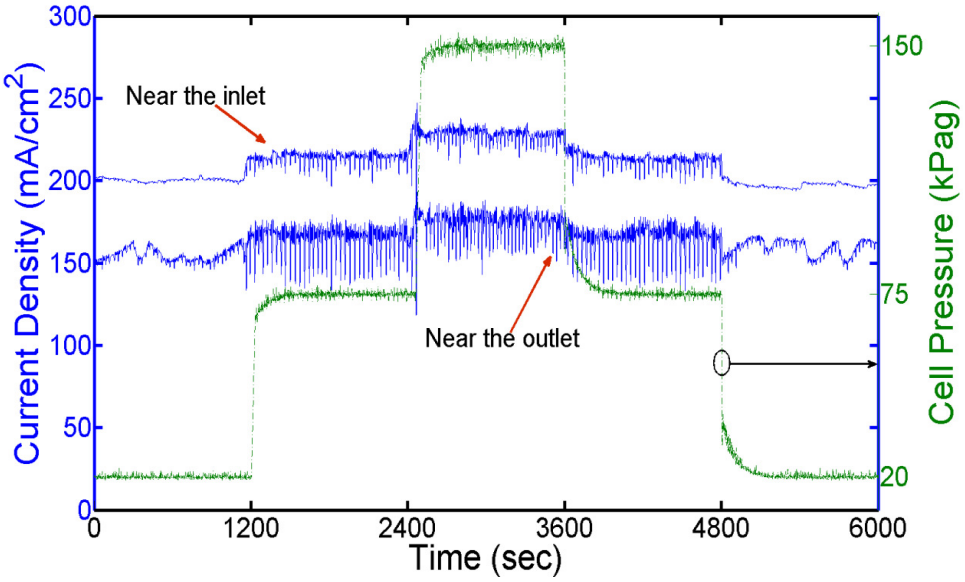

Figure 4.29: Dynamic characteristic of the local current density for different cell backpressures near the inlet and outlet regions. Measurement conditions: cell potential of 0.7 V, cell operating temperature of 65 °C, stoichiometry of 2 for the cathode air, stoichiometry of 1.2 for the anode hydrogen gas, fully humidified for both cathode and anode gas stream.

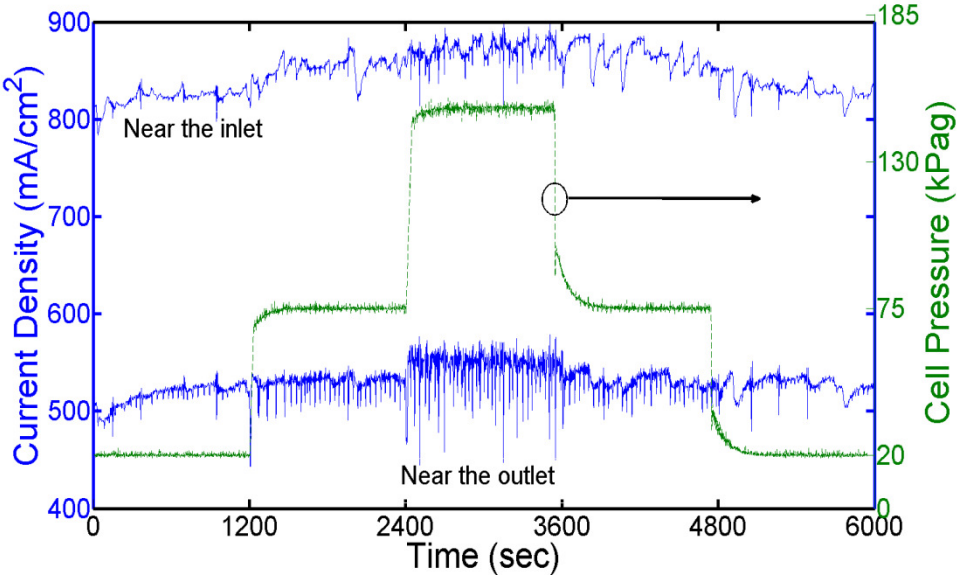

Figure 4.30: Dynamic characteristic of the local current density for different cell backpressures near the inlet and outlet regions. Measurement conditions: cell potential of 0.3 V, cell operating temperature of 65 °C, stoichiometry of 2 for the cathode air, stoichiometry of 1.2 for the anode hydrogen gas, fully humidified for both cathode and anode gas stream.

considerable fluctuation (instability) in the local current density shown for the higher pressures of 75 kPag and 150 kPag. This is further exemplified by the results shown in Figures 4.32 and 4.33 for the degree of fluctuations in regions near the inlet and outlet for the cell potential of 0.3 V but at different cell pressures. These results can be obtained by zooming in the local current density measurement for the two regions of the cell at the pressures of 20 kPag and 150 kPag, respectively, which correspond to the time increment between 0-1200 sec and 2400-3600 sec, respectively. These observations can be attributed to fact is that the saturation pressure of the water vapour is only affected by the temperature; hence, the mole fraction (partial pressure) of water vapour decreases with increasing the total backpressure in the flow channels. However, the mole fraction of oxygen in the gas mixture increases with increasing operating backpressure [125]. This may lead to enhance the magnitude of the local current density. On the other hand, the severe fluctuation of local current density, especially near the outlet region can be attributed to the negative impact of the cell backpressure on the reactant diffusion coefficient through the electrode structures. Further, flooding phenomenon can be accelerated because the high backpressure hindered movement of the product water toward the cell exit. The findings of the present work is consistent with the work described in [126] for the effect of the cell backpressure on the water management in a PEMFC.

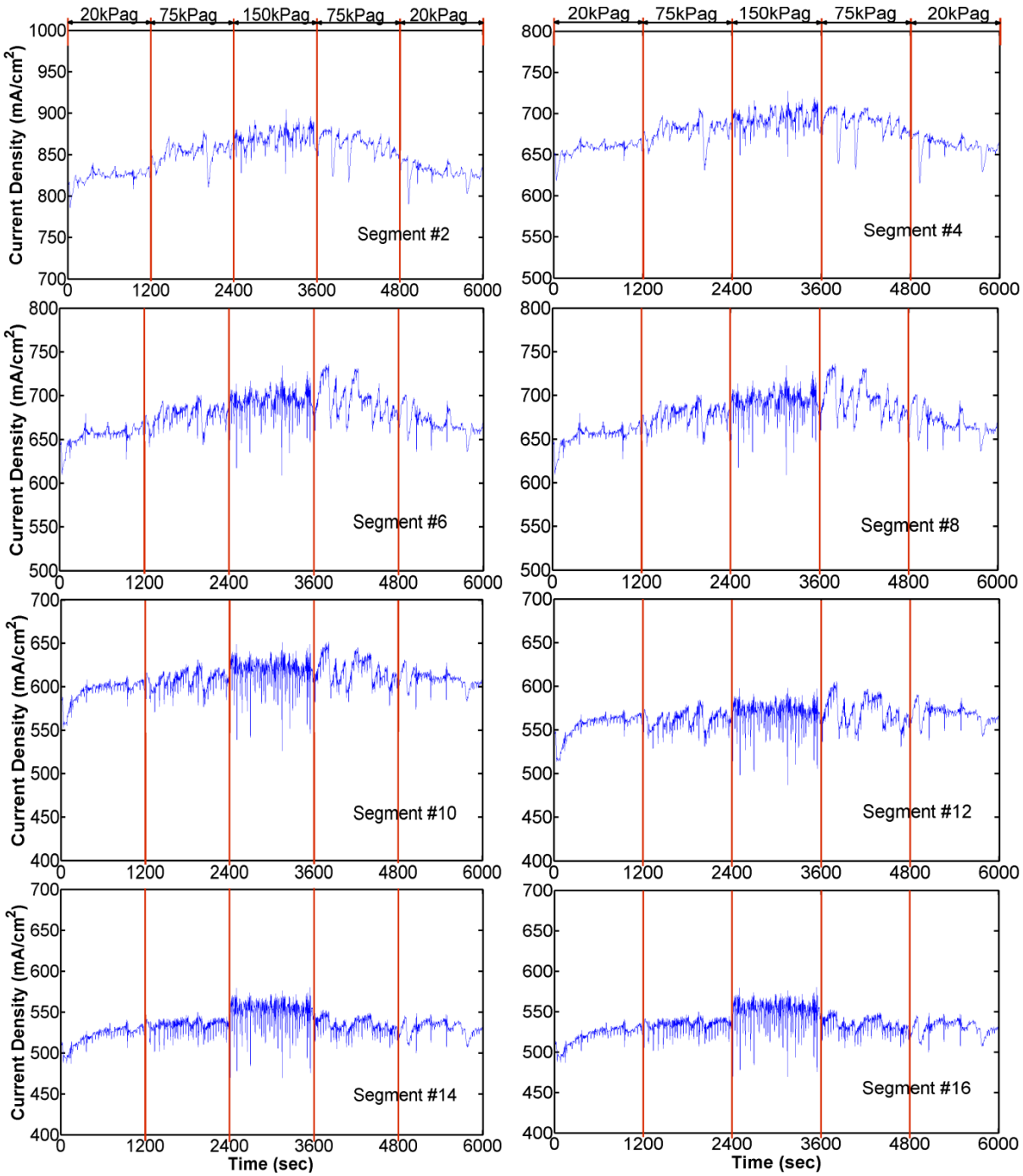

Figure 4.31: Dynamic characteristics of the local current density along the flow channel for the segments with even number under different cell backpressures. Measurement conditions: cell potential of 0.3 V, cell operating temperature of 65 °C, stoichiometry of 2 for the cathode air, stoichiometry of 1.2 for the anode hydrogen gas, fully humidified for both cathode and anode gas stream.

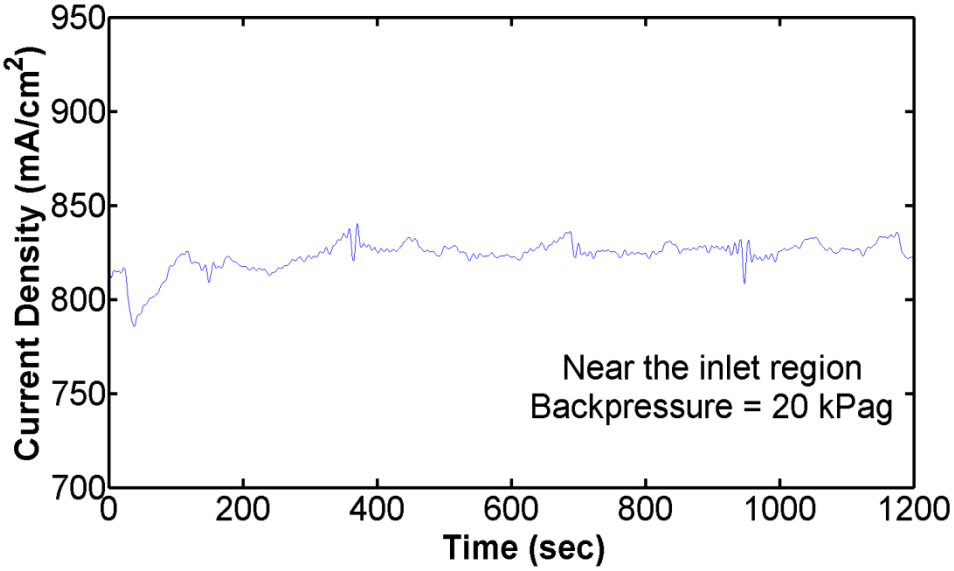

(a)

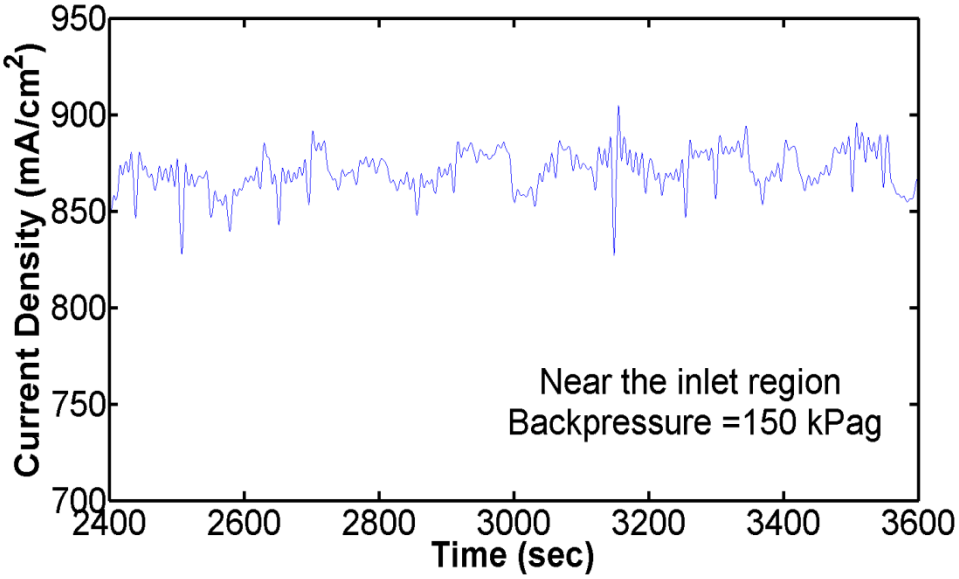

(b)

Figure 4.32: Dynamic characteristics of the local current density in region near the inlet for the different cell backpressures of 20 kPag (a) and 150 kPag (b), respectively. Measurement conditions: cell potential of 0.3 V, stoichiometry of 2 for the cathode air, cell operating temperature of 65 °C, stoichiometry of 1.2 for the anode hydrogen gas, fully humidified for both cathode and anode gas stream.

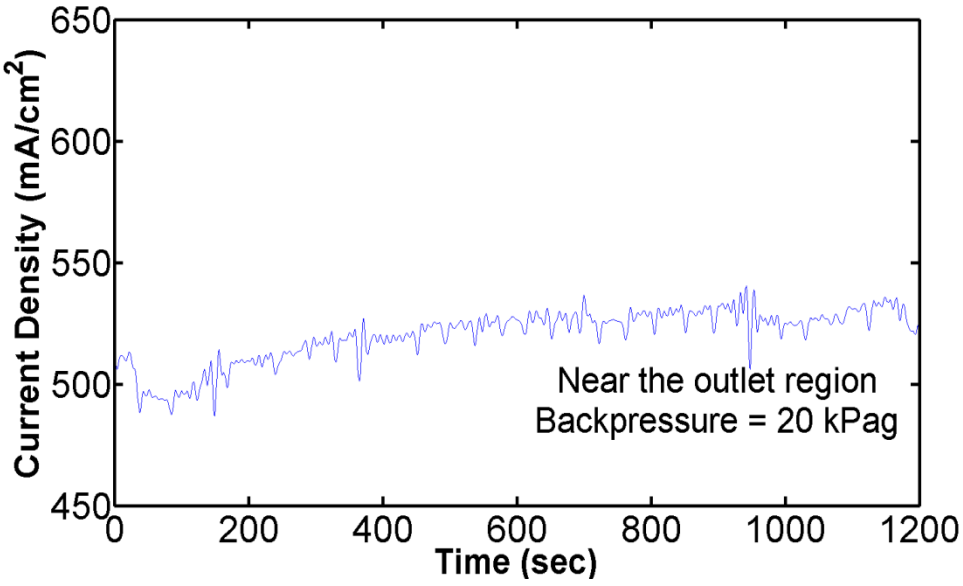

(a)

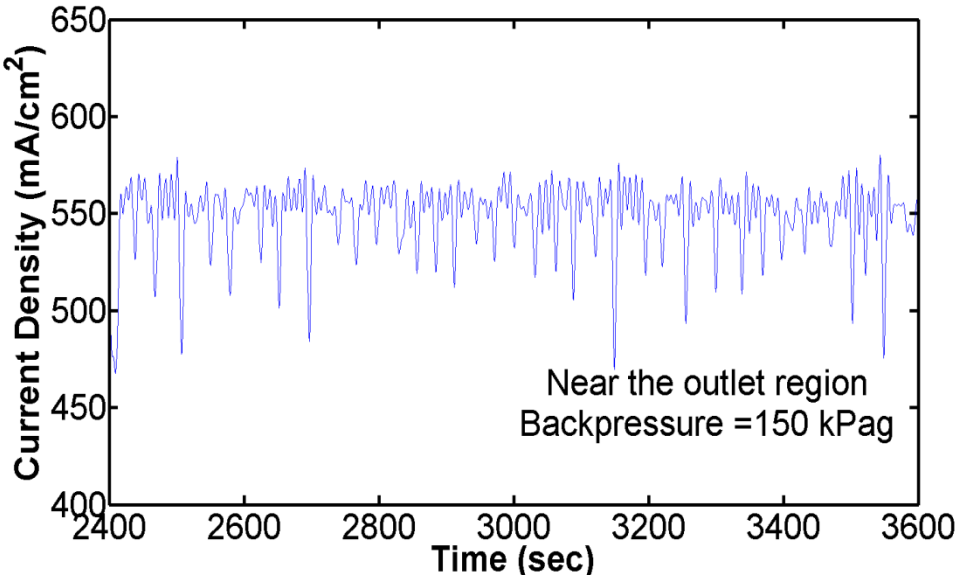

(b)

Figure 4.33: Dynamic characteristics of the local current density in region near the outlet for the different cell backpressures of 20 kPag (a) and 150 kPag (b), respectively. Measurement conditions: cell potential of 0.3 V, stoichiometry of 2 for the cathode air, cell operating temperature of 65 °C, stoichiometry of 1.2 for the anode hydrogen gas, fully humidified for both cathode and anode gas stream.

4.3.3 Effect of Inlet Relative Humidity (RH)

The degree of humidification in the reactant streams plays a crucial role in membrane hydration and water content in the electrode structures [121, 127]. Figure 4.34 (a) and (b) shows the dynamic characteristics of the local current density near the inlet and outlet regions, respectively. While, Figure 4.35 shows the dynamic characteristic of the local current density variation along the flow channels of a PEMFC for different reactant humidification levels of 25, 50, and 100%. Figure 4.36 is generated by magnifying the regions of 25% and 100% to obtain better resolutions. The current profiles are generated under the same operating conditions and cell potential of 0.3 V, the anode and cathode stoichiometry ratios of 1.2 and 2, respectively. For the inlet relative humidity of 25%, Figures 4.34 and 4.35 show that the local current density near the inlet region is lower when compared to those with a relative humidity of 50 and 100%, and the variations of the local current density are also low between the inlet and outlet regions.

The other important observation is that the cell performance fluctuation at the inlet and outlet regions. Due to the change of the water content in the electrode structures (hydration/dehydration), accompanied with less water formation, the local current density profile depends accordingly. As the relative humidity increases to 50%, improving in the local current densities near the inlet and outlet regions when compared with the relative humidity of 25%. The high cell performance can be attributed to better membrane hydration and proton conductivity (and lower Ohmic overpotential) at reactant of relative humidity of 50%. As the inlet humidity is increased to 100%, the cell performance is improved at the inlet region, but is degraded in the region near the outlet, as shown in Figure 4.35. This suggests that the external reactant humidification has two conflicting impacts (positive and negative) on the dynamic behavior of local current density in the regions near the inlet and outlet, respectively. This observation may signify that the water flooding issue in the cathode side can be minimized by avoiding the high degree of relative humidity in the reactant streams, which are found to be consistent with experimental results recently published [117, 120].

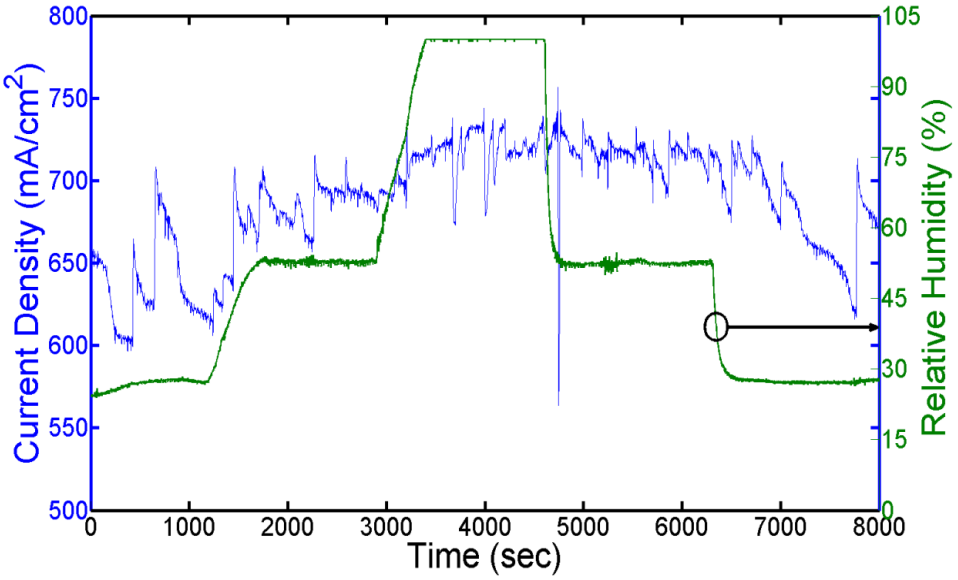

(a): Near the inlet region

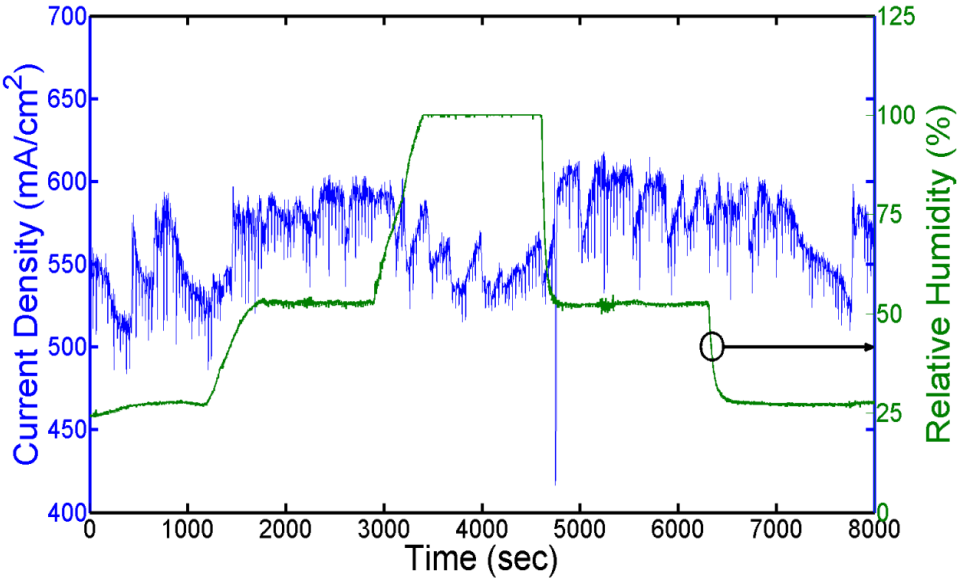

(b): Near the outlet region

Figure 4.34: Dynamic characteristics of the local current density for different levels of the reactant relative humidity near the inlet (a) and outlet (b) regions, respectively. Measurement conditions: cell potential of 0.3 V, cell operating temperature of 65 °C, cell backpressure of 50 kPag , stoichiometry of 2 for the cathode air, and stoichiometry of 1.2 for the anode hydrogen gas.

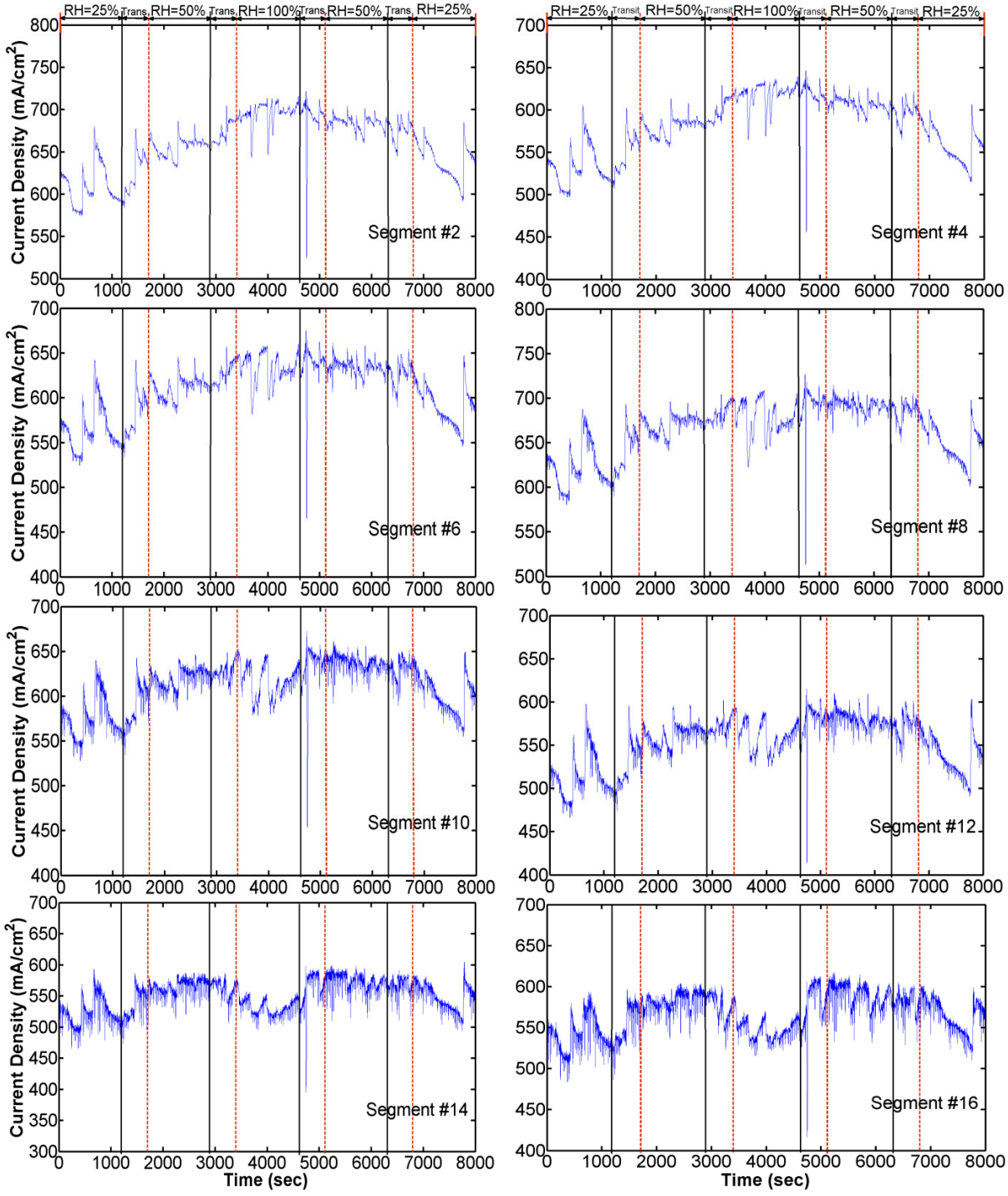

Figure 4.35: Effect of reactant relative humidity on the dynamic characteristics of the local current density along the flow channels for even segment numbers. Measurement conditions: cell potential of between 0.3 V, cell backpressure of 50 kPag, stoichiometry of 2 for the cathode air and 1.2 for the anode hydrogen gas.

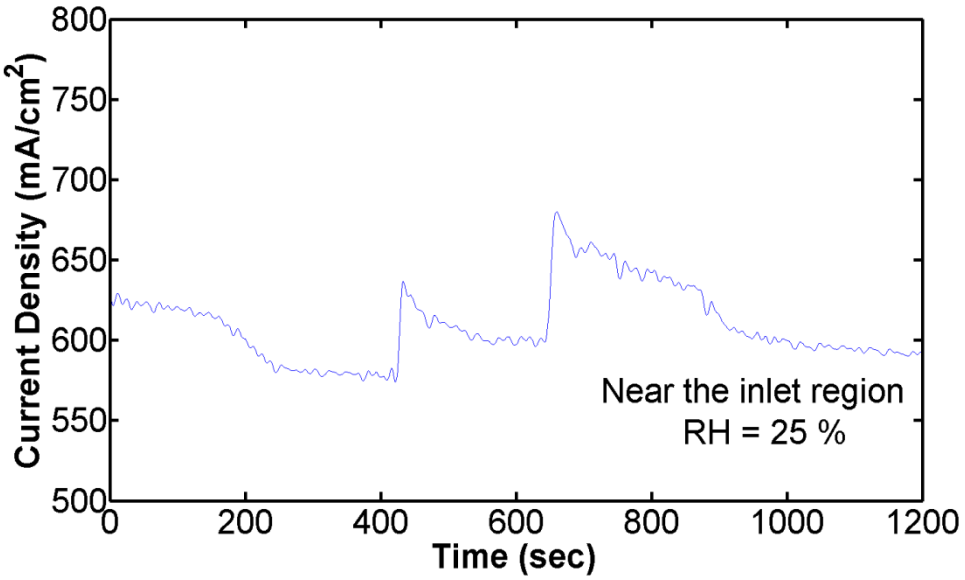

(a)

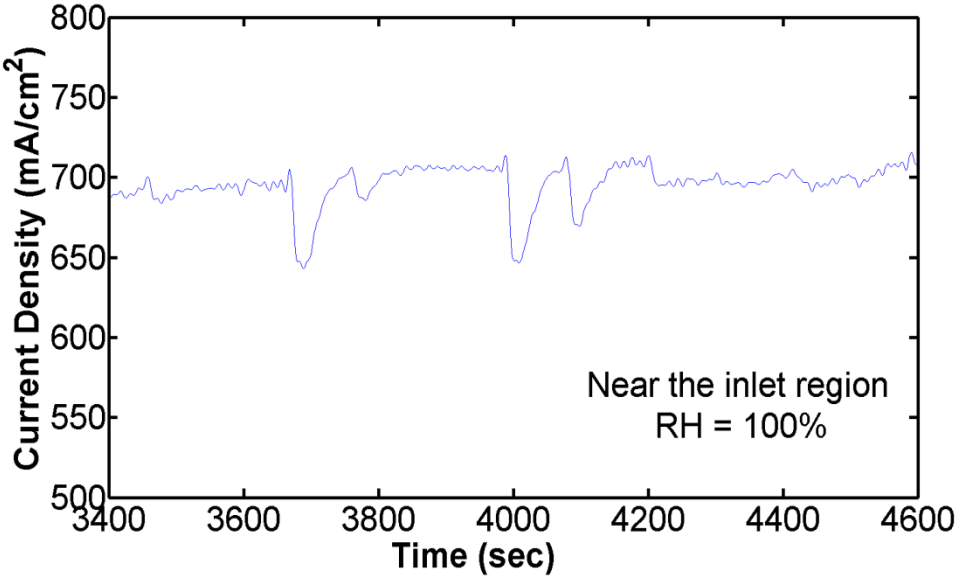

(b)

Figure 4.36: Effect of reactant relative humidity (RH) on the dynamic characteristics of the local current density near the inlet region of the tested PEMFC: (a) for RH = 25% and (b) for RH = 100%. Measurement conditions: cell potential of 0.3 V, cell backpressure of 50 kPag, stoichiometry of 2 for the cathode air and 1.2 for the anode hydrogen gas.

Part (IV)

Local Temperature Distribution Measurements in a PEMFC with Multiple Straight Flow Channels

4.4 Local Temperature Distribution Measurements in a PEMFC with Multiple Straight Flow Channels

4.4.1 Temperature Distribution across PEMFC for Different Current Densities

In order to obtain temperature profiles across the PEMFC, 48 thermocouples are placed in different locations within the experiment set-up. In addition to the 44 thermocouples implanted in the flow filed plates, as explained in section 3.3, two thermocouples are placed in the environment chamber to measure the surrounding temperature, while the other two are attached to the endplates on the anode and cathode sides, respectively as illustrated in Figure 3.20.

Figure 4.37 shows the temperature distributions across the cell for three different current densities of 300, 500, and 850 mA/cm^2. The environment temperature is maintained at 65 ^{o}C. The anode and cathode stoichiometry ratios are fixed at 1.5 and 3, respectively. Fully humidified gas streams are supplied at a temperature of 65 ^{o}C, with atmospheric pressure to the cell at both the cathode and anode sides. The temperature measurements are conducted at a sample rate of one reading every five seconds over a 30-minute period for each operating condition. Figure 4.37 shows the temperature profiles across the fuel cell for different regions and cell components including environment chamber (Envi), cathode endplate (Plate (C)), reaction site for the cathode (reaction 1) and anode (reaction 2) , respectively, as well as the anode endplate (Plate (A)). The temperature measurements shown in Figure 4.37 are obtained as mean values of temperatures recorded for each current density, over a period of time after the cell reached the steady state. It is seen that the highest temperature in the profile is recorded at the top surface of GDL for the cathode side (reaction 1) for all current densities tested. At high current density, it is seen that the temperature of the anode side of the cell (reaction 2) is lower than the cathode side by more than 1 ^{o}C. This can be attributed to the heat generation resulting from the electrochemical oxygen reduction reaction occurring over the cathode side's catalysis layer.

The other important observation is the existence of considerable differences between the temperatures of both cathode (reaction 1) and anode (reaction 2) and their corresponding endplate temperatures. Figure 4.37 shows that increasing the overall current density from 300 mA/cm^2 to 850 mA/cm^2 leads to increasing the internal cell temperature by 6.5 ^{o}C and 14 ^{o}C above the endplate and environment temperatures, respectively. This suggests that noticeable non-uniform temperature distribution exists across the PEMFC components especially at high current density (low cell voltage). Figure 4.37 also indicates that an effective cooling method should be implemented to remove the excessive heat generated, in order to avoid hot spot formations inside an operational PEMFC.

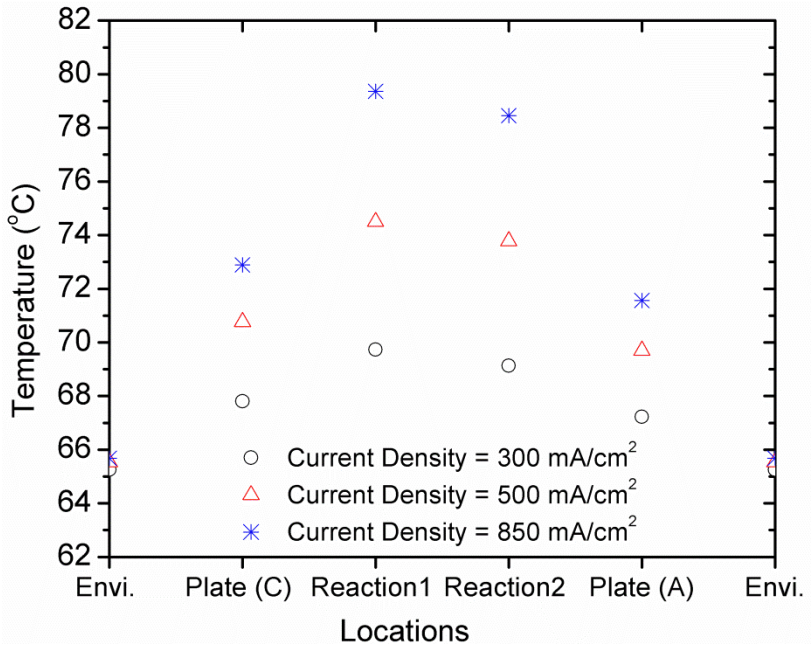

Figure 4.37: Temperature measurement profiles across the PEMFC for various current densities. Measurement conditions: cell current densities 300, 500 and 850 mA/cm^2, cell backpressure of atmospheric, environment and reactant supplied temperatures are fixed of 65 °C, stoichiometry of 3 for the cathode air and 1.5 for the anode hydrogen gas, fully humidified for both cathode and anode gas stream of 65 ^{o}C.

4.4.2 Temperature Distribution along Flow Channel for Various Current Densities

Figures 4.38 and 4.39 show the temperature profiles along the flow channel for the cathode and anode sides of PEMFC, respectively, and for different current densities of 300, 500, and 850 mA/cm^2. It is seen that the temperature gradient between the inlet and outlet is not considerably high when the current density is low at 300 mA/cm^2, but it becomes more noticeable when the current density increases due to the larger heat generation inside the cell. Obviously, the flow channels can be divided into three different regions in terms of temperature values, especially at high current density. These three sections are: up, middle and down-stream. Temperatures of the up- and down-stream sections are comparatively lower than the middle-section of the flow channels. In the up and down-stream sections, convective heat transfer to the surrounding area is significant, resulting in lower temperature. This may decrease reaction rate and, in turn, heat generation, thus amplifying temperature gradient. In the middle section, temperature is higher compared to the up- and down-stream sections. This may result in more hydration of the membrane and a higher rate of the oxygen reduction reaction (ORR) in the middle section of the channels, which can be the result of increasing water activity toward the outlet as the membrane gains the water produced by the ORR. There also exist various heat transfer processes, such as water vapor condensation and the release of latent heat, convective heat transfer due to the temperature gradient, and an electrochemical reaction that leads to reactant heat being released [128, 129]. In the downstream section, there is lower temperature compared to the middle section area. This may be caused by the following factors: oxygen depletion leading to a lower rate of electrochemical reaction and thus lower heat release, and water accumulation in the flow channels as well as in the GDL pores, which prevents the oxygen from reaching the catalyst layer [130]. Further, convective heat transfer at the edge of the flow field plate decreases the temperature, as mentioned previously.

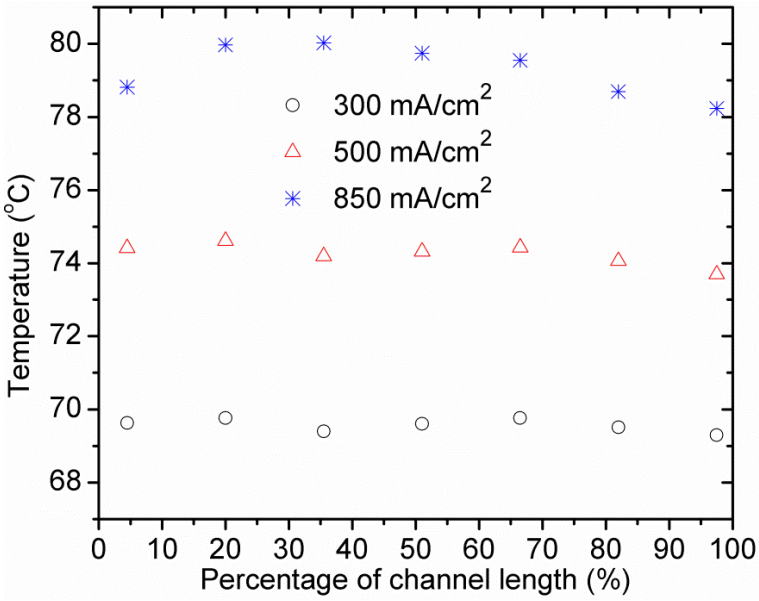

Figure 4.38: Local temperature distributions along the flow channel in PEMFC at the cathode side for various current densities. Measurement conditions: cell current densities 300, 500 and 850 mA/cm^2, cell backpressure of atmospheric, environment and reactant supplied temperatures are fixed at 65 °C, stoichiometry of 3 for the cathode air and 1.5 for the anode hydrogen gas, fully humidified for both cathode and anode gas stream of 65 °C.

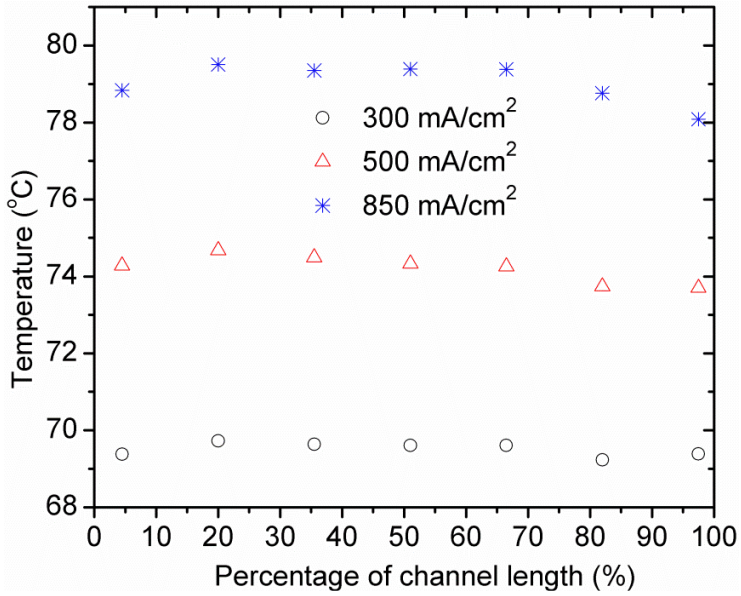

Figure 4.39: Local temperature distributions along the flow channel in PEMFC at the anode side for various current densities. Measurement conditions: cell current densities 300, 500 and 850 mA/cm^2, cell backpressure of atmospheric, environment and reactant supplied temperatures are fixed at 65 °C, stoichiometry of 3 for the cathode air and 1.5 for the anode hydrogen gas, fully humidified for both cathode and anode gas stream of 65 °C.

4.4.3 Temperature Profiles along Flow Channel for both Anode and Cathode Sides

Figure 4.40 shows the temperature profiles along the flow channels for both the cathode and anode sides, along the flow channels of the PEMFC. The dotted line with star marks represents the temperature profile for the anode side, and the dashed line with circle marks represents the temperature profile for the cathode side. Figure 4.40 indicates that the non-uniform distribution of the local temperature over the surfaces for anode and cathode sides at current density of 850 mA/cm^2. At such high current density, it is seen from Figure 4.40 that the temperatures along the flow channel at the cathode side are higher than the anode side, especially in the up- and down-stream sections of the flow channel. Although the hydration of the membrane near the down-stream section of the flow channel can be the highest at the high current density, the depletion of reactant and the accumulated liquid water is due to the electrochemical reaction along the flow channel, especially at the cathode side. This may reduce the reactant transport (diffusion) through the porous structure of GDL in order to reach the reaction site at the catalyst layer, which will lead to lower the local values of both local temperature and current density [131]. Thus, Figure 4.40 shows that the temperatures at the downstream section are decreased by 1.5 ^{o}C when compared to the middle-section. Figure 4.40 also indicates that the cathode side holds a higher temperature than the anode side by 1 ^{o}C along the flow channels except in the down-stream section. This can be attributed to the excessive heat generation that takes place on the cathode side of the PEMFC due to the ORR. Further, water transport by the electro-osmotic drag from the anode to the cathode side may lead to local membrane dehydration at the up- and middle-steam sections of the flow channel. This effect may increase the local temperature especially on the anode side. Since the temperature differences between the anode and cathode are small and temperature profiles present similar trends, only the temperature distribution on the cathode side will be discussed in following subsection.

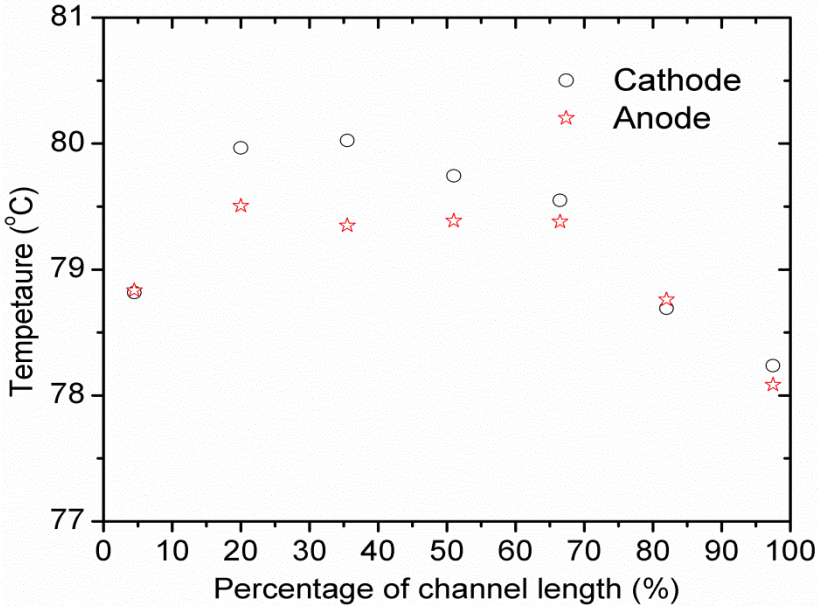

Figure 4.40: Temperature distribution along the flow channel in PEMFC for anode and cathode at various current densities. Measurement conditions: cell current density of 850 mA/cm^2, cell backpressure of atmospheric, environment and reactant supplied temperatures are fixed at 65 °C, stoichiometry of 3 for the cathode air and 1.5 for the anode hydrogen gas, fully humidified for both cathode and anode gas stream of 65 °C.

4.4.4 Effect of Air Stoichiometry on Temperature Distributions along the Flow Channel

The effect of the air stoichiometric ratio on the temperature distributions along the straight channel (in the flow direction) and in the direction normal to the flow at the cathode side of the PEMFC is investigated for three different values of 3, 4.5, and 5.5, as shown in Figure 4.41 (a) and (b), respectively. The effect of the air stoichiometry ratio on the overall cell potential is shown in Figure 4.42. The temperature profiles in this figure are obtained at the current density of 850 mA/cm^2. Fully humidified reactants on both the anode and cathode sides are set to the environment chamber temperature of 65 °C. It is seen from Figure 4.41 (a) and (b) that the local temperatures are the highest in middle section and then decrease toward the channel's up- or downstream sections as well as the side edges. The reduction in the local cell temperature in the up- and downstream sections as well as near the side edges can be attributed to convective heat transfer to the surrounding area where the temperature is lower

than the cell temperature. Further, the reactant starvation and water formation (accumulation/flooding), especially along the flow direction, may lead to a reduction in temperature at the downstream section as explained previously. Figures 4.41 (a) and (b) clearly show that the value of the local cell temperature over the MEA surface can be fairly reduced with maintaining the same temperature profile along the flow channel by increasing the air flow rate streams. The reason for this reduction can be explained as follows: the temperature inside the cell and over the reaction site is expected to be higher than 80 ^{o}C, while the reactant streams supplied to the cell are at temperature of 65 ^{o}C. Therefore, it is expected that the reactants act as cooler media and the local temperature inside the fuel cell decreases with a higher reactant flow rate accordingly. It can be observed that a higher air stoichiometry ratio or decreasing the cell's overall current density lowers the local temperature distributions in the PEMFC. However, Figure 4.42 indicates that increasing the air stoichiometry ratio has a positive impact on the overall cell potential. This can be attributed to better water removal capabilities from the cathode flow channels, as well as a higher reactant concentration over the reaction site, even though, increasing the air stoichiometric ratio reduces the overall PEMFC system efficiency.

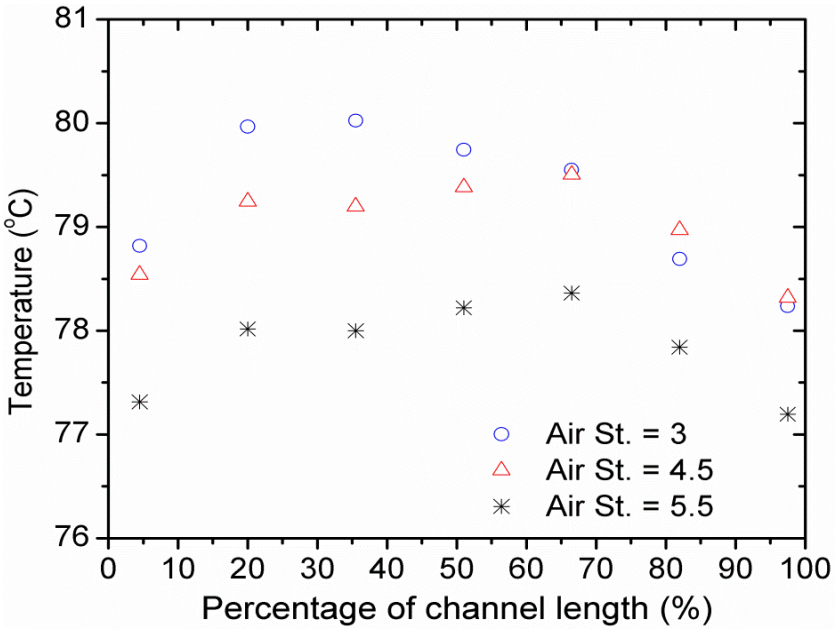

(a)

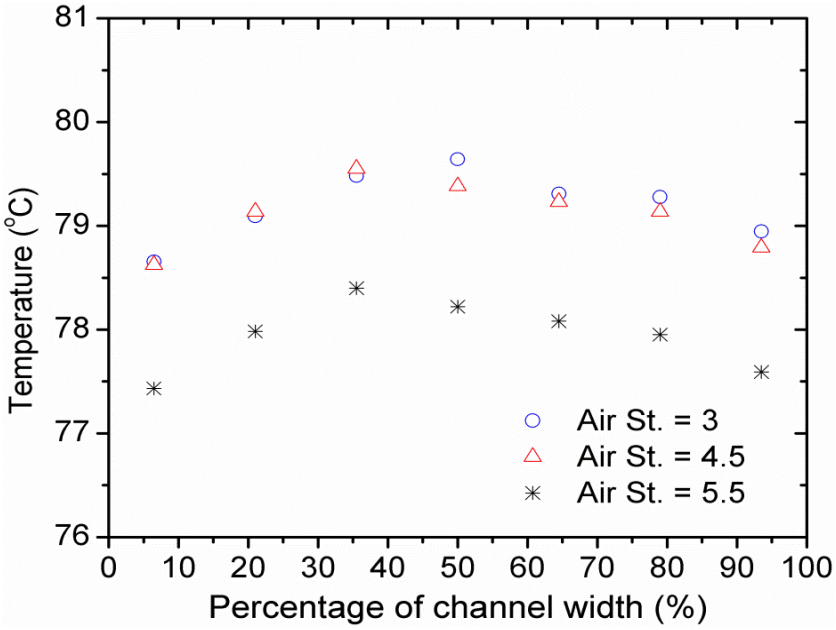

(b)

Figure 4.41: Temperature distribution (a) in flow direction and (b) in normal direction of the flow for the cathode side and different cell air stoichiometry ratios of 3, 4.5, and 5.5. Measurement conditions: cell current density of 850mA/cm^2, environment and reactant supplied temperatures are fixed at 65 °C, stoichiometry of 1.5 for the anode hydrogen gas, fully humidified for both cathode and anode gas stream of 65 °C.

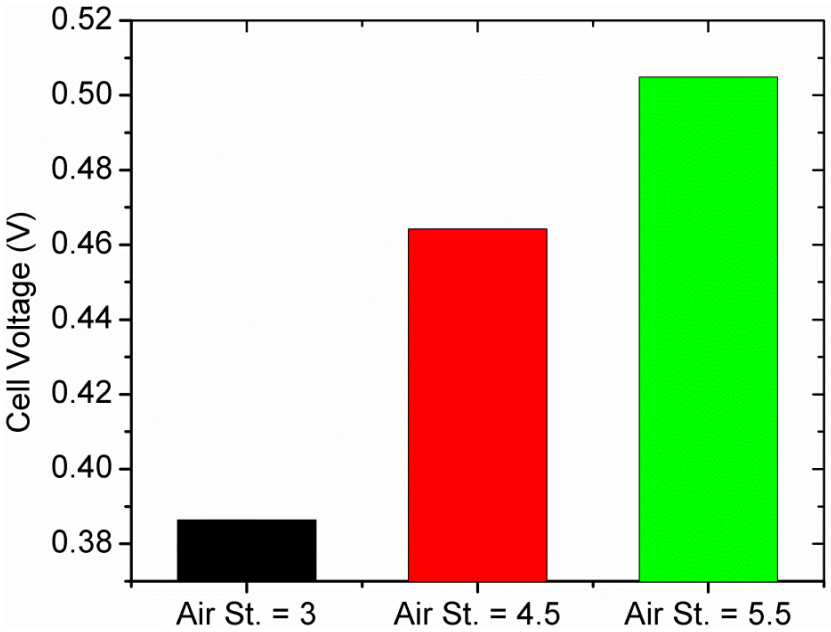

Figure 4.42: The effect of the air stoichiometry ratio on the overall cell potential for different cathode side and different cell air stoichiometry ratios of 3, 4.5, and 5.5. Measurement conditions: cell current density of 850mA/cm^2, environment and reactant supplied temperatures are fixed at 65 °C, stoichiometry of 1.5 for the anode hydrogen gas, fully humidified for both cathode and anode gas stream of 65 ^{o}C.

4.4.5 Effect of Cell Backpressure on the Temperature Distributions along the Flow Channel

Figures 4.43 (a) and (b) show the effect of the reactant backpressure on the local temperature distributions, and the overall cell potential for the operating fuel cell, respectively, which is one of the important phenomena to be studied in this work. During the experiment, three backpressure values of 0, 75, and 150 kPag are investigated. Other operating parameters such as environment chamber and supplied reactant temperatures are fixed at 65 ^{o}C, and stoichiometry ratios are fixed at 1.5 and 3 for the fuel and air, respectively. It can be observed that raising the reactant backpressure is not affecting the original profile (trend) of the local temperature distributions along the flow channel. It is obvious from Figure 4.43 (a) that increasing the reactant backpressure from 0 to 75 kPag will not affect the general local temperature profile over the electrode surface. However,

increasing the backpressure from 75 to 175 kPag causes the temperature profile to be shifted by 1.5 ^{o}C. The enhancement in the local temperature values can be attributed to the increase in the electrochemical activities as a result of higher reactant concentration. Further, Figure 4.43 (b) indicates that although the overall performance is considerably enhanced by 24% when the reactant backpressure is changed from 0 to 75 kPa, while increasing the reactant backpressure from 0 to 150 kPa results in only an 18% increase in the overall cell performance. This suggests that applying excessive reactant backpressure in a cell with straight flow channels can lead to a negative impact on the cell's performance. This is due to inadequate product water removal resulting from excessive backpressure, especially if the cell is operating at high current density and is near the concentration polarization region (I-V curve), similar to the case under investigation. It can be seen that the negative impact caused by insufficient water management can overcome the improvement gained from the higher reactant concentration over the MEA surface that results from high reactant backpressure. This observation of the effect of reactant backpressure on the overall cell performance is found to be in agreement with work conducted using the visualization technique as described in [126].

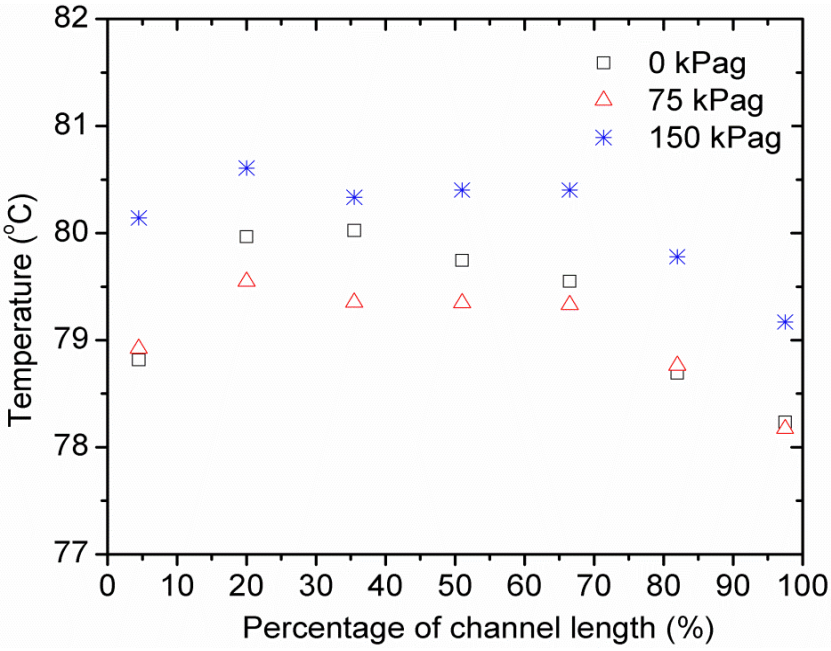

(a)

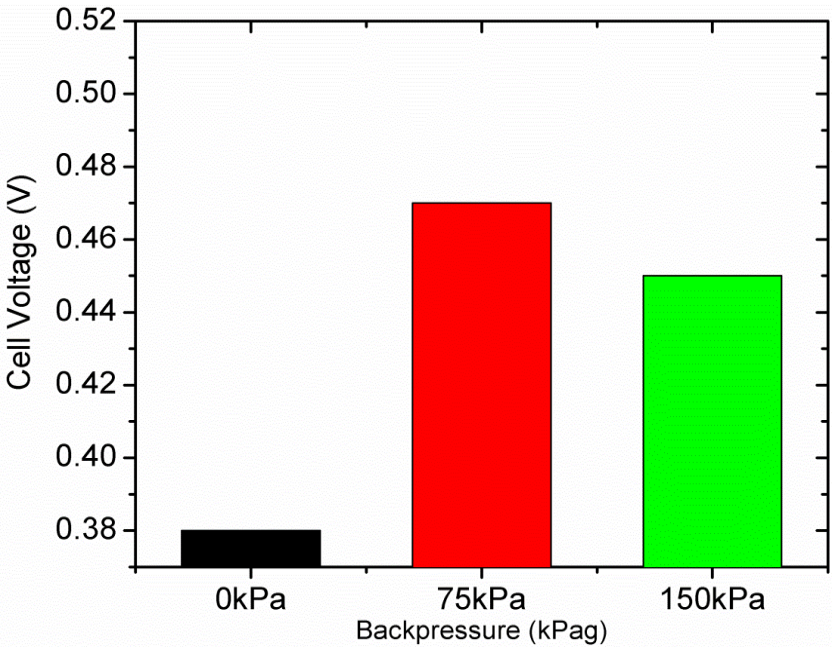

(b)

Figure 4.43: Temperature distribution along the flow channel at the cathode side for different cell pressures of 0, 75, 150 kPag (a) and their corresponding cell potentials (b). Measurement conditions: cell current density of 850 mA/cm^2, environment and reactant supplied temperatures are fixed at 65 °C, stoichiometry of 3 for the cathode air and 1.5 for the anode hydrogen gas, fully humidified for both cathode and anode gas stream of 65 °C.

Part (V)
Combined Measurements of the Current and Temperature Distribution in a PEMFC

4.5 Combined Current and Temperature Distribution Measurements

Simultaneous measurements of local current and temperature distributions are conducted in order to determine the relationship between the local current density and temperature distributions in PEMFC, as described in Section 3.5.4. The local current density distributions are measured on the anode side of operational PEMFC, while local temperature distribution measurements are collected simultaneously on the cathode side. In this section, the effect of various values of air stoichiometric ratios and cell backpressures on the local current density and temperature distributions are investigated and analyzed.

4.5.1 Relation between the Local Current and Temperature Distributions in PEMFC

Figure 4.44 shows the relationship between the local current density and temperature profiles near the inlet region of a single PEMFC when only the cell voltage is changed in a cycle between 0.7 V and 0.3 V. This Figure is obtained at a cell backpressure of 50 kPag, stoichiometry of 2 for the cathode air and 1.2 for the anode hydrogen gas, fully humidified for both cathode and anode gas streams at a cell temperature of 65 ^{o}C. The surrounding temperature inside the environment chamber is fixed at 65 ^{o}C. Figure 4.44 shows that the local temperature for the inlet region increases by 11 ^{o}C when the cell potential is decreased from 0.7 V to 0.3 V, with all other key operating conditions are maintained constant.

In the case of a decrease in the overall cell potential from 0.7 V to 0.3 V, it seems that the local current density and temperature profiles are directly related, such that an increase in the overall current density is associated with an increase in the temperature profile. On the other hand, Figure 4.44 indicates that increasing the cell potential from 0.3 V to 0.7 V is associated with decreasing the cell temperature to its initial value. This can be attributed to the higher electrochemical activity taking place over the MEA surface as a result of decreasing the cell potential. In contrast, a high cell potential leads to an opposite impact on both local current density and temperature profiles. Generally, it is obvious that the change in the local temperature is very slow when compared with the local current density, but both of them required about 3000 sec to reach their peaks.

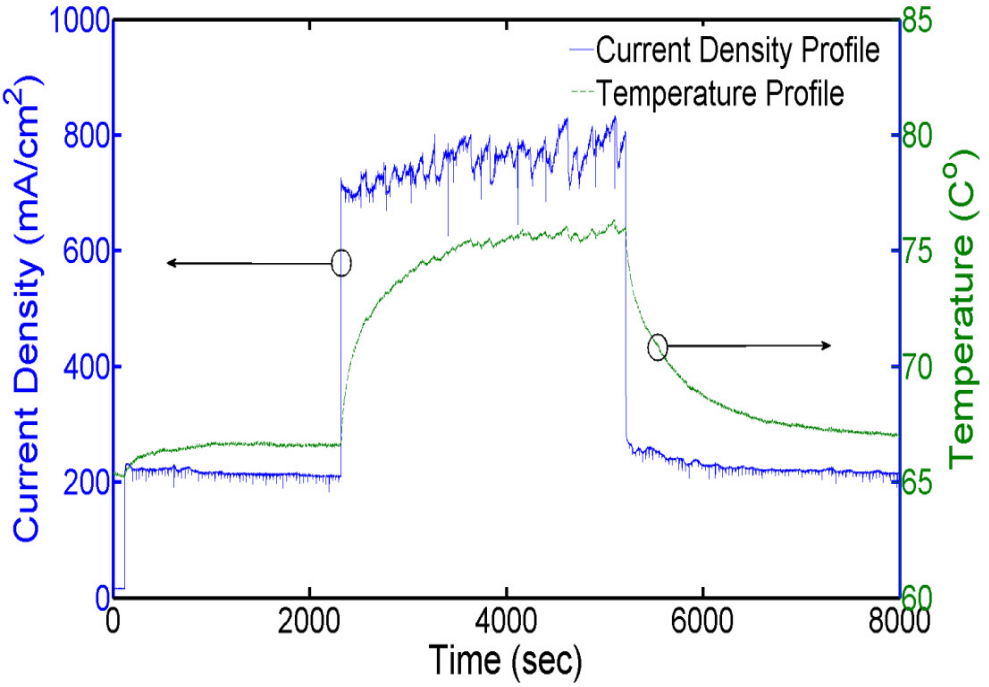

Figure 4.44: Dynamic characteristics of the local current density and temperature profiles near the inlet region of PEMFC. Measurement conditions: cell potential varied between 0.7 V and 0.3 V, cell backpressure of 50 kPag, stoichiometric of 2 for the cathode air and 1.2 for the anode hydrogen gas, fully humidified for both cathode and anode gas stream.

4.5.2 Effect of Air Stoichiometry on the Current and Temperature Distributions

Figures 4.45 and 4.46 show the effect of different air stoichiometry ratios of 2 and 5 on the local current and temperature distributions in an operating PEMFC for co-flow arrangement and cell potentials 0.7 V and 0.3 V, respectively. In Figures 4.45 and 4.46, (a) and (b) indicate the local current density at the air stoichiometries of 2 and 5, while (c) and (d) denote their corresponding temperature distributions. The hydrogen stoichiometry ratio of 1.2 and the fully humidified reactants on both the anode and cathode are set to the initial cell operating temperature of 65 °C.

Figures 4.45 and 4.46 indicate that the local current density and temperature values decrease gradually along the direction of the gas flow from inlet to outlet for cell potentials of 0.7 V and 0.3 V. However, the slope of local current density profiles is steeper than the

temperature profiles, especially for cell potential of 0.3 V. This may be caused by the gradual consumption of reactants along the flow direction in serpentine flow channels, as discussed previously. Generally, Figures 4.45 (b) and 4.46 (b) reveal that the temperature is quite high near the inlet region of the flow channels due to the faster electrochemical activity that takes place in the region near the inlet. At the high cell potential of 0.7 V, the average cell temperature of 66 ^{o}C is lower than the cell temperature of 76 ^{o}C, measured at the cell potential of 0.3 V. This can be attributed to the small amount of heat generated in the cell. The other important observation is that increasing the air stoichiometry from 2 to 5 has a negligible impact on local temperature over the MEA surface.

At the low cell potential of 0.3 V, the average cell temperature of 75 ^{o}C is considerably high when compared to the environment and reactant temperatures of 65 ^{o}C. This can be attributed to the larger heat generation in the cell, considering that the environment chamber temperature is fixed at 65 ^{o}C. Further, it shows that the temperature profile presents a similar trend to the local current density for the air stoichiometry ratio of 2 and 5. The highest temperature is measured near the cell inlet, while the lowest one is near the outlet, and the temperature difference between them is about 1.25 ^{o}C. As the air stoichiometry ratio increases from 2 to 5, both the local current density and temperature magnitude increase accordingly, this can be due to increased local reactant concentrations and better water management especially near the outlet region. Higher reactant concentration results in faster electrochemical activity over the MEA and may lead to increasing the local temperature value. Further, a higher air stoichiometry ratio will hold higher heat capacity in the reactant streams. Figure 4.46 indicates that the effect of a higher air stoichiometry ratio in PEMFC with serpentine flow channels presents an opposite impact on the temperature profile in the case of straight flow channels, as shown in Figure 4.41. This can be attributed to the differences in the flow channel designs as well as the operation conditions.

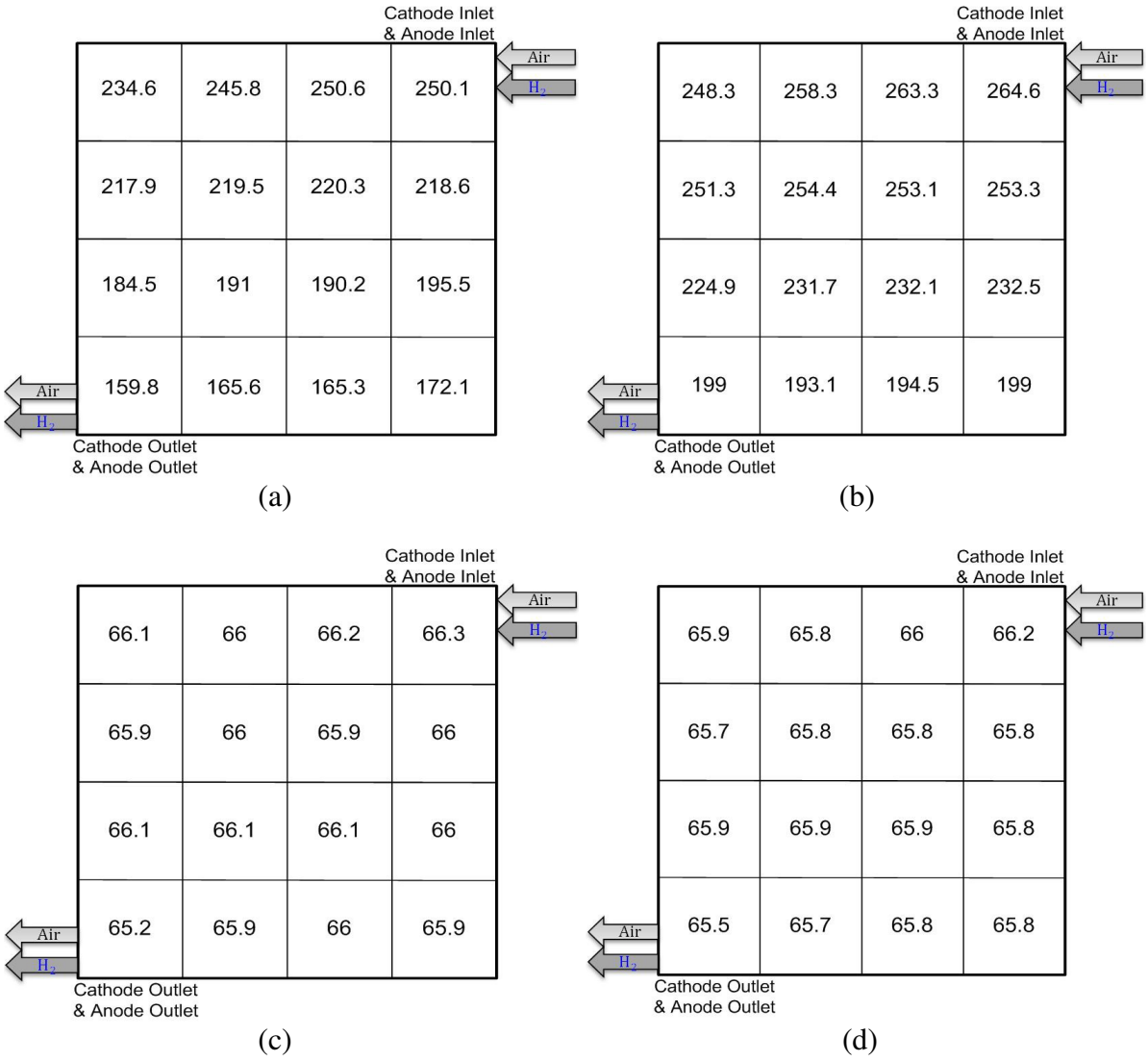

Figure 4.45: Effects of air stoichiometry ratios of 2 (a) and 5 (b) on the local current density and their corresponding temperature distributions (c) and (d) along the flow channels in PEMFC, respectively. Measurement conditions: cell potential of 0.7 V, cell backpressure of 50 kPag, stoichiometry of 1.2 for the anode hydrogen gas, fully humidified for both cathode and anode gas stream.

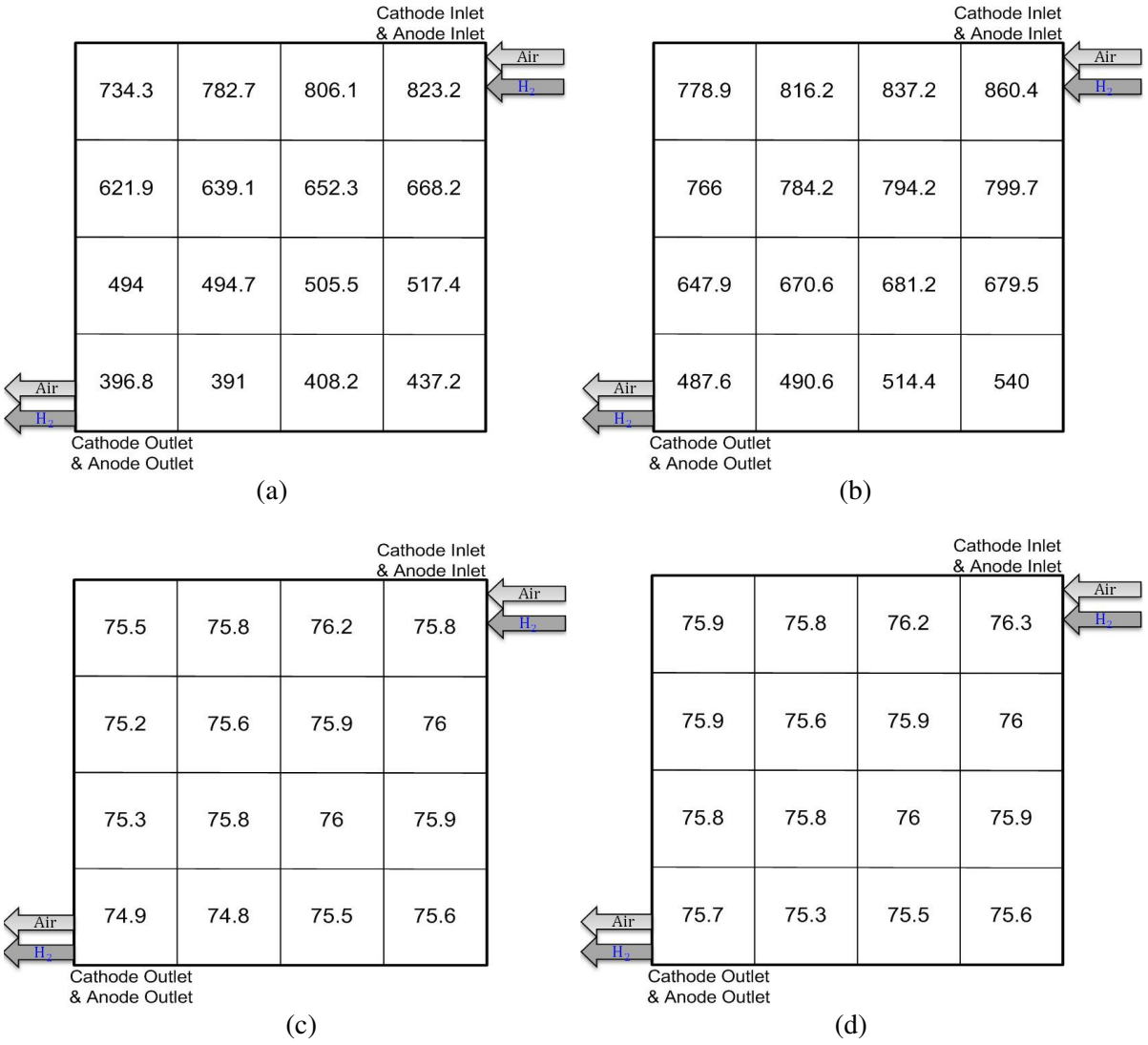

Figure 4.46: Effects of air stoichiometry ratios of 2 (a) and 5 (b) on the local current density and their corresponding temperature distributions (c) and (d) along the flow channels in PEMFC, respectively. Measurement conditions: cell potential of 0.3 V, cell backpressure of 50 kPag, stoichiometry of 1.2 for the anode hydrogen gas, fully humidified for both cathode and anode gas stream.

4.5.3 Effect of the Cell Backpressure on the Current and Temperature Distributions

Local current and temperature distributions for different cell backpressures of atmospheric and 150 kPag are also investigated and the results are presented in Figures 4.47 and 4.48 for cell potentials of 0.7 V and 0.3 V, respectively. These figures are obtained under the identical operating conditions as those of Figures 4.45 and 4.46, except that the air stoichiometry is fixed at 2. The two figures indicate that an increase in the cell pressure from an atmospheric pressure to 150 kPag may lead to a slight increase in both local current density and temperature values, without changing their initial profiles, for both 0.7 V and 0.3 V. It is seen that the local temperature profile for a cell potential of 0.3 V increases (shift up) by almost 2.5 ^{o}C when the cell backpressure is increased by 150 kPag. The local current density profile presents a similar trend to the local temperature when the cell backpressure increases. It is observed that the highest local temperature is measured near the inlet and middle regions in the PEMFC, while the lowest temperature is measured near the outlet region. Low operating voltage results in both higher local current density and heat generation flux, and local temperatures may increase accordingly. It can be seen from Figure 4.48 that decreasing operating voltage to 0.3 V may lead to an increase the inside cell temperature over the MEA. Hence, this reduction in the cell potential results in a 12 ^{o}C difference between the inside cell and its surrounding or endplate temperatures, which are commonly taken as the fuel cell's operating temperature in many studies. It also indicates that taking these temperatures to monitor the fuel cell temperature can be a misleading measurement of the actual operating conditions, especially at high current density.

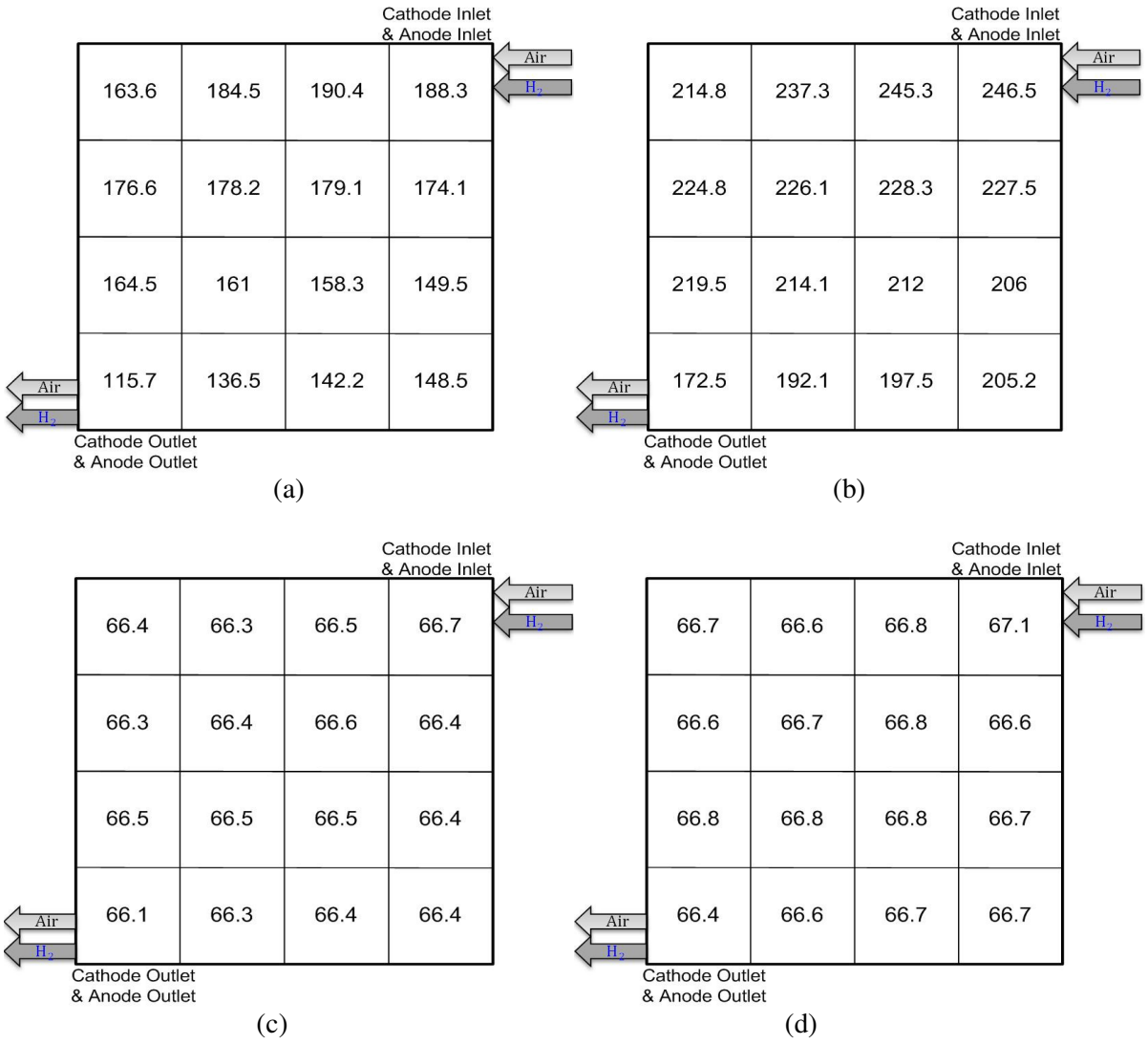

Figure 4.47: Effects of cell backpressures of 0 kPag (a) and 150 kPag (b) on the local current density and their corresponding temperature distributions (c) and (d) along the flow channels in PEMFC, respectively. Measurement conditions: cell potential of 0.7 V, cell backpressure of 50 kPag, stoichiometry of 1.2 for the anode hydrogen gas, fully humidified for both cathode and anode gas stream.

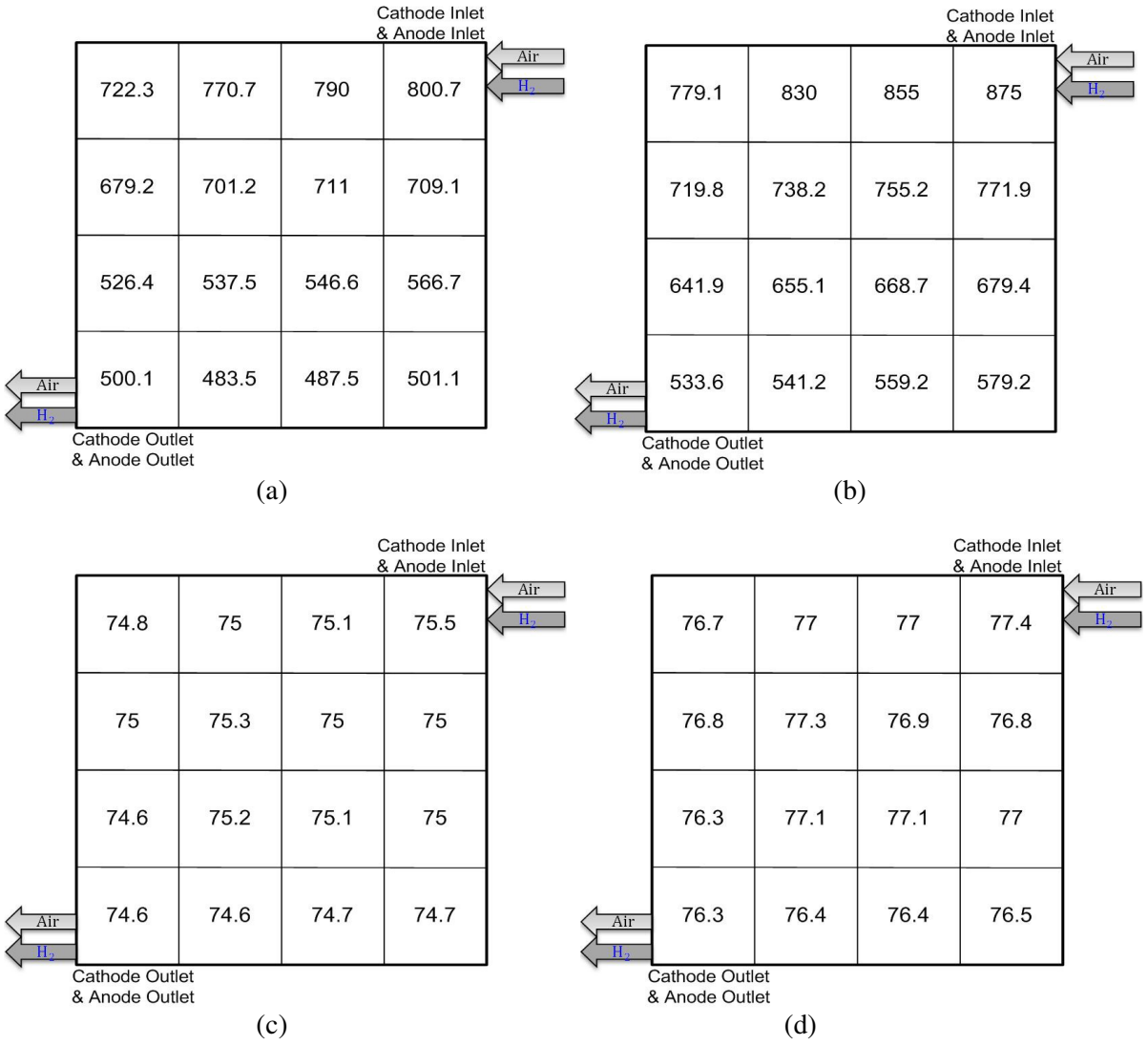

Figure 4.48: Effect of cell backpressures of 0 kPag (a) and 150 kPag (b) on the local current density and their corresponding temperature distributions (c) and (d) along the flow channels in PEMFC, respectively. Measurement conditions: cell potential of 0.3 V, stoichiometry of 1.5 for the anode hydrogen gas and 2 for air, fully humidified for both cathode and anode gas stream.

4.6 Summary

In this chapter, the results for the local current and temperature distributions over the MEA surface of the PEMFC are presented. The effect of various design and operating

conditions on temperature and current profiles as well as the overall cell performance are investigated. An experimental study of both the local current and temperature distributions in PEMFC has been conducted using the segmented flow field plate and printed circuit board technique (PCB). Moreover, the temperature distribution over the MEA is also measured by thermocouples. The results are summarized as follows:

- The effect of different reactant flow arrangements between the anode and cathode flow streams, including co-, cross-, and counter-flow, on the current distribution under steady state conditions has been investigated. The results showed that the current distribution is directly affected by the reactant flow arrangement. The co-flow arrangement yields considerable current density variations from the anode/cathode inlets to the exits, while the counter-flow arrangement produces the most uniform distribution for current density. In the case of the co-flow arrangement and under steady state conditions, the current density is the highest near the flow channel inlets and generally decreases monotonically along the flow direction, becoming almost aligned with the reactant stream flow arrangement (flow channel layout). It is also found that the cross-flow arrangement results in the most complex local current profile over the MEA surface. Thus, it is concluded that the flow arrangements have a predominant impact on the current density distribution, especially at high current density operation in modern PEMFCs.
- The limiting hydrogen concentration at the anode side, due to the low stoichiometry condition, has a major effect on the current distribution and cell performance.
- The effects of key operating conditions such as stoichiometry ratios, inlet humidity levels, and cell backpressure and temperature on the local current density distributions for co-, counter-, and cross flow arrangements under steady state conditions are examined. It is observed that the local current density distribution over the MEA is directly affected by the cell operating conditions, along with the configuration of the flow arrangement. Increasing both the air and hydrogen stoichiometry ratios improves the cell performance and lowers the variations of the current distribution, and increasing the operating backpressure and temperature improves cell performance but has a negligible impact on

the local current distribution. For the co-flow and cross-flow arrangements, supplying air and hydrogen at 50% relative humidity shows the best cell performance. The 100% relative humidity condition results in large variations of local current distribution. For the counter-flow arrangement, the 100% relative humidity condition shows better performance with similar local current distribution profiles. It is also found that among the different flow configurations tested under the various operating conditions, the counter-flow arrangement provided the optimum average current density and the lowest variations in the local current densities along the flow channels.

- Since the dynamic characteristics of PEMFC performance is important, especially for automotive applications exposed to continuous variations in load and speed, the local current distribution during dynamic operation is, therefore, investigated experimentally. The fluctuation of the local current density increases as the cell voltage is reduced, corresponding to the increase in the average cell current density or cell loading. Increasing the stoichiometry ratio of the cathode supply gas significantly reduces the local current density fluctuations. The fluctuation is also lower near the flow inlet than near the flow exit because more water is accumulated near the flow exit. Although, pressurizing the cell enhances cell performance, it causes more severe fluctuations of the current density due to more water condensation. Further, it is observed that both the magnitude and the fluctuation of the local current density are strongly influenced by the degree of humidity in the reactant gas stream. The phenomena observed closely related to water distribution and transport within the cell structure.

- In-situ, non-destructive temperature measurement is performed on the PEMFC with multiple straight and serpentine flow channels, using micro thermocouples embedded in the arrays of blind holes and at the top of reaction sites. Temperature distribution is obtained along the flow channel on both the cathode and anode sides and only along the flow channels at the cathode side for parallel and serpentine flow channels, respectively. The results indicate that the temperature distribution inside the PEMFC is very sensitive to

the current density. The temperature distribution inside the PEMFC seems to be virtually uniform at low current density, while temperature variation increases up to 2 ^{o}C at high current density. The results signify that the temperature variation inside the PEMFC is high enough to be considered taking into account that active area for the cell under investigation is only 50 cm^2.

- Simultaneous measurements are conducted in order to determine the relationship between the local current density and temperature distributions in the PEMFC. It is found that the local current density distribution is closely related to the temperature distribution along the flow channels, especially at high values of both current density and cell backpressure.

Chapter 5
Summary and Future Work

In this research, two different experimental techniques have been employed systematically to understand the distributions of both local current density and temperature over the reaction site of Proton Exchange Membrane Fuel Cell (PEMFC), with different flow arrangements and under various operating conditions. This detailed understanding is required to enhance both the reliability and durability of the PEMFC, along with cost reduction. An experimental study of the local current distribution in the PEMFC has been conducted using the segmented flow field plate and printed circuit board (PCB) technique, whereas thermocouples have been used to obtain the temperature distributions in the PEMFC. This thesis highlights: (1) the effect of the three common and practical flow arrangements including co-, counter-, and cross-flow arrangements on the local current distribution profile under steady state conditions; (2) the effect of different operating conditions such as the reactant stoichiometry ratio, cell pressure, cell temperature, cell potentials, and relative humidity on the local current density distribution; (3) the dynamic characteristics of local current density in PEMFC under different operating conditions; and (4) the temperature distribution in a single PEMFC with straight and serpentine flow channels as employed in industrial fuel cells at different operating conditions. The technical advantages/disadvantages of implementing either straight or serpentine flow fields in PEMFC are directly related to the complexity of the fuel cell system and its overall performance as discussed in Chapter 1 of this thesis. Such a contribution is required for improving the design of the PEMFC system. For example, analyzing the dynamic characteristics of the PEMFC is important in order to understand the challenges faced by PEMFC in automotive applications, where loads change continuously.

The main contributions of this thesis are summarized as follows:

- The reactant flow arrangement has a significant effect on the local current distribution. The co-flow arrangement results in considerable current density variations from the anode/cathode inlets to exits, while the counter-flow arrangement produces the most uniform distribution for current density. However, the cross-flow arrangement results in the most complex local current density profile over the MEA surface among the three

configurations compared. The observed influence of the flow arrangement on the local current density signifies that some regions inside the cell present a fast electrochemical reaction rate (e.g inlet region), while other regions present a low reaction rate (e.g. outlet region). From an industrial point of view, this important observation is closely related to the durability of the PEMFC because it implies that some regions over the MEA surface degrade faster than others. Thus, selecting the proper type of flow arrangement (e.g counter-flow) along with the optimum operating conditions is one of the key elements to overcome the PEMFC's drawbacks.

- Low fuel (hydrogen) stoichiometry ratio at the anode side can be considered a limiting factor, which has a significant impact on the local current distribution and cell performance.

- Increasing both the air and hydrogen stoichiometry ratios improves cell performance, lowers variations of the current distribution, and significantly reduces fluctuations in the local current density.

- Increasing the operating backpressure improves the magnitude of the local current distribution, and consequently enhances the overall cell performance. However, it causes more severe fluctuations especially at high current densities. Combining the effect of the two essential observations (the backpressure and reactant stoichiometry ratios) is very useful in the practical PEMFC applications. To reduce or eliminate the fluctuation problem and obtain reliable performance, a higher stoichiometry ratio is required. However, this employs expensive, on-site fuel cell accessories such as compressors and blowers and better sealing techniques.

- Fully humidified or dried reactant streams for air and hydrogen results in a negative impact on the local current distribution as well as overall cell performance. The effect of the relative humidity of reactant streams on the local current density profiles varies from one region to another over the MEA surface. However, it is found that for the co-flow and cross-flow arrangements, supplying air and hydrogen at 50% relative humidity shows an optimum cell performance and the 100% relative humidity condition results in large variations of local current distribution. From an industrial point of view, this is a crucial

contribution because it proposes that a simple humidification unit with less complex accessories is capable of providing sufficient humidification for PEMFC.

- The fluctuation of the local current density at low cell potential (high current density) is more noticeable than at high cell potential (low current density). The degree of fluctuation of the local current density is also lower near the flow inlet than near the flow exit.

- The temperature distribution inside the PEMFC is significantly affected by the amount of current density drawn from the cell. It is found that the temperature distribution inside the PEMFC can be virtually uniform at low current density, while the temperature variation over the MEA surface increases up to 2 ^{o}C at low cell potential (high current density). Further, operating the fuel cell at high current density can lead to an increase in the temperature difference of 12 ^{o}C between the inside cell temperature and its surrounding or the endplate temperatures. The steep temperature gradient across the fuel cell necessitates the need for an effective cooling system capable of removing the heat generated over the reaction site, to avoid hotspot formation inside an operational PEMFC. This observation also indicates that taking the endplate temperatures to monitor the fuel cell temperature can be misleading, especially at high current density.

- The close relationship between of both the local current density and temperature distributions is observed near the inlet region of serpentine flow channels at the cathode side, especially at low cell potential.

- Finally, this thesis provides an experimental database for numerical and experimental studies, and it develops optimum operational strategies in the industrial implementation of PEMFCs. It also demonstrates that many drawbacks including reliability, durability, and cost of an operational PEMFC can be reduced considerably by choosing the best possible cell structure and optimum operating conditions.

Potential Areas for Future Studies are highlighted as Follows:

- One of the methods under investigation to improve the water management inside an operational PEMFC is the modification of the flow channel surface wettability characteristics from hydrophilic to hydrophobic. It is worthwhile to investigate the effect

of the surface modification on the local current density distribution and its dynamic characteristic with using different flow channels and GDL coating materials.

- The simultaneous relationship between the local current density distribution and water formation is a promising area of research to explore. An optical window can be used in lieu of the graphite plate on the cathode side; hence, a high speed charge-coupled device camera can be used for visualization of water generation along the flow channels, and PCB can be used on the anode side to measure the local current distributions.

References

1. Hooders G. Fuel cell technology handbook. *SAE International and CRC Press* 2002.

2. Larminie J, Andrew D. Fuel Cell Systems Explained, Second Edition. *John Wiley & Sons* 2003.

3. Murphy OJ, Cisar A, Clarke E. Low-cost light weight high power density PEM fuel cell stack. *Electrochimica Acta* 1998,**43**:3829-3840.

4. Li X. Principles of fuel cells. *Taylor & Francis* 2006.

5. Lee Y. Effects of Water Transport and Freezing on the Performance Characteristics of Polymer Electrolyte Fuel Cells. *Thesis for the Degree of Doctor of Philosophy* 2009.

6. Inaba M, Kinumoto T, Kiriake M, Umebayashi R, Tasaka A, Ogumi Z. Gas crossover and membrane degradation in polymer electrolyte fuel cells. *Electrochimica Acta* 2006,**51**:5746-5753.

7. Cheng X, Zhang J, Tang Y, Song C, Shen J, Song D*, et al.* Hydrogen crossover in high-temperature PEM fuel cells. *Journal of Power Sources* 2007,**167**:25-31.

8. Wu H, Berg P, Li X. Non-isothermal transient modeling of water transport in PEM fuel cells. *Journal of Power Sources* 2007,**165**:232-243.

9. Yun C, Radoslav A. Platinum Monolayer Electrocatalysts for the Oxygen Reduction Reaction: Improvements Induced by Surface and Subsurface Modifications of Cores. *Advances in Physical Chemistry* 2011.

10. Li H, Tang Y, Wang Z, Shi Z, Wu S, Song D*, et al.* A review of water flooding issues in the proton exchange membrane fuel cell. *Journal of Power Sources* 2008,**178**:103-117.

11. Moreira J, Sebastian PJ, Ocampo AL, Castellanos RH, Cano U, Salazar MD. Dependence of PEM fuel cell performance on the configuration of the gas diffusion electrodes. *Journal of New Materials for Electrochemical Systems* 2002,**5**:173-175.

12. Yoon Y, Lee W, Park G, Yang T, Kim C. Effects of channel and rib widths of flow field plates on the performance of a PEMFC. *International Journal of Hydrogen Energy* 2005,**30**:1363-1366.

13. Blunk R, Abd Elhamid MH, Lisi D, Mikhail Y. Polymeric composite bipolar plates for vehicle applications. *Journal of Power Sources* 2006,**156**:151-157.

14. Cho E, Jeon U, Ha H, Hong S, Oh I. Characteristics of composite bipolar plates for polymer electrolyte membrane fuel cells. *Journal of Power Sources* 2004,**125**:178-182.

15. Li X, Sabir I. Review of bipolar plates in PEM fuel cells: Flow-field designs. *International Journal of Hydrogen Energy* 2005,**30**:359-371.

16. Pollegri A, P. S. US Patent No. 4,197,178,. 1980.

17. Zamel N. Effective Transport Properties of the Gas Diusion Layer of PEM Fuel Cells. *Ph.D Thesis* 2011.

18. Li J, Wang C-Y, Su A. Prediction and Experimental Validation of In-Plane Current Distribution Between Channel and Land in a PEFC. *Journal of The Electrochemical Society* 2008,**155**:B64-B69.

19. Carrette L, Friedrich K, Stimming U. Fuel Cells: Principles, Types, Fuels, and Applications. *Chem.Phys. Chem* 2000,**1**:162-193.

20. Olgun H, Ersoz A, Kaya D, Tiris M, Akgun F, Ozdogan S. Simulation Study of a PEM Fuel Cell System with Steam Reforming. *International Journal of Green Energy* 2004,**1**:313 - 325.

21. Pérez LC, Brandão L, Sousa JM, Mendes A. Segmented polymer electrolyte membrane fuel cells—A review. *Renewable and Sustainable Energy Reviews* 2011,**15**:169-185.

22. Cleghorn S, Derouin C, Wilson M, Gottesfeld S. A printed circuit board approach to measuring current distribution in a fuel cell. *Journal of Applied Electrochemistry* 1998,**28**:663-672.

23. Rajalakshmi N, Raja M, Dhathathreyan KS. Evaluation of current distribution in a proton exchange membrane fuel cell by segmented cell approach. *Journal of Power Sources* 2002,**112**:331-336.

24. Sauer D, Sanders T, Fricke B, Baumhöfer T, Wippermann K, Kulikovsky A*, et al.* Measurement of the current distribution in a direct methanol fuel cell--Confirmation of parallel galvanic and electrolytic operation within one cell. *Journal of Power Sources* 2008,**176**:477-483.

25. Freunberger S, Reum M, Evertz J, Wokaun A, Büchi F. Measuring the Current Distribution in PEFCs with Sub-Millimeter Resolution. *Journal of The Electrochemical Society* 2006,**153**:A2158.

26. Abdullah A, Okajima T, Mohammad A, Kitamura F, Ohsaka T. Temperature gradients measurements within a segmented H2/air PEM fuel cell. *Journal of Power Sources* 2007,**172**:209-214.

27. Hsieh S, Huang Y. Measurements of current and water distribution for a micro-PEM fuel cell with different flow fields. *Journal of Power Sources* 2008,**183**:193-204.

28. Wieser C, Helmbold A, Gülzow E. A new technique for two-dimensional current distribution measurements in electrochemical cells. *Journal of Applied Electrochemistry* 2000,**30**:803-807.

29. Nishikawa H, Kurihara R, Sukemori S, Sugawara T, Kobayasi H, Abe S*, et al.* Measurements of humidity and current distribution in a PEFC. *Journal of Power Sources* 2006,**155**:213-218.

30. Dohle H, Mergel J, Ghosh PC. DMFC at low air flow operation: Study of parasitic hydrogen generation. *Electrochimica Acta* 2007,**52**:6060-6067.

31. Stumper J, Campbell SA, Wilkinson DP, Johnson MC, Davis M. In-situ methods for the determination of current distributions in PEM fuel cells. *Electrochimica Acta* 1998,**43**:3773-3783.

32. Lin R, Gülzow E, Schulze M, Friedrich KA. Investigation of Membrane Pinhole Effects in Polymer Electrolyte Fuel Cells by Locally Resolved Current Density. *Journal of The Electrochemical Society* 2011,**158**:B11.

33. Gagliardo J, Owejan J, Trabold T, Tighe T. Neutron radiography characterization of an operating proton exchange membrane fuel cell with localized current distribution measurements. *Nuclear Instruments and Methods in Physics Research Section A: Accelerators, Spectrometers, Detectors and Associated Equipment* 2009,**605**:115-118.

34. LaDou J. Printed circuit board industry. *International Journal of Hygiene and Environmental Health* 2006,**209**:211-219.

35. Brett DJL, Atkins S, Brandon NP, Vesovic V, Vasileiadis N, Kucernak A. Localized Impedance Measurements along a Single Channel of a Solid Polymer Fuel Cell. *Electrochemical and Solid-State Letters* 2003,**6**:A63.

36. Schulze M, Gülzow E, Schönbauer S, Knöri T, Reissner R. Segmented cells as tool for development of fuel cells and error prevention/prediagnostic in fuel cell stacks. *Journal of Power Sources* 2007,**173**:19-27.

37. Noponen M, Mennola T, Mikkola M, Hottinen T, Lund P. Measurement of current distribution in a free-breathing PEMFC. *Journal of Power Sources* 2002,**106**:304-312.

38. Noponen MH, T. Mennola, T. Mikkola, M. Lund, P. Determination of mass diffusion overpotential distribution with flow pulse method from current distribution measurements in a PEMFC. *Journal of Applied Electrochemistry* 2002,**32**:1081-1089.

39. Hottinen T, Noponen M, Mennola T, Himanen O, Mikkola M, Lund P. Effect of ambient conditions on performance and current distribution of a polymer electrolyte membrane fuel cell. *Journal of Applied Electrochemistry* 2003,**33**:265-271.

40. Noponen M, Ihonen J, Lundblad A, Lindbergh G. Current distribution measurements in a PEFC with net flow geometry. *Journal of Applied Electrochemistry* 2004,**34**:255-262.

41. Mench MM, Wang CY. An In Situ Method for Determination of Current Distribution in PEM Fuel Cells Applied to a Direct Methanol Fuel Cell. *Journal of The Electrochemical Society* 2003,**150**:A79.

42. Mench M, Wang CY, Ishikawa M. In Situ Current Distribution Measurements in Polymer Electrolyte Fuel Cells. *Journal of The Electrochemical Society* 2003,**150**:A1052.

43. Dong Q, Mench M, Cleghorn S, Beuscher U. Distributed Performance of Polymer Electrolyte Fuel Cells under Low-Humidity Conditions. *Journal of The Electrochemical Society* 2005,**152**:A2114.

44. Yang X, Burke N, Wang C, Tajiri K, Shinohara K. Simultaneous Measurements of Species and Current Distributions in a PEFC under Low-Humidity Operation. *Journal of The Electrochemical Society* 2005,**152**:A759.

45. Ghosh P, Wüster T, Dohle H, Kimiaie N, Mergel J, Stolten D. In situ approach for current distribution measurement in fuel cells. *Journal of Power Sources* 2006,**154**:184-191.

46. Freunberger SA, Reum M, Wokaun A, Büchi FN. Expanding current distribution measurement in PEFCs to sub-millimeter resolution. *Electrochemistry Communications* 2006,**8**:1435-1438.

47. Strickland D, Litster S, Santiago G. Current distribution in polymer electrolyte membrane fuel cell with active water management. *Journal of Power Sources* 2007,**174**:272-281.

48. Hicks M, Kropp A, Schmoeckel, R. A. *ECS Trans* 2006,**1**:605-612.

49. Brett D, Atkins S, Brandon N, Vesovic V, Vasileiadis N, Kucernak A. Measurement of the current distribution along a single flow channel of a solid polymer fuel cell. *Electrochemistry Communications* 2001,**3**:628-632.

50. Wu J, Yi B, Hou M, Hou Z, Zhang H. Influence of Catalyst Layer Structure on the Current Distribution of PEMFCs. *Electrochemical and Solid-State Letters* 2004,**7**:A151.

51. Liu Z, Mao Z, Wu B, Wang L, Schmidt VM. Current density distribution in PEFC. *Journal of Power Sources* 2005,**141**:205-210.

52. Bender G, Wilson MS, Zawodzinski TA. Further refinements in the segmented cell approach to diagnosing performance in polymer electrolyte fuel cells. *Journal of Power Sources* 2003,**123**:163-171.

53. Bansal R. Fundamentals of engineering electromagnetics. *Taylor & Francis Group* 2006.

54. Liang D, Shen Q, Hou M, Shao Z, Yi B. Study of the cell reversal process of large area proton exchange membrane fuel cells under fuel starvation. *Journal of Power Sources* 2009,**194**:847-853.

55. Geiger A, Eckl R, Wokaun A, Scherer GG. An Approach to Measuring Locally Resolved Currents in Polymer Electrolyte Fuel Cells. *Journal of The Electrochemical Society* 2004,**151**:A394-A398.

56. Wilkinson M, Blanco M, Gu E, Martin JJ, Wilkinson DP, Zhang JJ*, et al.* In Situ Experimental Technique for Measurement of Temperature and Current Distribution in Proton Exchange Membrane Fuel Cells. *Electrochemical and Solid-State Letters* 2006,**9**:A507-A511.

57. Hakenjos A, Muenter H, Wittstadt U, Hebling C. A PEM fuel cell for combined measurement of current and temperature distribution, and flow field flooding. *Journal of Power Sources* 2004,**131**:213-216.

58. Hakenjos A, Hebling C. Spatially resolved measurement of PEM fuel cells. *Journal of Power Sources* 2005,**145**:307-311.

59. Hogarth W, Steiner J, Benziger J, Hakenjos A. Spatially-resolved current and impedance analysis of a stirred tank reactor and serpentine fuel cell flow-field at low relative humidity. *Journal of Power Sources* 2007,**164**:464-471.

60. Wang L, Liu H. Separate measurement of current density under the channel and the shoulder in PEM fuel cells. *Journal of Power Sources* 2008,**180**:365-372.

61. Higier A, Liu H. Optimization of PEM fuel cell flow field via local current density measurement. *International Journal of Hydrogen Energy* 2010,**35**:2144-2150.

62. Sun H, Zhang G, Guo L-J, Liu H. A novel technique for measuring current distributions in PEM fuel cells. *Journal of Power Sources* 2006,**158**:326-332.

63. Natarajan D, Van Nguyen T. Current distribution in PEM fuel cells. Part 2: Air operation and temperature effect. *AIChE Journal* 2005,**51**:2599-2608.

64. Natarajan D, Van Nguyen T. Current distribution in PEM fuel cells. Part 1: Oxygen and fuel flow rate effects. *AIChE Journal* 2005,**51**:2587-2598.

65. Meng H, Wang CY. *Journal of The Electrochemical Society* 2005,**152**:A1733.

66. Hauer K-, Potthast R, Wüster T, Stolten D. Magnetotomography--a new method for analysing fuel cell performance and quality. *Journal of Power Sources* 2005,**143**:67-74.

67. Wang C. Fundamental Models for Fuel Cell Engineering. *Chemical Reviews* 2004,**104**:4727-4766.

68. Vie P. Thermal conductivities from temperature profiles in the polymer electrolyte fuel cell. *Electrochimica Acta* 2004,**49**:1069-1077.

69. Mench M, Buford D, Davis T. *Proceeding of ASME, Internal Mechanical Engineering Congress & Exposition, Washington, DC* 2003:415-428.

70. Abdul-Aziz A, Alkasab K. Performance of serpentine passages in the cooling system of a phosphoric acid fuel cell stack. *Experimental Thermal and Fluid Science* 1994,**8**:101-111.

71. Adzic M, Heitor M, Santos D. Design of dedicated instrumentation for temperature distribution measurements in solid oxide fuel cells. *Journal of Applied Electrochemistry* 1997,**27**:1355-1361.

72. Wang M, Guo H, Ma C. Temperature distribution on the MEA surface of a PEMFC with serpentine channel flow bed. *Journal of Power Sources* 2006,**157**:181-187.

73. Shimoi R, Masuda M, Fushinobu K, Kozawa Y, Okazaki K. Visualization of the Membrane Temperature Field of a Polymer Electrolyte Fuel Cell. *Journal of Energy Resources Technology* 2004,**126**:258.

74. Shimoi R, Masuda M, Fushinobu K, Kozawa Y, Okazaki K. Visualization of the Membrane Temperature Field of a Polymer Electrolyte Fuel Cell. *Journal of Energy Resources Technology* 2004,**126**:258-261.

75. Fabian T, O'Hayre R, Prinz FB, Santiago JG. Measurement of Temperature and Reaction Species in the Cathode Diffusion Layer of a Free-Convection Fuel Cell. *Journal of The Electrochemical Society* 2007,**154**:B910-B918.

76. Lee S-K, Ito K, Ohshima T, Noda S, Sasaki K. In Situ Measurement of Temperature Distribution across a Proton Exchange Membrane Fuel Cell. *Electrochemical and Solid-State Letters* 2009,**12**:B126-B130.

77. David N, Wild P, Jensen J, Navessin T, Djilali N. Simultaneous In Situ Measurement of Temperature and Relative Humidity in a PEMFC Using Optical Fiber Sensors. *Journal of The Electrochemical Society* 2010,**157**:B1173-B1179.

78. Tüber K, Pócza D, Hebling C. Visualization of water buildup in the cathode of a transparent PEM fuel cell. *Journal of Power Sources* 2003,**124**:403-414.

79. Meier F, Eigenberger G. Transport parameters for the modelling of water transport in ionomer membranes for PEM-fuel cells. *Electrochimica Acta* 2004,**49**:1731-1742.

80. Mukundan R, Borup RL. Visualising Liquid Water in PEM Fuel Cells Using Neutron Imaging. *Fuel Cells* 2009,**9**:499-505.

81. Bellows R, Lin M, Arif M, Thompson A, Jacobson D. Neutron Imaging Technique for In Situ Measurement of Water Transport Gradients within Nafion in Polymer Electrolyte Fuel Cells. *Journal of The Electrochemical Society* 1999,**146**:1099-1103.

82. Satija R, Jacobson DL, Arif M, Werner SA. In situ neutron imaging technique for evaluation of water management systems in operating PEM fuel cells. *Journal of Power Sources* 2004,**129**:238-245.

83. Park J, Li X, Tran D, Abdel-Baset T, Hussey DS, Jacobson DL*, et al.* Neutron imaging investigation of liquid water distribution in and the performance of a PEM fuel cell. *International Journal of Hydrogen Energy* 2008,**33**:3373-3384.

84. Alaefour I, Karimi G, Jiao K, Li X. Measurement of current distribution in a proton exchange membrane fuel cell with various flow arrangements – A parametric study. *Applied Energy* 2012,**93**:80-89.

85. Alaefour I, Karimi G, Jiao K, Shakhshir SA, Li X. Experimental study on the effect of reactant flow arrangements on the current distribution in proton exchange membrane fuel cells. *Electrochimica Acta* 2011,**56**:2591-2598.

86. Jiao K, Alaefour I, Karimi G, Li X. Cold start characteristics of proton exchange membrane fuel cells. *International Journal of Hydrogen Energy* 2011,**36**:11832-11845.

87. Jiao K, Alaefour I, Karimi G, Li X. Simultaneous measurement of current and temperature distributions in a proton exchange membrane fuel cell during cold start processes. *Electrochimica Acta* 2011,**56**:2967-2982.

88. Alaefour I, Li X. Dynamic Response of the Local Current Density in Proton Exchange Membrane Fuel Cells with Different Operating Conditions. *International Journal of Hydrogen Energy* 2011:Under review.

89. Alaefour I, Li X. The Effect of the Air Stoichiometry on Dynamic Behavior of Local Current Density in Proton Exchange Membrane Fuel Cell. *ECS Transactions* 2012,**42**.

90. Alaefour I, Qi L, Jiao K, Park J, Li X. Temperature Distribution in a PEM Fuel Cell with Multiple Straight Flow Channels. *Hydrogen Fuel cell conference-Vancouver*

91. Alaefour I, Karimi G, Li X. Experimental Study of Current Distribution in Proton Exchange Membrane Fuel Cell: Experimental Setup and Flow Arrangement Effect. *Green Energy Conference* 2010.

92. Alaefour I, Jiao K, Karimi G, Li X. Measurement of the Dynamic Response of the Local Current Density Distribution in PEMFC for Various Operating Conditions. *Fuel Cell Seminar & Exhibition 2011* 2011, :Florida.

93. Hydrogenics. FACTS S-Series User Guide 2003.

94. Greenlight. FCATS G20 Test Station-Self Commissioning Guide 2010.

95. Mughal A, Li X. Experimental diagnostics of PEM fuel cells. *International Journal of Environmental Studies* 2006,**63**:377-389.

96. MacDonald C. Effect of Compressive Force on PEMFC performance *University of Waterloo* 2009:Master Thesis.

97. National-Instruments. Measuring Temperature with Thermocouples-a Tutorial 1996.

98. Kim JS, Park, J. B., Kim, Y. M., Ahn, S. H.*, Sun, Hee-Young, Kim, Kyung-Hoon, and Song, Tae-Won. "Fuel Cell End Plates: A review. *International Journal of Precision Engineering and Manufacturing, Korean Society of Precision Engineering* 2008,**9**:39-46.

99. http://www.watlow.com/reference/refdata/0310.cfm.

100. http://www.omega.com/.

101. www.therm-x.com.

102. Omega. CC Cement High Temperature Cement. *User's Guide*.

103. council Usfc. Fuel Cell Test Station Requirements and Verification Procedure. *Document Number: USFCC 04-011* 2006,**B**.

104. Michalski L, Eckersdorf K, Kucharski J, J. M. Temperature Measurement, Second Edition. *John Wiley & Sons, Ltd* 2002.

105. Heitor M, Moreira A. Thermocouples and Samples Probes for Combustion Studies. *Progress in Energy and Combustion Science* 1993,**19**:259-278.

106. Measurement ASTM Committee on Temperature. Manual on the Use of Thermocouples in Temperature Measurement (4th Edition): (MNL 12). In: ASTM International; 1993.

107. Holman J. Experimental Methods for Engineers *McGraw-Hill* 2001.

108. Tavoularis S. Measurment in Fluid Mechanics. *Cambridge,* 2009.

109. Hwnag J, Chang W, Peng R, Chen P, Su A. Experimental and numerical studies of local current mapping on a PEM fuel cell. *International Journal of Hydrogen Energy* 2008,**33**:5718-5727.

110. Rob L. Borup MR, John R Davey, Jacob Spendelow, Muhammad Arif, David Jacobson, Daniel Hussey In-Situ PEM fuel cell water measurements *2008 Fuel Cell Simenar & exposition issue of ECS transactions* 2008.

111. Jiao K, Park J, Li X. Experimental investigations on liquid water removal from the gas diffusion layer by reactant flow in a PEM fuel cell. *Applied Energy* 2010,**87**:2770-2777.

112. Yuan J, Sundén B. Numerical Analysis of Heat Transfer and Gas Flow in PEM Fuel Cell Ducts by a Generalized Extended Darcy Model. *International Journal of Green Energy* 2004,**1**:47-63.

113. Park J, Jiao K, Li X. Numerical investigations on liquid water removal from the porous gas diffusion layer by reactant flow. *Applied Energy* 2010,**87**:2180-2186.

114. Wang Y, Al Shakhshir S, Li X. Development and impact of sandwich wettability structure for gas distribution media on PEM fuel cell performance. *Applied Energy* 2011,**88**:2168-2175.

115. Patel S, Bansode AS, Sundararajan T, Das SK. The Performance Analysis of a Multi-Duct Proton Exchange Membrane Fuel Cell Cathode. *International Journal of Green Energy* 2008,**5**:35-54.

116. Lee Y, Kim B, Kim Y. An experimental study on water transport through the membrane of a PEFC operating in the dead-end mode. *International Journal of Hydrogen Energy* 2009,**34**:7768-7779.

117. Lee Y, Kim Y, Jang Y, Choi J. Effects of external humidification on the performance of a polymer electrolyte fuel cell. *Journal of Mechanical Science and Technology* 2007,**21**:2188-2195.

118. Mughal A, Li X. Experimental diagnostics of PEM fuel cells. *International Journal of Environmental Studies* 2006,**63**:377-389.

119. Hasan A, Guo S, Wahab M. Single-Channel Analysis of Proton Exchange Membrane Fuel Cell. *International Journal of Green Energy* 2010,**7**:208-221.

120. Williams M, Kunz H, Fenton J. Operation of Nafion®-based PEM fuel cells with no external humidification: influence of operating conditions and gas diffusion layers. *Journal of Power Sources* 2004,**135**:122-134.

121. Jiao K, Li X. Water transport in polymer electrolyte membrane fuel cells. *Progress in Energy and Combustion Science* 2011,**37**:221-291.

122. Perng S, Wu H, Jue T, Cheng K. Numerical predictions of a PEM fuel cell performance enhancement by a rectangular cylinder installed transversely in the flow channel. *Applied Energy* 2009,**86**:1541-1554.

123. Qu S, Li X, Hou M, Shao Z, Yi B. The effect of air stoichiometry change on the dynamic behavior of a proton exchange membrane fuel cell. *Journal of Power Sources* 2008,**185**:302-310.

124. Kandlikar S, Lu Z. Thermal management issues in a PEMFC stack - A brief review of current status. *Applied Thermal Engineering* 2009,**29**:1276-1280.

125. Yan Q, Toghiani H, Causey H. Steady state and dynamic performance of proton exchange membrane fuel cells (PEMFCs) under various operating conditions and load changes. *Journal of Power Sources* 2006,**161**:492-502.

126. Sang H, Chang S. Experimental Study of Effects of Operating Conditions on Water Transport Phenomena in the Cathode of Polymer Electrolyte Membrane Fuel Cell. *Journal of Fuel Cell Science and Technology* 2011,**8**:064501.

127. Zhang J, Li H, Shi Z, Zhang J. Effects of Hardware Design and Operation Conditions on PEM Fuel Cell Water Flooding. *International Journal of Green Energy* 2010,**7**:461-474.

128. Nguyen T, Ralph W. A Water and Heat Management Model for ProtonExchange-Membrane Fuel Cells. *Journal of the Electrochemical Society* 1993: pages 2178-2186.

129. Jung S, Nguyen T. An Along-the-Channel Model for Proton Exchange Membrane Fuel Cells. *Journal of The Electrochemical Society* 1998,**145**:1149-1159.

130. Dannenberg K, Ekdunge P, Lindbergh G. Mathematical model of the PEMFC. *Journal of Applied Electrochemistry* 2000,**30**:1377-1387.

131. Ju H, Meng H, Wang C-Y. A single-phase, non-isothermal model for PEM fuel cells. *International Journal of Heat and Mass Transfer* 2005,**48**:1303-1315.